Novel N-type Π-conjugated Polymers for All-polymer Solar Cells

by

Yinghui He

A thesis
presented to the University of Waterloo
in fulfillment of the
thesis requirement for the degree of
Doctor of Philosophy
in
Chemical Engineering

Waterloo, Ontario, Canada, 2017

Examining Committee Membership

The following served on the Examining Committee for this thesis. The decision of the Examining Committee is by majority vote.

External Examiners	Prof. Alex Adronov (McMaster University)
	Prof. Alan Sellinger (Colorado School of Mines)
Supervisors	Prof. Yuning Li (University of Waterloo)
	Dr. Dario Bassani (University of Bordeaux)
Internal Members	Prof. Aiping Yu (University of Waterloo)
	Dr. Lionel Hirsch (University of Bordeaux)
Other Member	Dr. Romain Perrier-Cornet (Canadian General-Tower Ltd)

Author's Declaration

This thesis consists of material all of which I authored or co-authored: see Statement of Contributions included in the thesis. This is a true copy of the thesis, including any required final revisions, as accepted by my examiners.

I understand that my thesis may be made electronically available to the public.

Statement of Contribution

This thesis contains materials from several published or submitted papers, some of which resulted from collaboration with my colleagues in the group.

- The content in Chapter 2 has been partially published in Yinghui He, Chang Guo, Bin Sun, Jesse Quinn and Yuning Li, *Chem. Commun*., 2015, 51, 8093–8096.
- The content in Chapter 3 has been partially published in Yinghui He, Chang Guo, Bin Sun, Jesse Quinn and Yuning Li, *Polym. Chem.*, 2015, 6, 6689–6697.
- The content in Chapter 4 has not been published yet. However, it is in a near-verbatim state to what is intended for submission.

Abstract

Organic solar cells (OSCs), also known as, organic photovoltaics (OPVs), appear as a promising technology for renewable energy owing to their light weight, great flexibility and low-cost fabrication process. So far most of the OPVs have been using fullerene derivatives, such as **PCBM** or **$PC_{71}BM$**, as the electron acceptor in the active layer, which have been proven to a bottleneck for this technology. Therefore, developing non-fullerene acceptors has become the new driving force for this field. All-polymer solar cells (all-PSCs) that have the advantages of robustness, stability and tunability have already achieved PCE up to 9%. However, there is still a significant gap between the all-PSCs and fullerene-based OSCs (PCE approaching 12%) despite tremendous effort that has been put into the optimization of both material and device. Thus, developing novel acceptor materials is imperative for improving the performance of all-PSCs. In this thesis, three classes of π-conjugated polymers were designed and synthesized for the application of all-PSC. The first class of polymers is based on an novel electron-deficient moiety, (3*E*,7*E*)-3,7-bis(2-oxoindolin-3-ylidene)-5,7-dihydropyrrolo[2,3-*f*]indole-2,6(1*H*,3*H*)-dione (IBDP). The IBDP-based polymers (**P1** and **P2**) showed balanced ambipolar transport property (electron mobility up to 0.10 $cm^2 V^{-1} s^{-1}$ and hole mobility up to 0.19 $cm^2 V^{-1} s^{-1}$) in OTFTs. In addition to the good charge transport properties, the IBDP polymers exhibited strong and broad adsorption profile across the visible and NIR region up 1100 nm as well as elevated LUMO levels at -3.70 eV. With these advantageous features, these IBDP polymers were used as acceptor with poly(3-hexylthiophene-2,5-diyl) (**P3HT)** as the donor in all-PSCs. After donor/acceptor ratio optimization, the resultant all-PSC devices showed high PCE of 3.38%, which is the highest PCE that has been obtained from **P3HT**-based all-PSCs so far. The second class consists of three (3*E*,7*E*)-3,7-bis(2-oxoindolin-3-ylidene)benzo[1,2-*b*:4,5-*b'*]difuran-2,6(3*H*,7*H*)-dione (IBDF)-based polymers that feature a new type of side chains that contain an ester group. The resultant IBDF polymers exhibited excellent electron transport properties with electron mobility up to 0.35 $cm^2 V^{-1} s^{-1}$ in OTFTs. When used as acceptor in

all-PSCs with **PTB7-Th** as donor, low PCEs (<0.4%) were obtained, which was found to be caused by the poor miscibility of the donor and acceptor, as well as the inferior bulk charge transport properties of the IBDF polymers. Finally, a new building block, dihydroxylnaphthalene diimide (NDIO), was introduced for the first time into π-conjugated polymers. Due to the alkoxy groups, the electron affinity of the NDIO polymer is significantly higher than the NDI analogues, which led to an enhanced electron transport property and more stable performance in OTFTs upon air-exposure. When used as acceptor in all-PSCs with **PTB7-Th** as the donor, a decent PCE of 3.25 % was realized. In particular, the FF (0.61) of the solar cell devices is much higher than those of the NDI polymers based all-PSCs, which was attributed to the balanced charge transport for both hole and electron in the active layer, as well as the suppressed bimolecular recombination.

Acknowledgements

I would like to express my sincerest gratitude to my two co-advisors, Prof. Yuning Li and Dr. Dario Bassani. Their expertise and insights have helped me greatly during the course of my PhD study. Moreover, their patience and continuous guidance allowed me to develop my research skills and gain knowledge every day in the last four years.

I am very much thankful for Dr. Wei Hong, who taught me all the organic synthesis skills that have got me though all those synthetic challenges throughout my PhD study, and Dr. Jesse Quinn, who has been a wonderful colleague and friend on every aspect in both research and life.

I would like to thank all the other colleagues Dr. Bin Sun, Dr. Chang Guo, Dr. Yunfeng Deng, Dr. Mylène Le Borgne and Dr. Shaoyun Chen who I have worked with, for their support and kind friendship. Moreover, I would like to recognize all my hard-working co-operative students especially Silvia Lee and Jane. I would also like to thank all my committee members: Prof. Aiping Yu, Dr. Lionel Hirsch, Prof. Alex Adronov, Prof. Alan Sellinger and Dr. Romain Perrier-Cornet.

Finally, I would like to acknowledge the unequivocal support from my family, my parents and wife. There is no word to describe how much I am grateful for everything they have done for me, which has given me the strength and courage to pursue my goals.

Table of Contents

List of Figures

List of Tables

List of Schemes

List of Symbols

e: elementary charge, 1.60218×10^{-19} C

ε: dielectric constant

E_g: optical band gap

EQE: external quantum efficiency

FF: fill factor

h: Planck's constant, 6.6207×10^{-34} m^2 kg s^{-1}

I_{DS}: drain-source current

I_{ON}/I_{OFF}: current ON/OFF ratio

J_{SC}: short-circuit current

λ_{max}: wavelength of incident light with maximum absorption

L: channel length

M_n: numerical average molecular weight

PDI: polydispersity index

PCE: power conversion efficiency

R_S: series resistance

R_{SH}: shunt resistance

V_{OC}: open-circuit voltage

V_{TH}: threshold voltage

V_G: gate voltage

V_{DS}: drain-source voltage

μ: charge carrier mobility

W: width, gate width

List of Abbreviations

AFM	Atomic Force Microscopy
BGBC	Bottom Gate Bottom Contact
CV	Cyclic Voltammetry
D-A	Donor-Acceptor
DDTS	Dodecyltrichlorosilane
DFT	Density Functional Theory
GPC	Gel Permeation Chromatography
HOMO	Highest Occupied Molecular Orbital
LUMO	Lowest Unoccupied Molecular Orbital
OFET	Organic Field Effect Transistor
OPV	Organic Photovoltaics
OTFT	Organic Thin Film Transistor
OSC	Organic Solar Cell
PDI	Polydispersity Index
RMS	Root Mean Square
TGBC	Top Gate Bottom Contact
TOF-SIMS	Time-of-Flight Secondary Ion Mass
UV-Vis	Ultraviolet-Visible
XRD	X-ray Diffraction

Other abbreviations and symbols are defined in the text

Chapter 1. Introduction

1.1 Research Context

As the demand for energy has been skyrocketing in last 30 years, nowadays it is imminent for us to seek new energy sources other than traditional ones such as petroleum and coal.[1] On the other hand, there are growing environmental concerns over the climate change and air pollution associated with using these traditional energy sources.[2] Therefore, numerous efforts have been spent finding new energy sources in the last two decades.[3,4] Solar energy is an ideal energy source, since it is completely renewable and environmentally friendly. Moreover, it is free of charge. A solar cell (Figure 1-1) is an electrical device that can convert solar energy into electricity, which can be of various uses such as residential supply and automotive transportation, without generating any air pollution or causing any negative impacts to the environment. As far as the technology of solar cell (also known as photovoltaics) has developed, it can be generally categorized into three generations.[5–7] The first generation of solar cells is based on single crystal silicon. With considerable efficiency and long lifespan, single crystal silicon solar cell panels are massively used for residential and plants nowadays, however, the initial production cost and heavy weight have refrained it from application in other areas, for instance, portable electronic devices.[8] The second generation of solar cells is called thin film solar cells, because they are made of thin layers of inorganic semiconductors such as cadmium telluride (CdTe) and copper indium gallium diselenium (CIGS). The combination of use of less material and lower production cost allows the manufacturers to produce and sell solar cells at a much lower price. However, it has turned out to be difficult to produce thin film solar cells in massive quantity with comparable efficiency level to that of single crystal silicon solar cells.[9] The third generation of solar cells usually refers to a variety of technologies that are still under research and development now, which include organic solar cells, dye sensitized solar cells and quantum dot solar cells. Organic solar cells, also known as organic photovoltaics (OPVs), are mainly based on organic semiconductors. Thus, they

have several distinguished features. First, they can be solution processed, which fundamentally allows the possibility of manufacturing a solar cell panel using printing technologies at high throughput. Compared with the fabrication of inorganic solar cells, using printing technologies will substantially lower the manufacturing cost and increase manufacturing efficiency.[10,11] Second, organic materials generally have light weight (due to the low density) and good flexibility. This feature is highly desired by the portable electronic devices.[12,13] Third, the diversity of organic materials provides means to tune and optimize the material properties to meet the criteria set by the applications.[14] Owing to these features, organic solar cells have been considered one of the promising photovoltaic technologies.

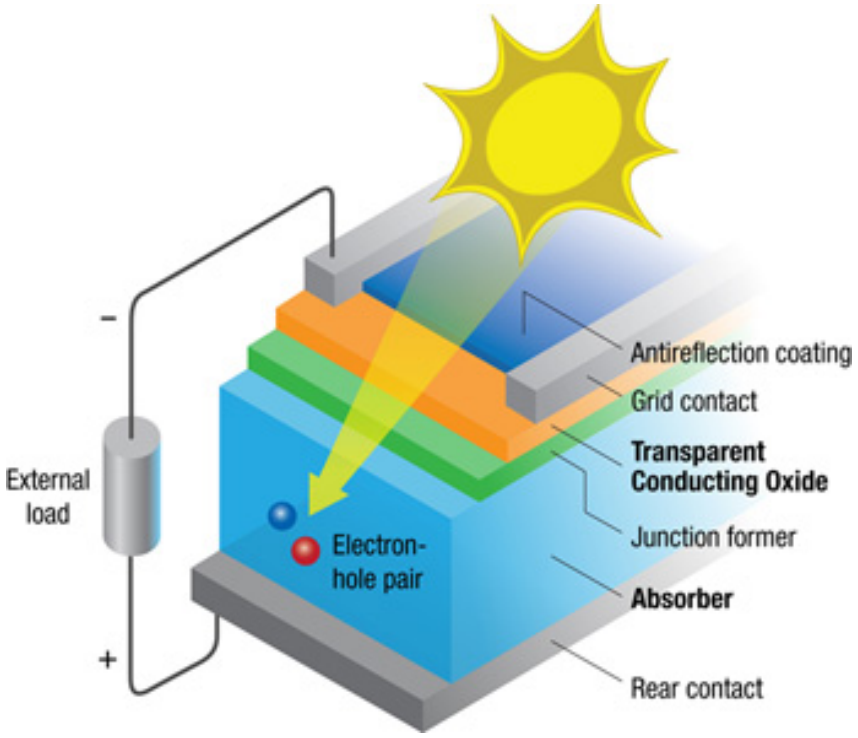

Figure 1-1 The illustration of the structure of a typical solar cell device.[15]

1.2 Organic Solar Cells

Solar cell is an electrical device that can steadily harvest the sunlight and generate electricity. In 1978, Morel *et al.* and Tang *et al*. individually introduced the first two organic solar cells with power-conversion efficiencies (PCEs) of around 1%.[16][17] As shown in Figure 1-2, the cell was based on the two-layer planar heterojunction of two organic materials: copper phthalocyanine (**CuPc**) as donor and 3,4,9,10-perylenetetracarboxyl-bis-benzimidazole (**PV**) as acceptor. These two organic layers were sandwiched between ITO-coated glass (front contact) and Ag (back contact) to form a solar cell. When the light photon reaches the front contact, it transmits through the front contact and to the **CuPc** layer, where the photon will be absorbed by **CuPc** and generates an exciton. As the exciton travels to the interface between **CuPc** and the PV, the exciton gets split into an electron and a hole, and then the electron will transfer to the PV layer. Finally, the hole and electron will be collected by respective electrodes, forming the photovoltaic current. The driving force for the charge separation is provided by the energy difference between the lowest unoccupied molecular orbital (LUMO) of the donor (**CuPc**) and highest occupied molecular orbital (HOMO) of the acceptor (**PV**). One improvement to the OSC device was to use C60 fullerene and its derivatives to replace the n-type **PV**, since fullerene has stronger electronegativity and higher electron mobility. In 1993, researchers introduced the use of fullerene derivative, [6,6]-phenyl-C61-butyric acid methyl ester (**PCBM**, Figure 1-3) as the acceptor in planar heterojunction OSCs.[18] However, the cell only demonstrated a low PCE of 0.04%. It was because the lifetime of the exciton in organic semiconductors (~10 nm)[19,20] is much shorter than that in single crystal silicon, which means only small portion of the generated excitons turn into charge carriers.[21] This problem was later addressed by introducing a bulk heterojunction (BHJ) system (Figure 1-4), which involves blending donor and acceptor materials in a single layer device. It was first

introduced by Hiramoto *et al*. through the co-evaporating donor and acceptor molecules simultaneously under high-vacuum condition.[22] In 1995, Heeger's group reported the first polymer–fullerene (**MEH-PPV** and **PCBM**) bulk heterojunction solar cell with a high PCE.[23] This opened a new rea of polymer–fullerene system in the field of high-efficiency OSCs. Up to now the polymer–fullerene solar cell's PCE has reached 11.7%[24], indicating remarkable progress towards a promising future.

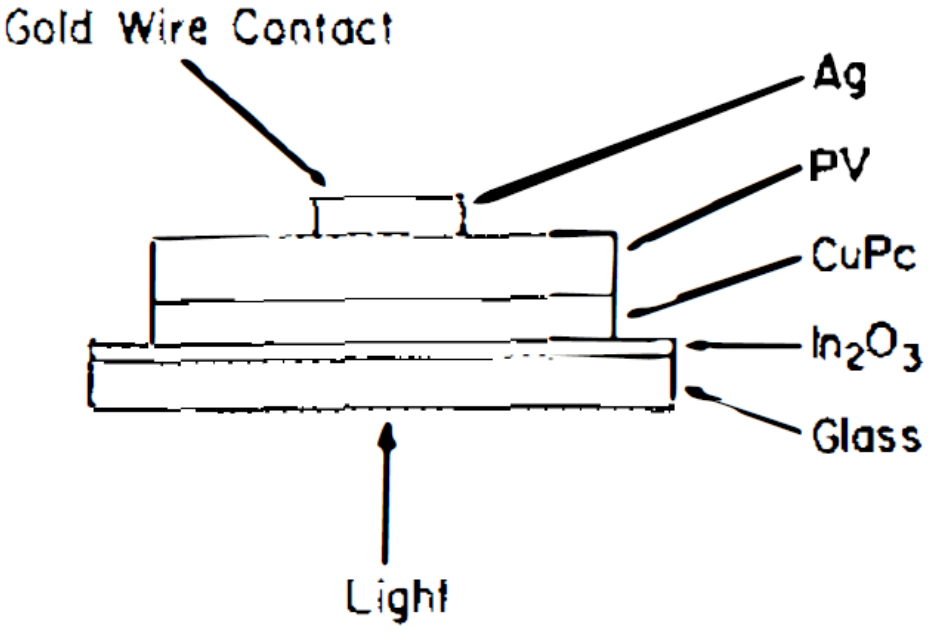

Figure 1-2 The device structure of the first OSC reported by Tang *et al*.[17]

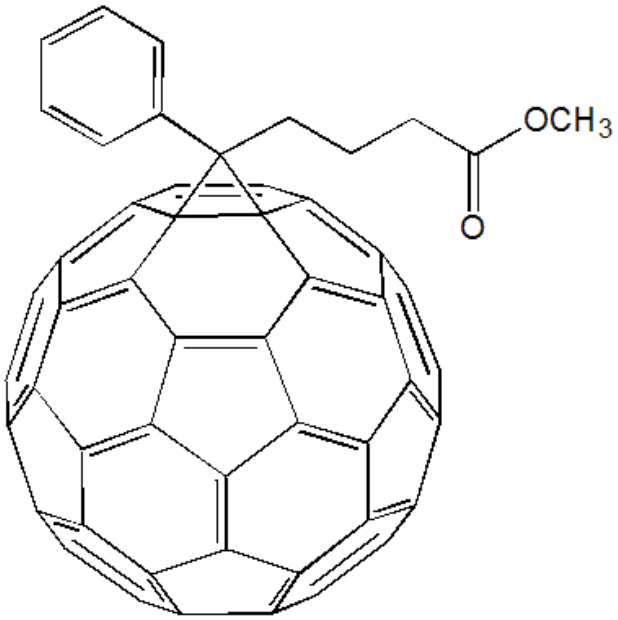

Figure 1-3 The chemical structure of **PCBM**.

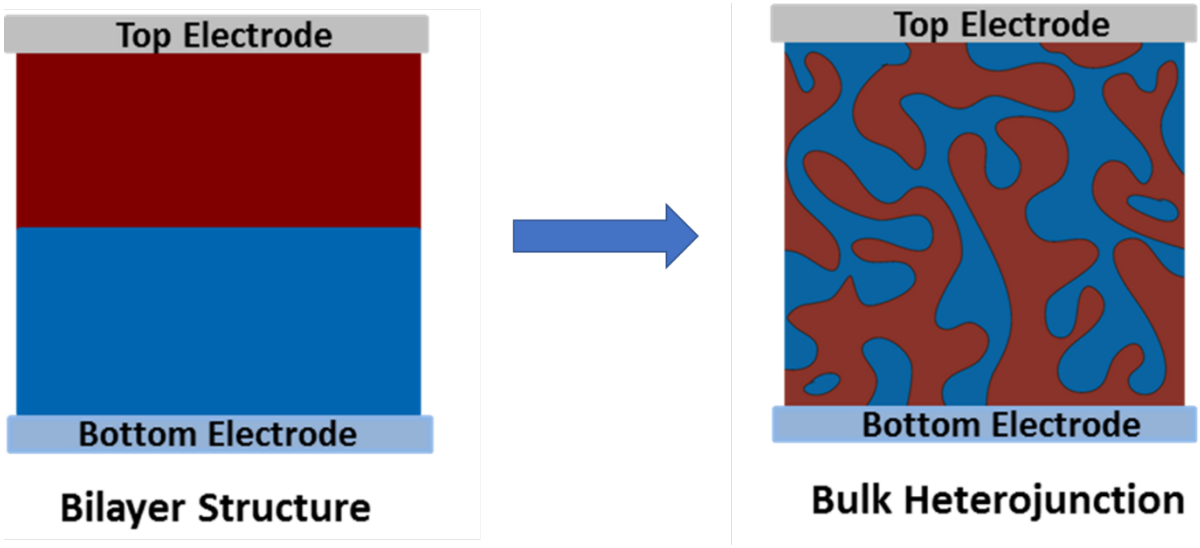

Figure 1-4 The concept of bulk heterojunction (BHJ) that is used for OSCs.

There are four parameters to characterize the performance of a solar cell: Open circuit voltage (V_{OC}), short circuit current density (J_{SC}), fill factor (FF) and power conversion efficiency (PCE), which all can be obtained from the V-J (voltage-current density) curve of a cell. As depicted in Figure 1-5, V_{OC} is the output voltage when J is at zero, which represents the maximum voltage that can be obtained from the cell. There are many factors that can influence V_{OC} of a solar cell (Figure 1-6). For organic solar cells, Cowan *et al*. proposed an equation derived from both theoretical study and experimental data[25]:

$$V_{OC} = \frac{1}{e}\left(E^{A}_{LUMO} - E^{D}_{HOMO} - \Delta\right) - \frac{kT}{e}\ln\left(\frac{N_e N_h}{N_C}\right)$$

Where N_e is termed the electron density in the acceptor domains and N_h is termed the hole density in the donor domains under open circuit conditions, and N_C is the density of states (DOS) at the conduction band edge of the donor and acceptor. The energy shift, Δ, arises from disorder within the phase separated donor and acceptor domains. J_{SC} is the measured current density when the external resistance is zero, which represents the maximum current density that can be obtained from the cell. This equation was also verified by Scharber's work,[26] which gave a simplified equation:

$$V_{OC} = \frac{1}{e}\left(E^{A}_{LUMO} - E^{D}_{HOMO}\right) - 0.3V$$

A simple way to increase the J_{SC} of a solar cell is to use a low bandgap and broaden the adsorption profile of semiconductor to promote the light harvesting and charge generation. In a device, however, J_{SC} could also be determined by several non-trivial factors such as exciton dissociation, charge transport (bulk charge transport mobility) and germinate recombination. Achieving a proper morphology of the active layer is a key to the intrinsic performance for given a combination of donor/acceptor. The preferred morphology of the active layer is a bi-continuous interpenetration network (Figure 1-7)[27]. Donor and acceptor domains should be twice the size of the exciton diffusion length (around 10 nm),

which allows excitons to diffuse to the donor–acceptor interface and thus achieves efficient exciton dissociation and charge generation. After charge separation at the donor–acceptor interface, holes and electrons must travel to the positive and negative electrodes through the continuous donor and acceptor networks, respectively. Although V_{OC} and J_{SC} can indeed be improved by employing these strategies, it remains a challenge to improve both values simultaneously. Narrowing the bandgap can improve J_{SC}, but V_{OC} may correspondingly be decreased because of the higher HOMO level that results. Researchers recently demonstrated that structural fine-tuning is a powerful approach for improving both V_{OC} and J_{SC} simultaneously.[28–31] For example, introducing a fluorine atom into the TT unit reduces both HOMO and LUMO levels simultaneously, while also improving V_{OC} and retaining the bandgap.[29,31] Fine-tuning the side-chain structure can also result in a similar effect. One example is to simultaneously lower both the HOMO and LUMO levels by replacing the electron-rich alkoxy side chain with the less electron-rich alkyl chain.[32] FF is the ratio of the maximum power output to the product of V_{OC} and J_{SC}. It is affected by many factors, including the balance of charge carrier mobility, interface recombination (bimolecular recombination), series and shunt resistances, film morphology and miscibility between the donor and acceptor. However, obtaining a clear understanding and the ability to modulate the FF remains a hurdle in the development of PSCs. Apart from the parameters above, the series resistance (R_S) and shunt resistance (R_{SH}) can also significantly affect the J-V curve, as shown in the equation below:

$$J = J_L - J_0 \exp\left(\frac{q(V + JR_S)}{nKT}\right) - \frac{V + JR_S}{R_{SH}}$$

Where J_L is the photocurrent, J_o is the dark saturation current and n is the ideality of the device. According to this equation, the higher R_S or the low R_{SH} is, the lower V_{OC} and FF will become. The

PCE is ratio of maximum output to the power input (100 mW/cm^2 for the standard AM1.5G spectrum multiplied by the area of the cell). Therefore, we have the expression for PCE:

$$PCE = \frac{J_{SC} \times V_{SC} \times FF}{100\ mW/cm^2}$$

Since PCE represents the overall performance of a solar cell, the focus of organic photovoltaics has been achieving high PCE to compete with silicon solar cells. With all these parameters affecting the PCE of a solar cell, improving the PCEs of OSCs presents a great challenge to the researchers. Although optimizing the fabrication process can probe the intrinsic maximum performance of the materials, more efforts should be made to develop novel materials with excellent properties that can simultaneously boost all those parameters in order for OSCs' performance to reach that of Silicon solar cells.

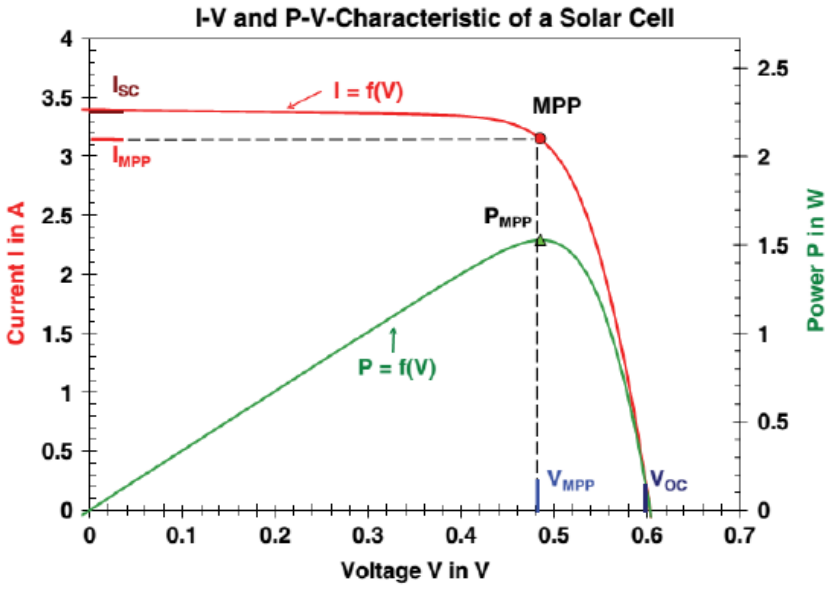

Figure 1-5 The J-V and P-V characteristics of a solar cell.[33]

Figure 1-6 Factors that can affect the V_{OC} in organic solar cells.

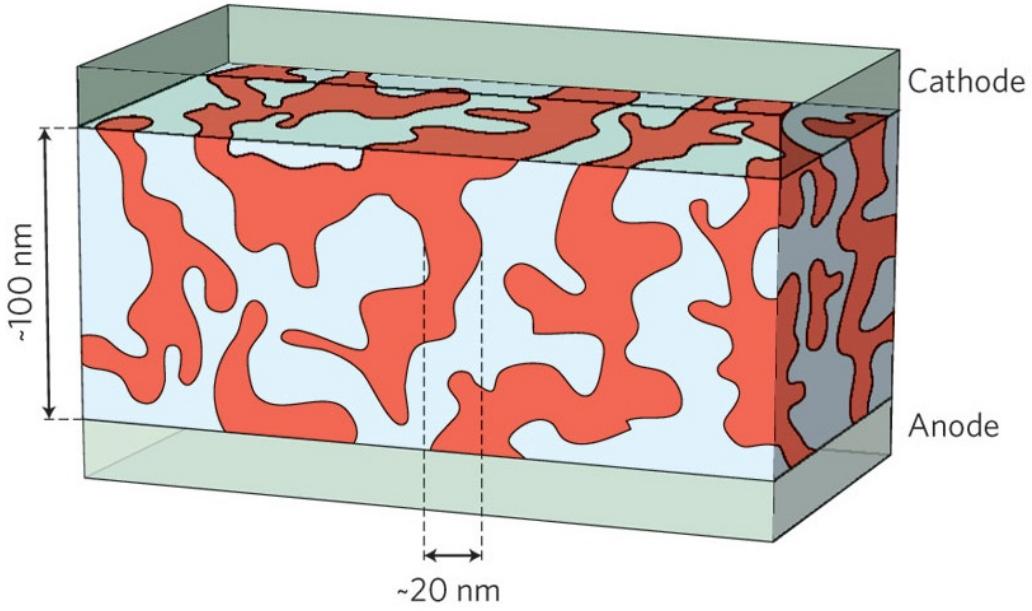

Figure 1-7 The ideal morphology (bi-continuous and interpenetrating network) for a bulk heterojunction of donor-acceptor.

1.3 Organic Semiconductors

Semiconductors are materials that show low conductivity at room temperature but significantly higher conductivity at elevated temperatures. This phenomenon can be explained by the band gap between valence band and conduction band in an inorganic solid. For a solid material, if the band gap is less than 3.0 eV[34], an appreciable number of electrons in the valence band will jump the gap and reach the conduction band (Figure 1-8). This behavior can be described by the following equation[35]:

$$n_i = A^{1/2} T^{3/2} \exp\left(-\frac{E_g}{2k_B T}\right)$$

where A is a constant depending on the characteristics of the valence and conduction bands of the material, T is the absolute temperature, and k_B is the Boltzmann constant. Thus, there will be free electrons populating in conduction band and the material becomes conductive when the temperature was increased. The modern theory of semiconductor physics is based on quantum mechanics to explain the movement of charge carriers in a crystal lattice. Depending on which type of charge carriers (electrons and holes) the material is conducting, the semiconductor can be categorized into 3 types: n-type (electron conduction), p-type (hole conduction) and ambipolar type (both electron and hole conduction). The semiconductor materials can be doped under precise conditions to control the charge carrier concentration and regions of p- and n-type dopants to realize hole conduction and electron conduction (Figure 1-9).

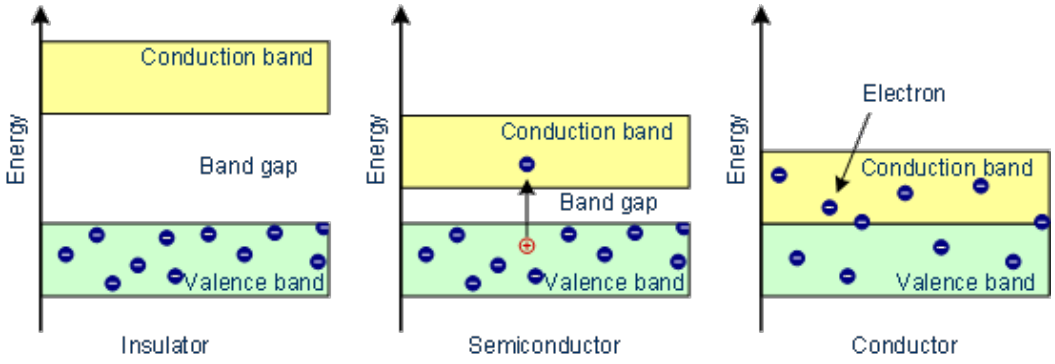

Figure 1-8 The difference among insulator, semiconductor and conductor.[36]

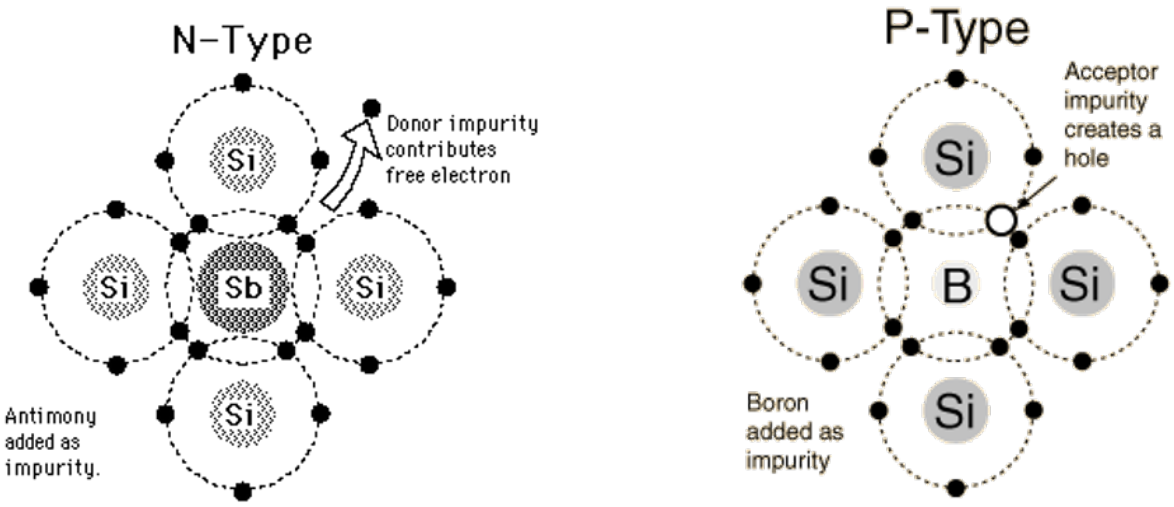

Figure 1-9 The illustration of impurity doping to realize n-type or p-type semiconductor.[37]

In the 1954, researchers discovered that polycyclic aromatic compounds can form semiconducting charge-transfer complex salts with halogens. Electrical conductivity of 0.12 S/cm was observed in perylene-iodine complex.[38] This finding showed that materials could carry charge. In theory, carbon is a Group IV atom with four valence electrons, which can form four bonds through orbital hybridization in three forms, sp, sp^2, and sp^3 (Figure 1-10). The sp^2 orbital is formed by hybridization of s, p_x and p_y orbitals along a plane separated from each other by 120 degrees. While the sp^2 orbitals can form the σ-bonding, the remaining p_z orbitals (out of plane) form delocalized orbitals, which are called the π-bonding. When two orbitals overlap to form the bonding, there will be two new orbitals: one bonding orbital and one anti-bonding orbital (marked with *). The bonding orbital will be occupied by two electrons with spin-up and -down, while the anti-bonding orbital is unoccupied. When many π-bonds are conjugated together, for example, π-conjugated polymers, these bonding/anti-bonding orbitals will form two continuous energy level bands, respectively as shown in Figure 1-11 and the π electrons will fill the energy levels from lowest to highest. The frontier orbital

of the π-orbitals is called HOMO (the highest occupied molecular orbital) and the frontier orbital of the π*-orbitals is called LUMO (the lowest occupied molecular orbital). This concept is similar to the top of the valence band and the bottom of the conduction band in inorganic semiconductors. As π-conjugation grows larger, the HOMO-LUMO band gap becomes smaller. If the band gap is small enough (< 3.0 eV), the organic material starts to have semiconducting properties, just like the inorganic semiconductors. For organic semiconductors, the HOMO and LUMO levels determine the type of charge carriers they can conduct. An organic semiconductor with a high HOMO level tends to transport positive holes and it is called a p-type semiconductor or an electron donor material, a term widely used for OSCs. In contrast, an organic semiconductor with a low LUMO level favors the transport of negative electrons and behaves as an n-type semiconductor or an electron acceptor material. Previous studies have already shown that a LUMO level that is close or below -4.0 eV is needed to stabilize the electron transport in the organic semiconductor.[39,40] Similarly, a HOMO level close or below -5.0 eV is also required for hole transport in organic semiconductor.[41,42] The HOMO and LUMO levels of an organic semiconductor are governed by the chemical functional groups in the π-conjugation. An electron deficient or electron-accepting moiety would decrease the energy levels such as carboxyl groups. On the other hand, an electron rich or electron-donating moiety would increase the energy levels such as alkoxyl groups. Due to the variety of functional groups available for organic compounds, the development of organic semiconductors becomes promising and diversified. In particular polymeric semiconductors have the merits of high mechanical robustness and fully compatibility with printing technology and therefore receive a lot of research attention.[43] For charge transport within π-conjugated polymer semiconductors, two aspects can be looked at: i) intrachain transport and ii) interchain transport (Figure 1-12). The

intrachain charge transport mainly depends on the effective π-conjugation length along the polymer backbone. Generally high coplanarity along the backbone will result in effective π-conjugation and hence efficient intrachain charge transport. The interchain charge transport is determined by the interchain distance and the charge transport between polymer chains is highly anisotropic. The most favored direction is along the π–π stacks, which usually has the shortest interchain distance among all directions and it is the most beneficial for charge hopping between chains. In general, since the intrachain transport is much faster than the interchain transport, interchain charge hopping is usually the rate limiting step.

Hybrid Orbitals and Geometry			
Atomic Orbitals Used	Hybrid Orbitals Formed	Geometry	Example Compound
s,p	Two sp orbitals	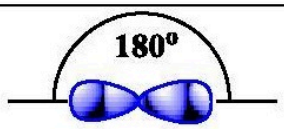 Linear	CO_2
s,p,p	Three sp^2 orbitals	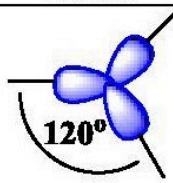 Trigonal Planar	SO_3
s,p,p,p	Four sp^3 orbitals	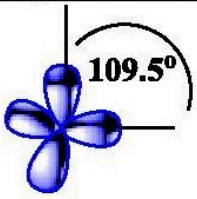 Tetrahedral	$GeCl_4$

Figure 1-10 The geometry of sp, sp^2 and sp^3 orbitals.

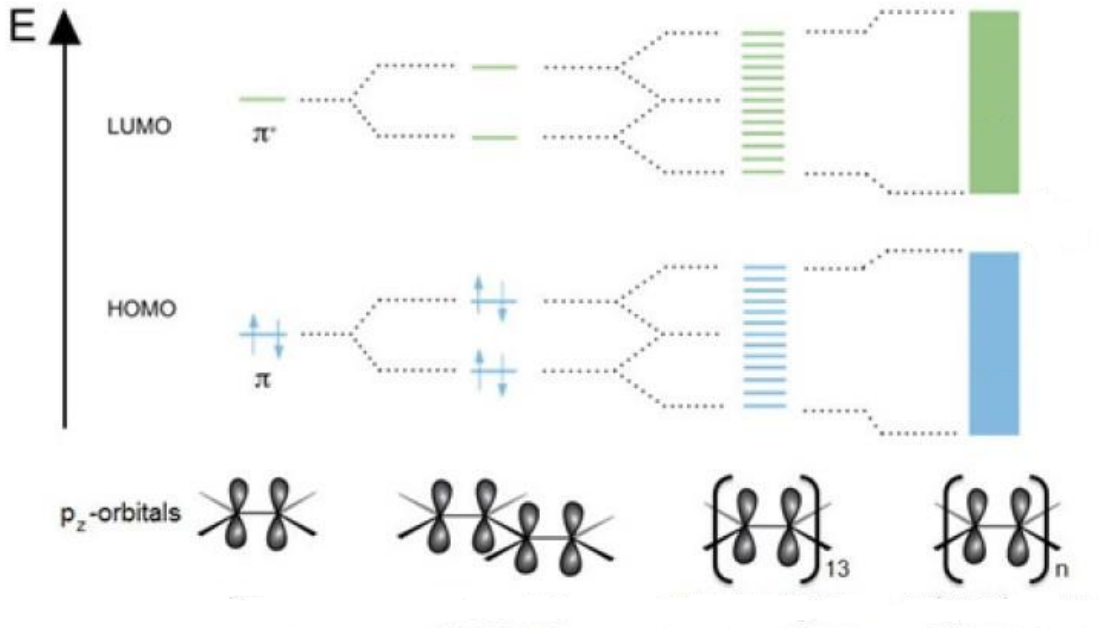

Figure 1-11 Energy band diagram of a π-conjugated polymer.[44]

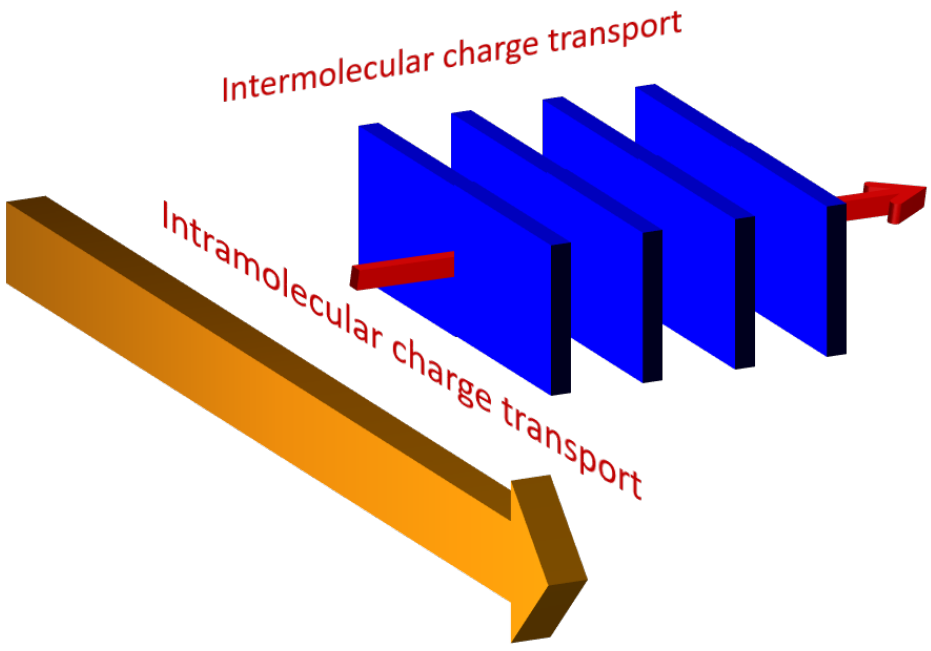

Figure 1-12 Intramolecular charge transport and intermolecular charge transport mechanism.

1.4 Π-conjugated Polymers for Organic Solar Cells

π-conjugated polymers/fullerene based solar cells (PSCs) initially have limited PCEs below 5% since the donor materials, mainly **MEH-PPV** or poly(3-hexylthiophene-2,5-diyl) (**P3HT**) in most cases, have narrow absorption range and low hole mobility.[45–48] In 2006, a novel low band gap polymer, poly[2,6-(4,4-bis-(2-ethylhexyl)-4*H*-cyclopenta[2,1-*b*;3,4-*b'*]dithiophene)-alt-4,7-(2,1,3-benzothiadiazole)] (**PCPDTBT**, Figure 1-13) was reported for PSCs and high PCE up to 5.5 % was achieved[49,50], which was attributed to the higher hole mobility and extended absorption up to 900 nm. **PCPDTBT** represents a new class of π-conjugated polymers, whose backbone is comprised of alternating donor-acceptor (D-A) arrangement. Herein, donors refer to those electron-rich moieties, for example, thiophene and bithiophene and acceptors refer to those electron-deficient moieties such as diketopyrrolopyrrole and naphthalene diimide. According to the orbital hybridization theory, the HOMO and LUMO levels of a D-A polymer are mainly determined by the donor building block and acceptor building block, which generally leads to an elevated HOMO level, deep-lying LUMO level and narrow bandgap. This provides a useful tool to optimize the energy band alignment and solar energy harvest. In addition, the induced intermolecular D–A interaction can shorten the π–π stacking distance to help bring about efficient charge transport in D–A polymers. Since then substantial progress has been made in development of various D–A polymers for high-performance PSCs[51] and recently PCEs over 10% were achieved with poly [[2,6'-4,8-di(5-ethylhexylthienyl)benzo[1,2-*b*;3,3-*b*]dithiophene] [3-fluoro-2[(2-ethylhexyl)carbonyl]thieno[3,4-*b*]thiophenediyl] (**PTB7-Th)** (Figure 1-13) as donor material in PSCs.[52,53] Nowadays, this low-bandgap polymer has been a research focus and served as a benchmark material in this field.[51] Numerous structural parameters such as side chain length and molecular weight, and fabrication conditions such as solvent, additives and post-treatments

were engineered to achieve higher PCE and establish more accurate structure-property relationships.[54–57] Due to these efforts and guidance, researchers were able to discover more donor materials and now the PCE of PSC has reached 11.7%.[24]

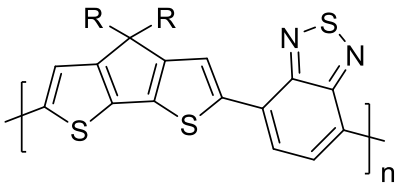

PCPDTBT

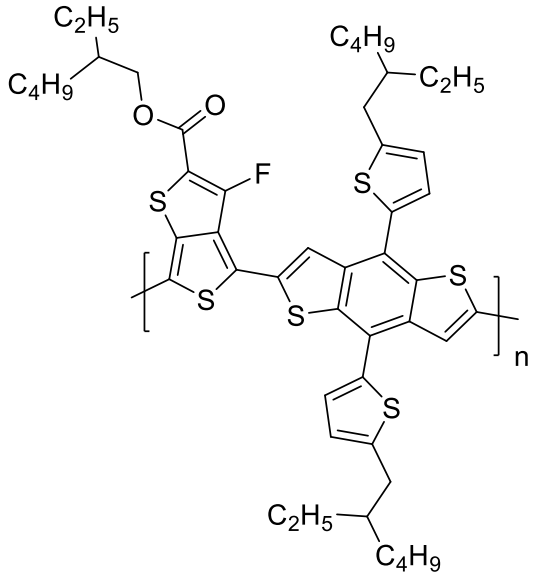

PTB7-Th

Figure 1-13 The chemical structure of polymer **PCPDTBT** and **PTB7-Th**.

On the other hand, the most commonly used acceptors in PSC are **PCBM** and **$PC_{71}BM$** (Figure 1-14). **$PC_{71}BM$** was used to replace **PCBM** in PSCs to extend the absorption to 380–500 nm and increase the electron affinity.[45] It has been demonstrated PSCs with **$PC_{71}BM$** showed enhanced device performance compared to those with **PCBM**.[58] With fullerene's excellent electron transport properties, high electron affinity and the ability to form favorable nanoscale network with donors, almost all reported high efficiency PSCs used these two fullerene derivatives as acceptor. However, fullerene derivatives also exhibit several non-trivial drawbacks that hinder its progress in practical

applications. First, the relatively low lowest unoccupied molecular orbital (LUMO) energy level (~4.1 to -4.3 eV)[59] set a limitation for the open-circuit voltage of the resultant cells.[60] Second, fullerene derivatives fullerenes have strong tendency to crystallize and aggregate causing a performance degradation in long term.[61–63] Third, fullerene derivatives have very poor light absorption profile in the visible and infrared region.[64] Besides, several studies have shown that fullerene will undergo dimerization under photo stress, which also hurts the device's long-term stability.[58,65] In this regard, alternative systems with non-fullerene acceptors attracted intensified research attention in recent years.[66–69]Among them, all-polymer solar cells (all-PSCs), consisting of polymer donors (PD) and polymer acceptors (PA), have recently been studied extensively as replacement for conventional fullerene based PSCs.[13,70–77] For example, Figure 1-15a represents the dramatically increasing trend in the number of SCI publications regarding all-PSCs. In accordance with these trends, the PCE values of all-PSCs have risen from 2% to 8% over the last three years (Figure 1-15b). Currently most of the acceptor polymers are based on the electron-deficient building block naphthalene diimide (NDI) and their all-PSCs have already achieved high PCEs over 9% with the efforts of material and device optimization.[78–83] Despite all these efforts, there is still a non-negligible gap in PCE between fullerene-based PSCs and all-PSCs. Specifically, the J_{SC} for PSCs can be up to 20 mA/cm^2 and only around 12 mA/cm^2 for all-PSCs.[66,84] Similarly, the FF for PSCs usually falls in the range of 60-80% while for all-PSCs the FF is rarely over 60%.[66,84] There are several factors accountable for this gap. First, the charge transport is fully anisotropic in polymer acceptors while it is isotropic in fullerene. Therefore enhancing the electron mobility of acceptor and matching the molecular orientation of donor and acceptor as face-to-face at the interface become keys for improving charge carrier generation, charge carrier transport, and the resulting PCE of all-PSCs.[85] In addition, precise control of the BHJ

morphology should be achieved in a rational manner. the blending of two polymers is less thermaldynamically favored due to the reduced gain of entropy by the presence of long polymer chains. Therefore, achieving an optimal BHJ morphology of polymer/polymer blend is particularly challenging. It is of great importance to control the molecular weight of both PD and PA to realize highly crystalline domains of PD and PA as well as well-intermixed D-A phases. One of the reasons accountable for the low FF in all-PSCs is the inferior electron transport property in those NDI-based polymers. For example, the space charge limited current (SCLC) measured electron mobility in **$PC_{71}BM$** is usually around 5×10^{-3} cm^2 V^{-1} s^{-1}[86,87] while that of the NDI-based polymers is usually on the order of 10^{-4} cm^2 V^{-1} s^{-1}.[73,74,83] On the other hand, NDI polymers have been found to show narrow adsorption (600-700 nm) and fairly low adsorption coefficient ($\sim10^4$ cm^{-1}) in the visible region. Therefore, future work should be focused on the development of new PA materials with high electron mobility and broader absorption in the visible-NIR region to bring new possibilities of achieving high performance all-PSCs.

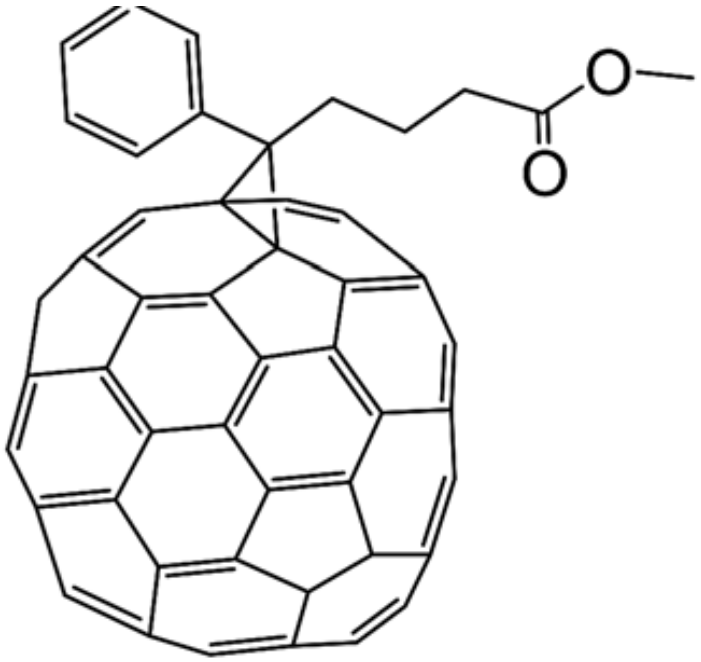

Figure 1-14 The chemical structure of **$PC_{71}BM$.**

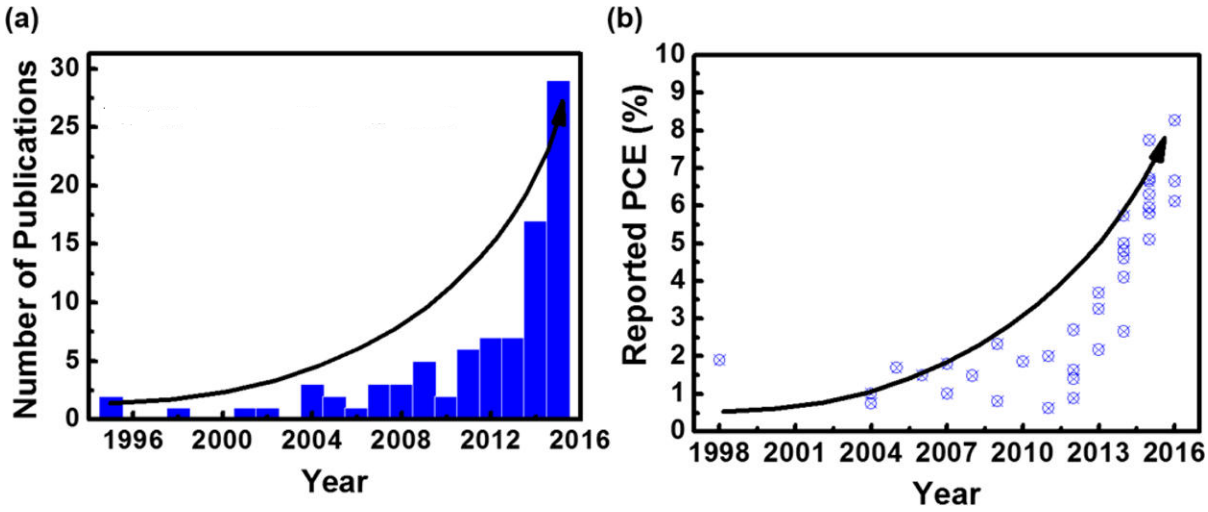

Figure 1-15 (a) Numbers of SCI papers on the key word: all-polymer solar cells and (b) efficiency enhancements regarding all-PSCs for the last two decades.[66]

1.5 Π-conjugated Polymers for Organic Thin Film Transistors

Charge mobility is one of the most important parameters to evaluate the charge transport property of a material. Organic thin film transistor (OTFT) is a useful tool to test the charge carrier mobility extrinsically. In the same time, OTFTs can be used for various applications such as logic circuits, biosensors, photodetectors and flexible displays. Figure 1-16 shows two types of OTFT devices: bottom gate bottom contact (BGBC) and top gate bottom contact (TGBC) structures, wherein the gate controls the current between the source and drain electrodes, similar to a tap that controls the water flow. The source electrode (S) is where the majority carriers enter the channel, the drain (D) is where the majority carriers leave the channel, and the gate (G) terminal controls the channel conductivity. By controlling the gate voltage, the current from source to drain can be adjusted for the transistor to function as a switch. In the last few years, several new polymer semiconductors with mobilities above 1 $cm^2 V^{-1} s^{-1}$ have been reported[88–91], outperforming amorphous silicon (0.1~1 $cm^2V^{-1}s^{-1}$).[92] Most of these high mibilities were achieved with polymers having alternating electron donating (D) and accepting (A) building blocks in the backbone.[14,93] These D-A polymers also have larger conjugated units. The strong intermolecular static attraction between backbones due to the D-A interaction and large overlapping area gives a much closer π-π stacking distance, which dramatically facilitates the inter-chain charge hopping. Thus, the D-A strategy has been widely adopted for developing high mobility π-conjugated polymers.

For complementary logic applications, p-type and n-type transistors with balanced hole and electron mobilities are required. While many high-performance p-type polymer semiconductors have been reported, high performance n-type unipolar polymer semiconductors are rare. Currently there are 4 n-type polymer semiconductors with electron mobility higher than 1 $cm^2 V^{-1} s^{-1}$ listed in Figure 1-17. For example, the widely investigated **P(NDI2OD-T2)** developed by Yan *et al*. achieved electron mobility as high as 0.85 $cm^2 V^{-1} s^{-1}$ in top gate bottom contact (TGBC) OTFTs.[94] In addition, the electron mobility can be improved to up to 3 $cm^2 V^{-1} s^{-1}$ by controlling the defect amount in the backbone.[95] Lei *et.al.* reported a PPV-like acceptor based polymer, **BDOPV-2T**, which displayed unipolar electron mobility up to 1.75 $cm^2 V^{-1} s^{-1}$. Recently, our group reported two electron deficient building blocks: pyridine-flanked diketopyrrolopyrrole (DPPy) and thiophene-S,S-dioxidized indophenine (IDTO). The DPPy-BT copolymer, PDBPyBT, showed record high electron mobility up to 6.3 $cm^2 V^{-1} s^{-1}$. These 4 polymers represent best n-type polymers available for OTFTs, while p-type polymer semiconductors can already achieve hole mobility up 52.7 $cm^2 V^{-1} s^{-1}$.[96]

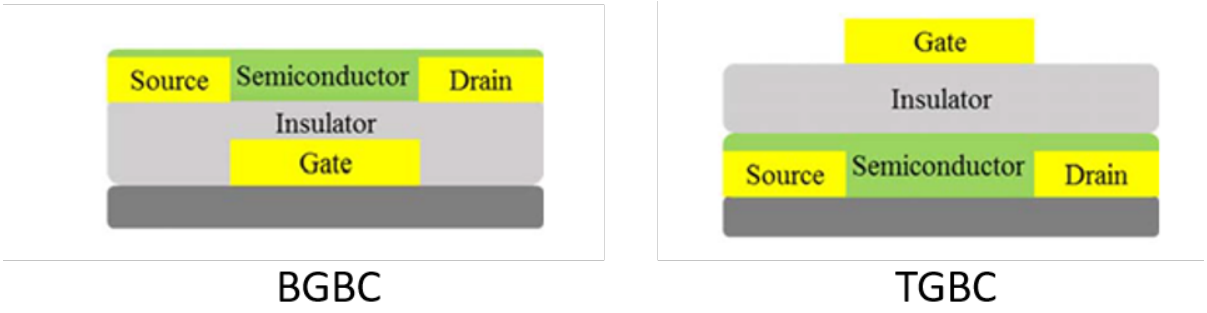

Figure 1-16 Two types of OTFTs (BGBC and TGBC) that are commonly used.

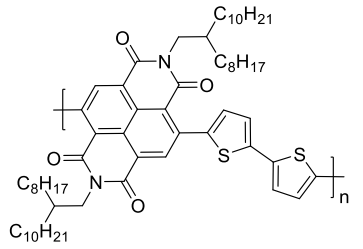

P(NDI2OD-2T)

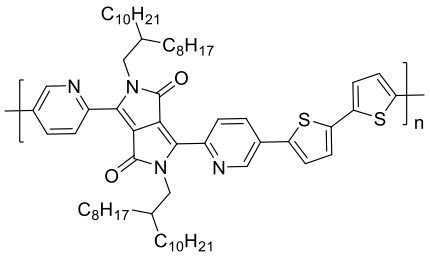

PDBPyBT

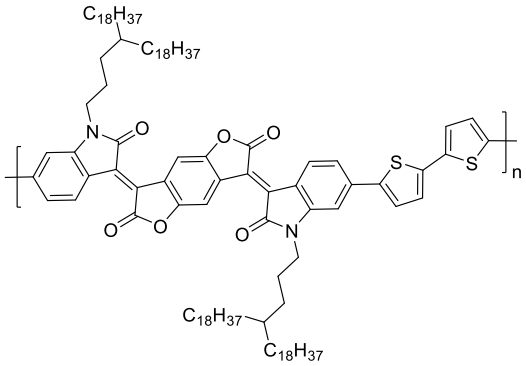

BDOPV-2T

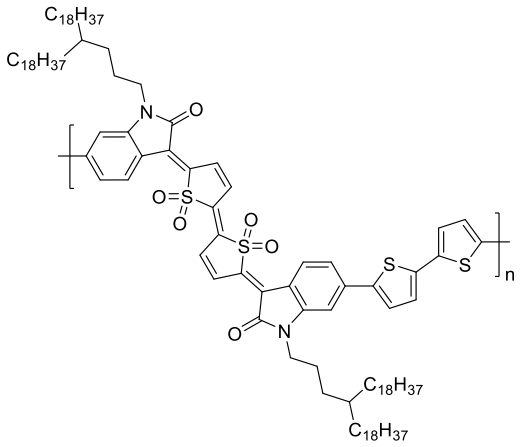

PIDTOBT

Figure 1-17 Some of the best n-type/n-type dominant polymer semiconductors available.

1.6 Objective and Structure of This Thesis

Despite the rapid development of all-PSCs in recent years, there is still a significant gap between all-PSCs and fullerene-based OSCs in terms of device performance. This is mainly due to relatively low charge mobility, low absorption coefficient and narrow absorption range in the visible and NIR region of the acceptor materials (mainly NDI polymers). Therefore, developing new n-type polymers that can overcome these drawbacks is of great importance. Due to the lack of suitable electron-deficient building

blocks available for π-conjugated polymers,[97] developing new n-type polymer semiconductors have been a huge challenge for material chemists. This is evident by the number of newly developed n-type polymers versus the number of p-type within last decade.[14,93] Therefore, the objective of this work is to develop novel electron deficient building blocks and n-type polymeric semiconductors with good electron transport properties and enhanced absorption profile, and then utilize them to improve the performance of all-PSCs. The strategy employed in this work is given as follows:

1) Develop a novel electron-deficient building block to construct D-A polymer semiconductors D-A polymers. Inspired by the high electron affinity of (3*E*,7*E*)-3,7-bis(2-oxoindolin-3-ylidene)-benzo[1,2-*b*:4,5-*b'*]difuran-2,6(3*H*,7*H*)-dione (IBDF) and the excellent electron transport properties of IBDF-based polymers[98–100], a new electron-deficient building block, (3*E*,7*E*)-3,7-bis(2-oxoindolin-3-ylidene)-5,7- dihydropyrrolo[2,3-*f*]indole-2,6(1*H*,3*H*)-dione (IBDP) is designed and synthesized. The resultant IBDP-based polymers will be characterized to study the optical and electronic properties. A suitable donor material and the standard device configuration will be used to fabricate the all-PSCs to investigate the photovoltaic properties of the polymers.

2) A new series of ester side chains will be designed and synthesized for IBDF-based polymers with enhanced solubility. The side chain for IBDF-based polymers will be engineered to optimize the electron transport property and then the resultant polymers will be used with a suitable donor in active layer of all-PSCs. The standard device configuration will be used in this work. The structure-property relationship will be studied using several tools, which include EQE, XRD, AFM and SCLC measurements.

3) A novel electron-deficient building block, dihydroxylnaphthalene diimide (NDIO), will be used for the first time to form a D-A polymer towards air-stable unipolar n-type charge transport. With

addition of alkoxy side chain, the LUMO and HOMO levels of the NDIO polymers are substantially lowered, yielding larger HOMO/LUMO offsets in all-PSCs, which is believed to help facilitate the electron transport and charge generation. The polymers will first be tested in OTFTs to evaluate the electron transport property in nitrogen and air, respectively, to test the performance robustness and stability in air. The all-PSCs will be fabricated using the NDIO polymers as acceptor in the standard device configuration. The structure-property relationship will be studied using several techniques, which includes external quantum efficiency (EQE), AFM and XRD and SCLC measurements.

The thesis is organized as follows:

1) In chapter 2, the design and synthesis of a novel electron deficient building block (IBDP) will be described and two IBDP polymers (**P1** and **P2**). The resultant polymers will then be characterized using several techniques such as atomic force microscope (AFM), X-ray diffraction (XRD), UV-Vis absorption spectroscopy and cyclic voltammetry (CV) will be used to study the optical and electronic properties. Then the polymer will be used for bottom-gate bottom-contact (BGBC) OTFTs to investigate their charge transport properties. Furthermore, the polymers will be used as acceptor in all-PSCs with **P3HT** as the donor. Only preliminary results will be presented due to the limited amount of materials.

2) In chapter 3, a series of ester side chains will be synthesized and used for the copolymers of IBDF and bithiophene (BT) to yield n-type dominant solution-processable IBDF-based polymers. First, the optical and electrochemical properties of these polymers will be systematically studied using UV and CV. Then the charge transport properties of these polymers will be evaluated in bottom-gate bottom-contact (BGBC) OTFTs. The polymers then will be mixed with **PTB7-Th**

in a standard device structure: ITO/PEDOT:PSS/Polymer blend/LiF/Al to investigate the photovoltaic properties. Finally, SCLC, external quantum efficiency (EQE), AFM and XRD will be used to study the structure-property relationships.

3) In chapter 4, a new building block, dihydroxylnaphthalene diimide (NDIO), will be used to form two NDIO-based unipolar n-type polymers. The polymers demonstrated deeper HOMO and LUMO levels. The polymers then will be mixed with **PTB7-Th** in a standard device structure: ITO/PEDOT:PSS/Polymer blend/LiF/Al. The all-PSCs will be characterized and compared with the bench mark PA material, **P(NDI2OD-T2)**. OTFTs, SCLC, external quantum efficiency (EQE), AFM and XRD will be used to study the structure-property relationships.

4) In chapter 5, the thesis work will be concluded and then some future work will be proposed for further study to this work.

Chapter 2. Synthesis and Characterization of IBDP-based Polymers

Part of this chapter was published in Yinghui He, Chang Guo, Bin Sun, Jesse Quinn and Yuning Li, *Chem. Commun*., 2015, 51, 8093–8096.

2.1 Introduction

D-A polymers are useful materials for low-cost organic electronics such as organic thin film transistors (OTFTs) and organic photovoltaics (OPVs) due mainly to their excellent charge transport properties and fine-tuned HOMO/LUMO levels.[21,43,101,102] In recent years, intensified research effort has been devoted to the development of novel electron-rich and -deficient building blocks in order to enhance the charge carrier mobility for a wider range of application of polymer semiconductors. While there are numerous electron-rich building blocks reported in literature, there are only a handful electron-deficient building blocks available.[14,103] Recently our group reported an novel electron deficient building block, (3*E*,7*E*)-3,7-bis(2-oxoindolin-3-ylidene)benzo[1,2-*b*:4,5-*b'*]difuran-2,6(3*H*,7*H*)-dione (IBDF, Figure 2-1)[98], which has been used for D-A polymers for OTFTs. Owing to the strong electron withdrawing capability of the IBDF moiety, IBDF-based D-A polymers showed excellent n-type or n-type dominant ambipolar charge transport performance with high electron mobility up to 1.74 $cm^2\ V^{-1}\ s^{-1}$.[98–100,104–106] However, it was found that the IBDF-based polymers required giant substituents such as 4-octadecyldocosyl (containing 40 carbon atoms) to render polymers soluble in commonly used solvents such as chloroform and chlorobenzene and precursors to such large substituents are not readily available.[98,99] This has greatly made the study of IBDF-based polymers very difficult. Herein we designed and synthesized a novel acceptor building block, namely (3*E*,7*E*)-3,7-bis(2-oxoindolin-3-ylidene)-5,7-dihydropyrrolo[2,3-*f*]indole-2,6(1*H*,3*H*)-dione (IBDP, Figure 2-1), which is a structural analogue to IBDF, where the lactones in the IBDF core are replaced with lactams

in the IBDP core. The newly designed IBDP core allows for substitution at four nitrogen atoms, potentially enabling solubilisation of the IBDP-based polymers with more easily accessible shorter substituents. We synthesized an the brominated IBDP monomer (compound **7** in Scheme 1) with readily available dodecyl and 2-decyltetradecyl substituents and used this IBDP unit as an acceptor and bithiophene or (*E*)-1,2-di(thiophen-2-yl)ethane as a donor to form two D-A polymers (**P1** and **P2** in Scheme 1). The two polymers will be first characterized by UV-Vis-IR absorption spectroscopy, cyclic voltammetry and used for BGBC OTFTs. Besides, the structure-property relationship will be investigated using AFM and XRD. Finally the two polymers will be used as acceptor in all-PSCs with **P3HT** as donor material and preliminary results will be presented.

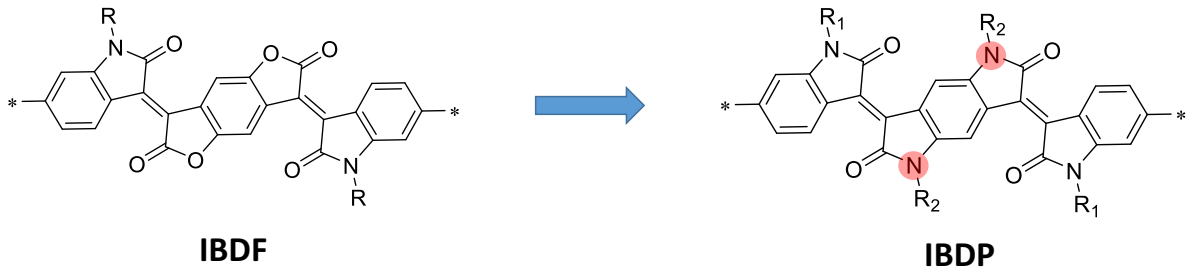

Figure 2-1 The chemical structures of IBDF and IBDP.

2.2 Results and Discussion

We started our study by conducting computational simulations on two model compounds: IBDF-Me and IBDP-Me (Figure 2-2), whose substituents are methyl groups for simplifying the calculation. The simulation results showed that IBDP-Me has a very small dihedral angle (~10°) between an indolin-2-

one unit and the pyrroloindoledione core, which is comparable to that of IBDF-Me (~8°). This indicates that IBDP has very similar coplanarity with IBDF.

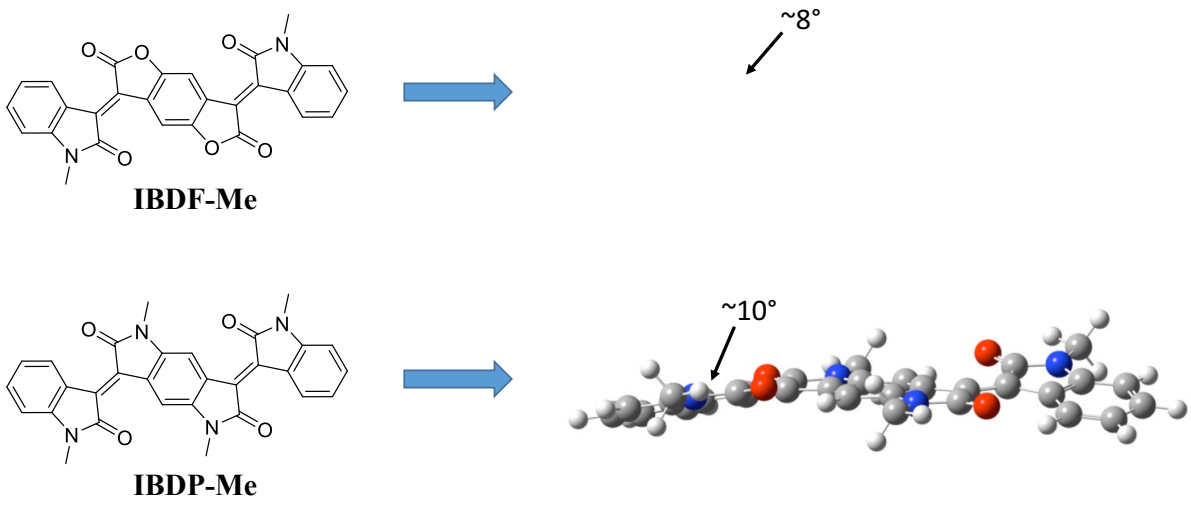

Figure 2-2 The chemical structures and optimized geometry of IBDF-Me and IBDP-Me.

The synthesis of the brominated IBDP monomer (**7**) could potentially obtained via the Aldol condensation of the corresponding isatin and pyrroloindoledione (Route 1 in Figure 2-3), or the oxindole and pyrroloindoletetraone (Route 2 in Figure 2-3). At first, we attempted to synthesize **7** via Route 1 and found the condensation did not yield **7** in neither acidic conditions nor basic conditions. We suspected one of the intermediates (Figure 2-3) of this reaction was very unstable, which might have failed the reaction. Therefore, we turned to Route 2, whose details are given in Scheme 2-1. First, *p*-phenylenediamine was *N,N'*-dialkylated with dodecyl bromide in ethanol to form **1**, which was used to prepare **4** following a similar synthetic route reported previously.[107] The synthesis of compound **6** was usually done by heating the isatin in hydrazine. In our case, however, such treatment only yielded the intermediate hydrazone. This was believed to be caused by the steric effect induced by the bulky

side chains since a similar isatin with a larger spacer group between isatin and alkyl branches was converted into oxindole in hydrazine.[108] Inspired by a two-step reduction reported in literature[109], we first chlorinated 6-bromo-1-(2-decyltetradecyl)indoline-2,3-dione with PCl_5 to give the intermediate **5**, which was then reduced with zinc to form **6**. Aldol condensation of **4** with two equivalents of **6** in refluxing acetic acid in the presence of a catalytic amount of HCl afforded monomer **7**. Two IBDP-based polymers **P1** and **P2** were synthesized via the Stille coupling polymerization of **6** with 5,5'-bis(trimethylstannyl)-2,2'-bithiophene and (*E*)-1,2-bis(5-(trimethylstannyl)thiophen-2-yl)ethene, respectively. The crude polymers were purified by Soxhlet extraction successively using acetone and hexanes to remove the oligomers and other impurities. Finally, the polymers were dissolved in chloroform to afford **P1** and **P2** in yields of 82% and 98%, respectively. Both polymers have very good solubility (>10 mg/mL) in several common solvents such as toluene, chloroform, chlorobenzene, and 1,2-dichlorobenzene at room temperature. The molecular weights of these polymers were measured by gel-permeation chromatography (GPC) at 140°C with 1,2,4-trichlorobenzene as eluent and polystyrene as standards. The number average molecular weight (M_n) and the polydispersity index (PDI) were determined to be 78 kDa and 2.1 for **P1** and 89 kDa and 1.6 for **P2** (Figure 2-4). The thermal stability of the polymers was characterized by thermogravimetric analysis (TGA). A 5% weight loss was observed at 384 °C for **P1** and 380 °C for **P2** (Figure 2-5), indicating good thermal stability of both polymers.

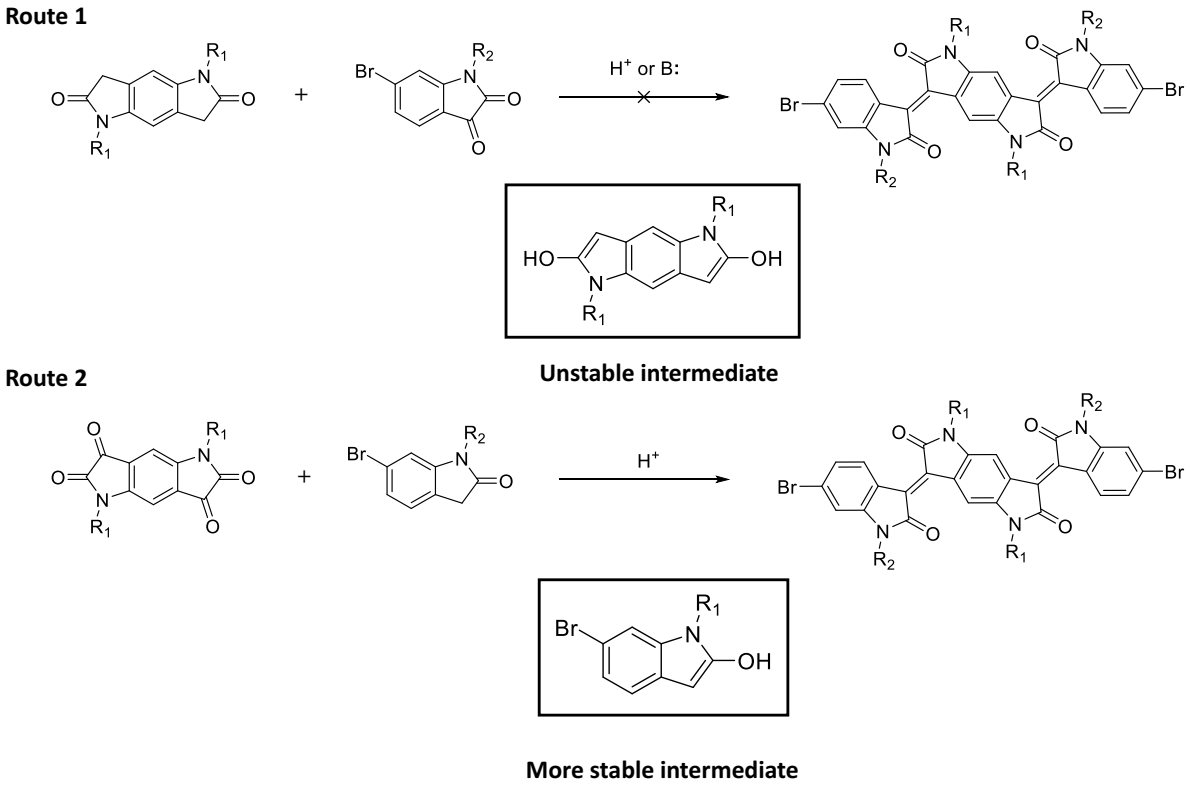

Figure 2-3 Two synthetic routes towards the brominated IBDP monomer.

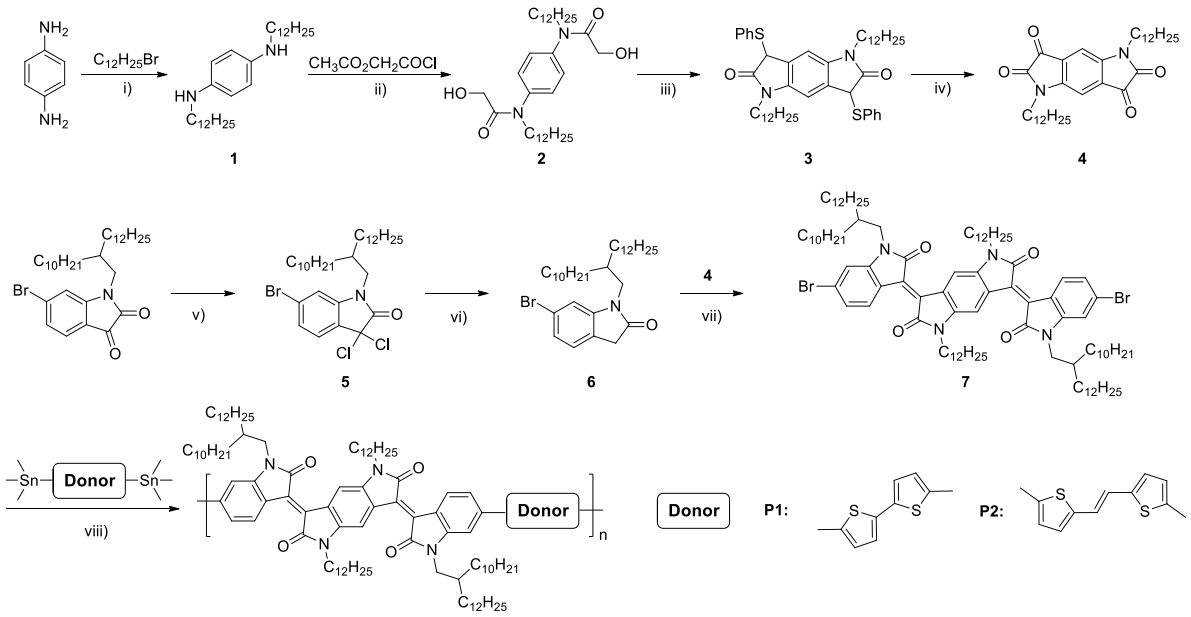

Scheme 2-1 Synthetic route towards the brominated IBDP monomer and IBDP-based polymers. Reaction conditions: i) Ethanol/reflux, 26%; ii) CH_2Cl_2/Et_3N/0 °C to r.t., THF/MeOH/H_2O/K_2CO_3/r.t., 43%; iii) CH_2Cl_2/oxalyl chloride/DMSO/Et_3N/-78 °C to r.t., CH_2Cl_2/thiophenol/TFAA/BF_3 • Et_2O/r.t., 28%; iv) THF/H_2O/ammonium cerium nitrate/r.t., 51%; v) Toluene/PCl_5/r.t.; vi) AcOH/Zn/r.t., 95%; vii) AcOH/HCl/reflux, 78%; viii) Chlorobenzene/P(*o*-tolyl)$_3$/Pd_2(dba)$_3$/120 °C, 82% for **P1** and 98% for **P2**.

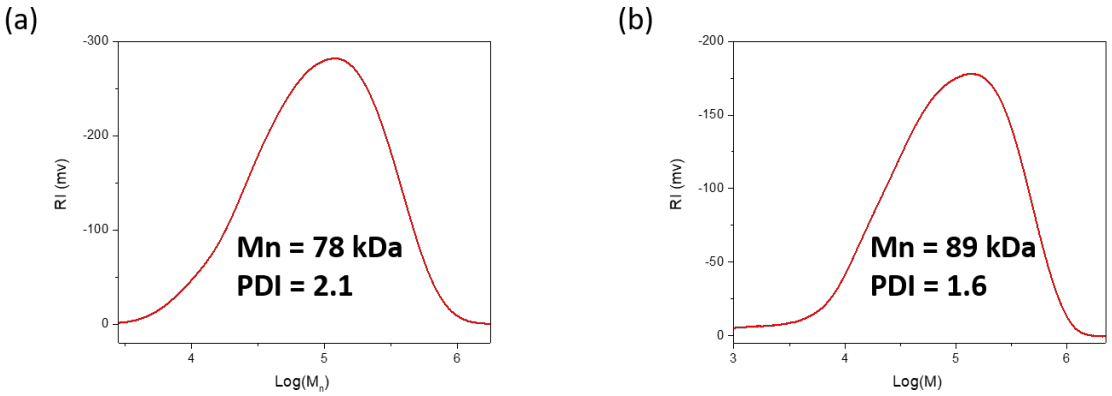

Figure 2-4 The molecular weight distribution for **P1** (a) and **P2** (b) obtained by HT-GPC.

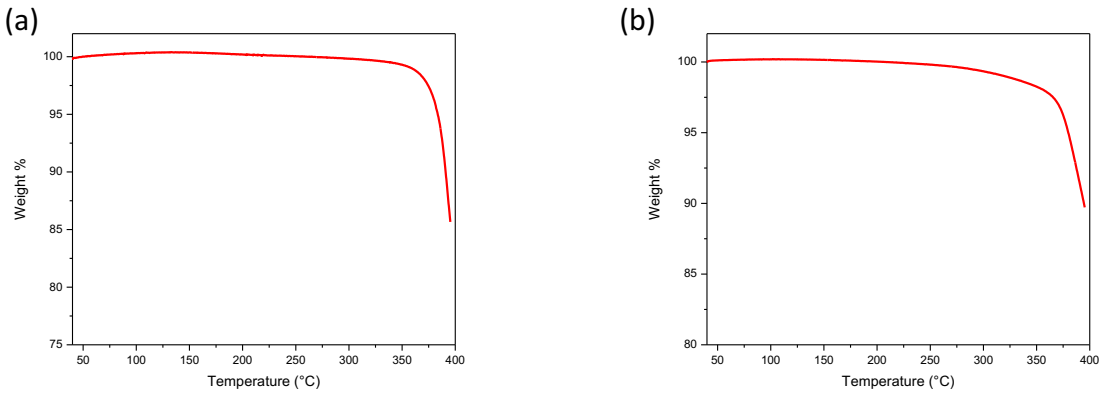

Figure 2-5 The TGA diagrams for **P1** (a) and **P2** (b) obtained in nitrogen.

The UV-Vis-IR absorption spectra of the polymers in solution and in thin film are shown in Figure 2-6. Both polymers exhibited typical dual band absorption, wherein the low energy band can be attributed to the internal charge transfer (ICT) transition and the high-energy band is the π-π* transition of IBDP moieties. In solution, the maximum absorption wavelengths (λ_{max}) are 699 nm for **P1** and 711 nm for **P2**. The λ_{max} of the **P1** film remained at 699 nm, but a prominent shoulder at 822 nm appeared, indicating the more extended conjugation of the polymer chains in the solid state. Interestingly, **P2** showed a blue-shift in absorption from solution (711 nm) to the film (698 nm), which is an indicatiion of the dominance of H-aggregate.[110] The adsorption coefficients of the peak for film absorption were determined to be 1.3×10^6 cm^{-1} and 1.1×10^6 cm^{-1} for **P1** and **P2** respectively, which are an order higher than the common donor materials that are being used for OSCs. For example, the adsorption coefficient for **PTB7-Th** is only on the order of 10^5 cm^{-1}.[52,53] The optical band gaps of the polymer films are calculated to be 1.23 eV for **P1** and 1.22 eV for **P2** using the absorption onsets. As shown in Figure 2-6, both polymer shown extended absorption into the NIR region up to 1100 nm. This is probably due

to the nitrogen donating effect that raised the HOMO levels of the polymers. Cyclic voltammetry (CV) was used to reveal electrochemical property of the polymers (Figure 2-7). By using the oxidative onset potentials, HOMO levels were calculated to be -5.60 eV and -5.39 eV for **P1** and **P2**, respectively. LUMO levels were calculated from the reduction onset potentials to be -3.71 eV and -3.70 eV for **P1** and **P2**, respectively. The LUMO levels are raised compared to the IBDF analogues by 0.1-0.2 eV.[111,112] Based on these HOMO/LUMO levels, **P1** and **P2** are suitable materials for ambipolar charge transport in OTFTs and potentially can be both the donor and acceptor materials in OSCs provided the compatible counterpart.

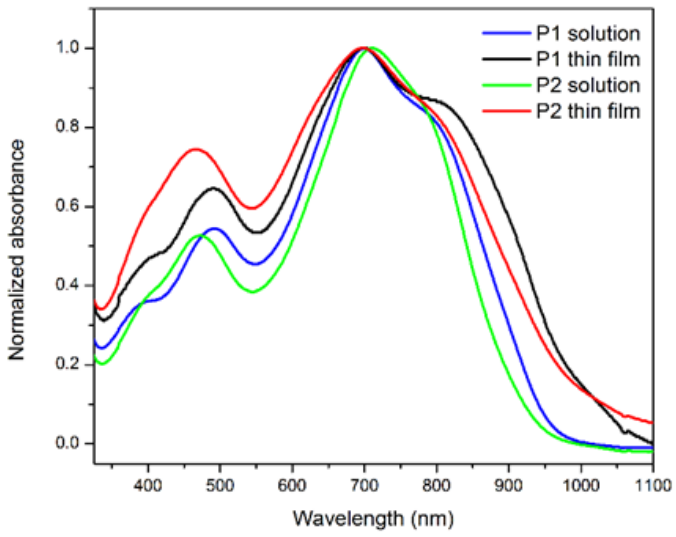

Figure 2-6 The UV-Vis-IR absorption spectra in solution (chloroform) and in thin film.

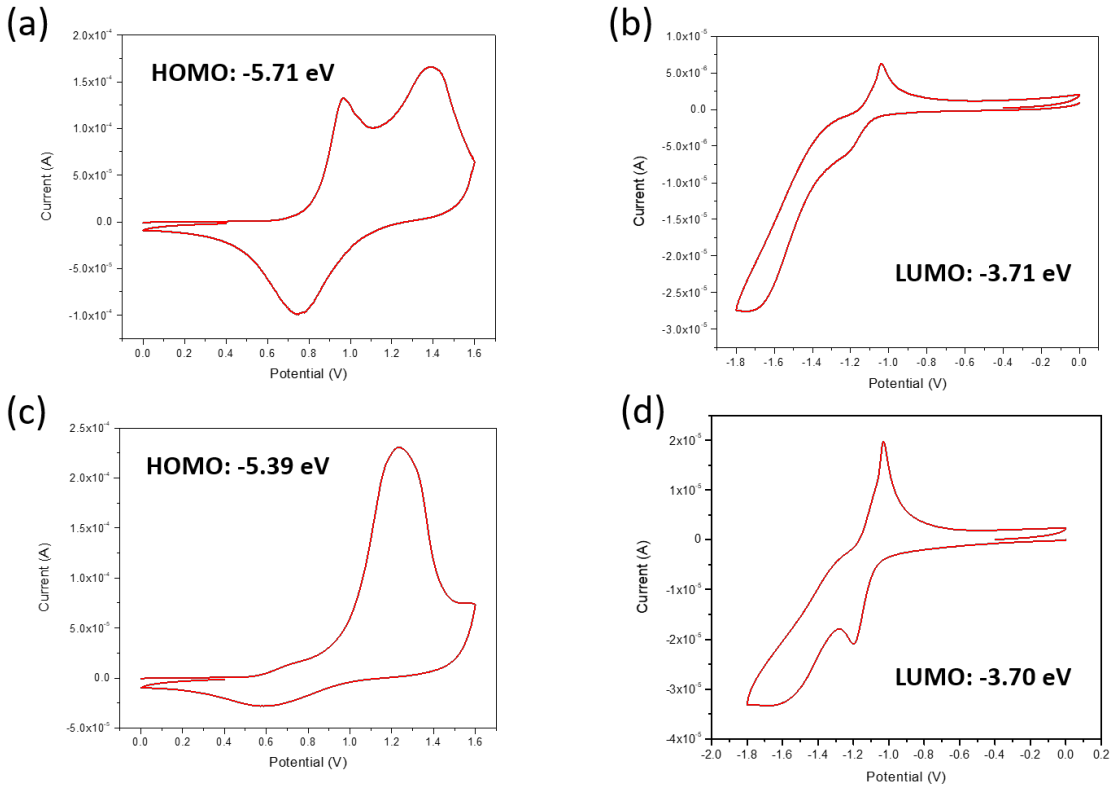

Figure 2-7 The cyclic voltammetry diagrams for **P1** (a and b) and **P2** (c and d) at a scan rate of 0.1 V/s. A scan rate of 0.05 V/s was also tried for these polymers. However, it had no impact on the onset potentials.

P1 and **P2** were evaluated as channel semiconductors in bottom-gate, bottom-contact OTFT devices fabricated on dodecyltrichlorosilane (DDTS) modified SiO_2/Si wafer substrates. Both polymers showed p-type dominant ambipolar charge transport behaviour (Table 2-1). For devices based on **P1**, the best performance with hole mobility of 0.19 $cm^2\ V^{-1}\ s^{-1}$ and electron mobility of 0.088 $cm^2\ V^{-1}\ s^{-1}$ was achieved for the 150 °C-annealed films (Figure 2-8). Annealing at a higher temperature of 200 °C led to a slight increase in the electron mobility (up to 0.089 $cm^2\ V^{-1}\ s^{-1}$), but a significant drop in the hole

mobility (0.057 cm^2 V^{-1} s^{-1}). For devices based on **P2**, the best overall performance with hole/electron mobilities of 0.10 cm^2 V^{-1} s^{-1}/ 0.075 cm^2 V^{-1} s^{-1} was obtained for the 200 °C-annealed polymer films (Figure 2-8). Annealing at a higher temperature of 250 °C did not further improve the device performance. The decent charge transport properties of these two polymers and their considerable absorption in the NIR region may enable the NIR detection application for **P1** and **P2**, which is limited by the lack of suitable materials that can response to NIR signals.[113–117]

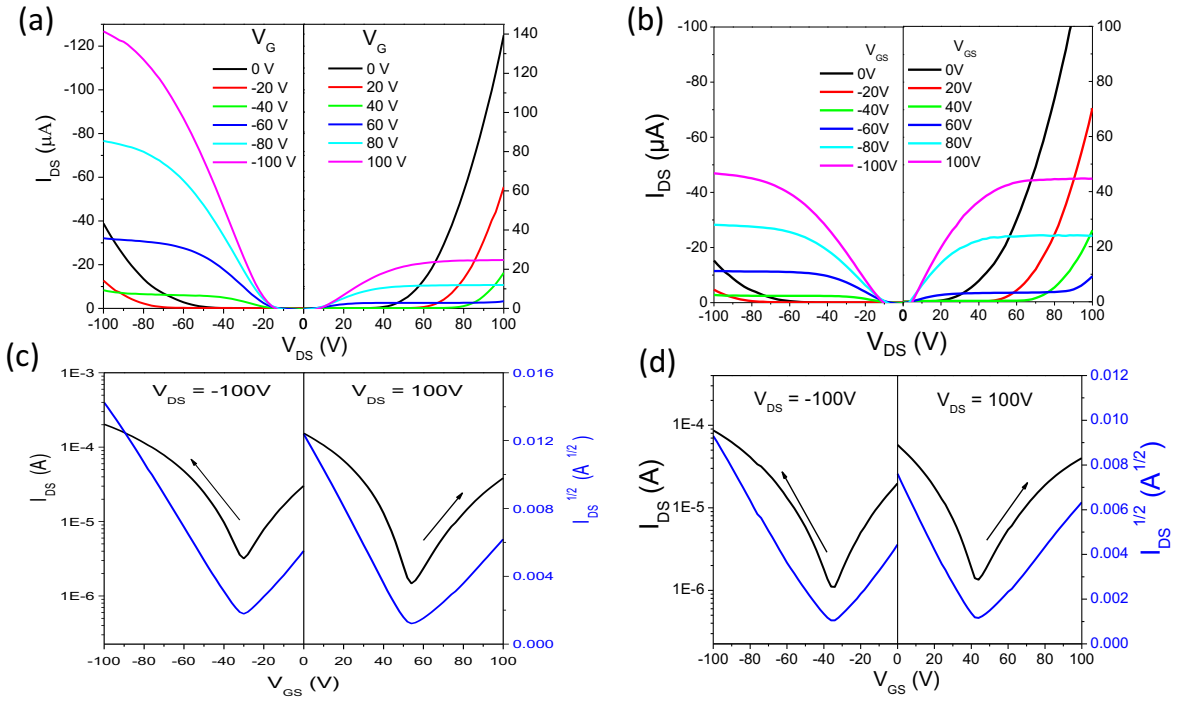

Figure 2-8 The output curves for OTFTs based on **P1** (a) and **P2** (b), and transfer curves for OTFTs based on **P1** (c) and **P2** (d). Device dimensions: channel length (L) = 30 μm; channel width (W) = 1000 μm.

Table 2-1 The summary of BGBC OTFT performance of **P1** and **P2**.

Polymer	Annealing temperature (°C)	Hole mobility[a] ($cm^2 V^{-1} s^{-1}$)	Electron mobility[a] ($cm^2 V^{-1} s^{-1}$)
P1	100	0.15 ± 0.02 (0.17)	0.063 ± 0.007 (0.071)
	150	0.16 ± 0.03 (0.19)	0.064 ± 0.017 (0.088)
	200	0.040 ± 0.014 (0.057)	0.073 ± 0.013 (0.089)
P2	100	0.055 ± 0.010 (0.062)	0.023 ± 0.003 (0.027)
	150	0.081 ± 0.012 (0.093)	0.037 ± 0.008 (0.045)
	200	0.10 ± 0.02 (0.10)	0.055 ± 0.016 (0.075)
	250	0.091 ± 0.020 (0.11)	0.055 ± 0.015 (0.067)

[a] The average mobility ± standard deviation (maximum mobility) calculated from the saturation regions of five devices.

We noticed that **P1** and **P2** showed lower charge transport performance than some of the IBDF based polymers.[99,100] One possible reason for their lower mobility is that an optimal side chain combination is not reached in these polymers. **P1** and **P2** showed greatly improved solubility due to the presence of four large side chains on IBDP. However, the excessively strong side chain interaction in the solid state might hinder the π-π stacking of the polymer main chains. Transmission X-ray diffraction (XRD) measurement was used to investigate the packing of polymer flakes of both polymers. **P1** and **P2** showed intense primary diffraction peaks at 2θ = 3.26° and 3.51°, which correspond to the interlayer lamellar *d*-spacing of 2.71 nm and 2.52 nm, respectively. The weak diffraction peak at 2θ = 25.04° for **P1** is originated from the π- π stacking distance of polymer chains, which was calculated to be 0.355 nm. No noticeable π- π stacking peak was observed for **P2**. The presence of four long side chains on IBDP might hinder the π-π stacking and lead to the lower carrier mobility of these IBDP polymers

compared to the IBDF polymers as discussed previously. The very weak diffraction peaks corresponding to the π-π stacking distances for both polymers might substantiate this side chain interference. Using shorter side chains may help strengthen the π-π interaction.[99,118] Furthermore, most of the high mobility IBDF polymers reported so far bear the 4-octadecyldocosyl side chain, which has a farther distance from the polymer backbone compared to the 2-decyltetradecyl side chain in **P1** and **P2**. The branching point of branched side chains was reported to have a great impact on the ordering of the polymer chains and the carrier mobility.[104,118,119] The use of branched side chains with a larger spacer between the branching point and the backbone such as 4-decylhexadecyl or four straight alkyl side chains on IBDP may lead to better charge transport performance. Following this work, Cao et al. used 4-decyltetradecyl as the side chain on IBDP and improved the mobility significantly.[108] The surface morphology of **P1** and **P2** thin films spin-coated on dodecyltrichlorosilane (DDTS) modified SiO_2/Si wafer substrates was examined by atomic force microscopy (Figure 18). **P1** thin films showed fibre-like domains, which grew slightly as the annealing temperature increased from 100 °C to 150 °C and remained similar at an annealing temperature of 200 °C. In general, **P2** thin films showed poorly defined domains compared to **P1** films, indicative of the less ordered chain packing of **P2**.

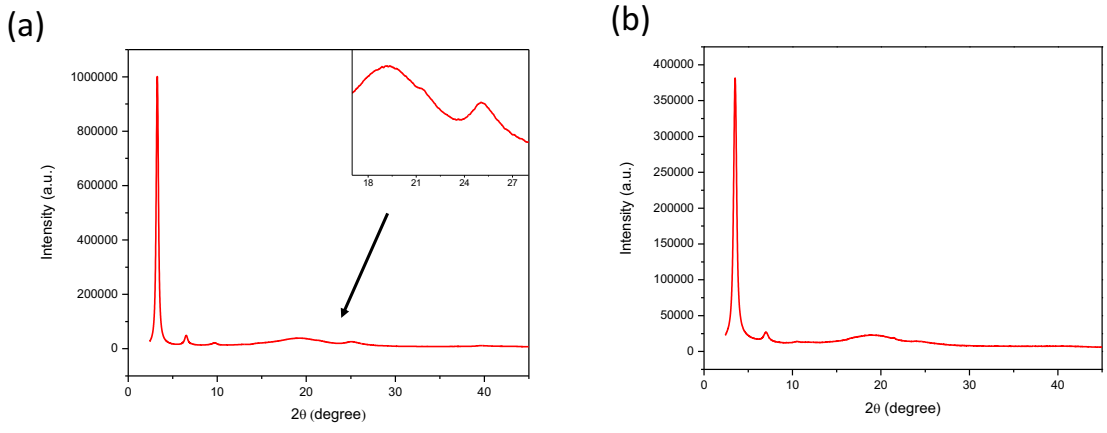

Figure 2-9 The transmission XRD patterns of **P1** flake (a) and **P2** flake (b).

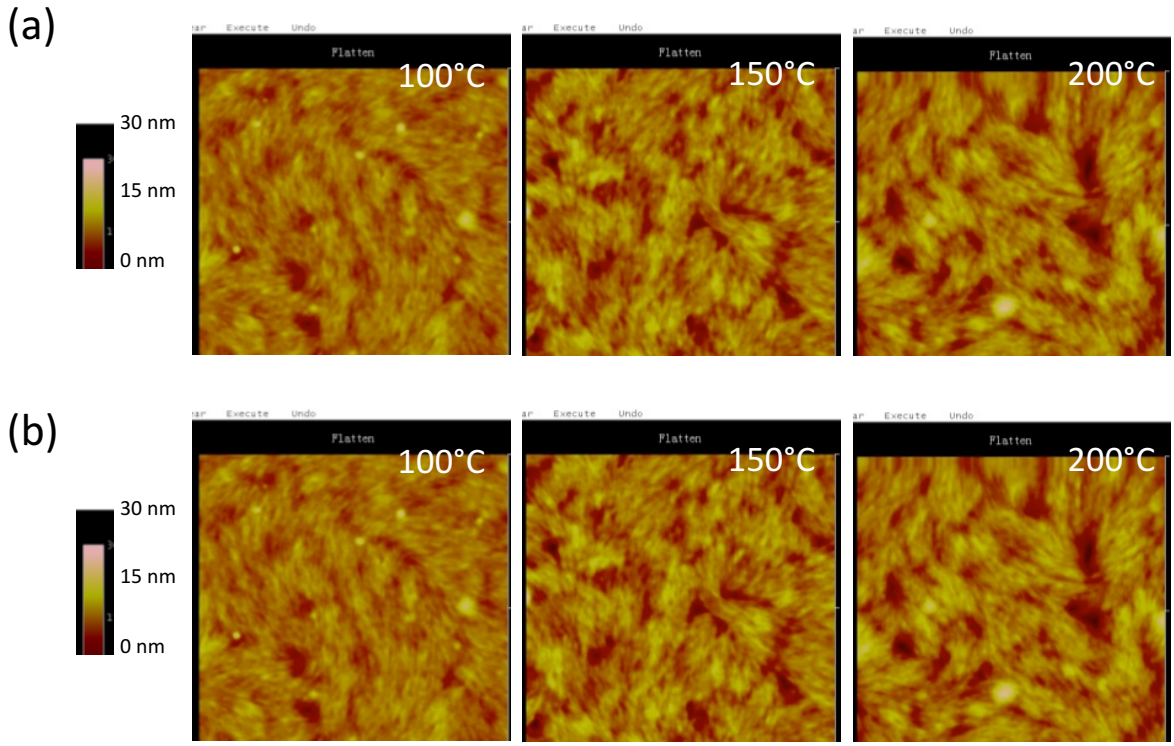

Figure 2-10 AFM height images (2μm × 2μm each) of **P1** (a) and **P2** (b) thin films on SiO_2/Si substrates annealed at different temperatures.

Given the absorption spectra and HOMO/LUMO levels of **P1** and **P2**, we chose the commercial regioregular **P3HT** as the donor material for the fabrication all-PSCs. The HOMO/LUMO offsets between **P3HT** and **P1** polymers are around 0.5 eV (Figure 2-11), which are very sufficient for exciton disassociation. Moreover, the IBDP polymers can provide considerable complementary absorption in the visible and NIR region (Figure 2-11), which has been a huge limitation for the **P3HT:PCBM** solar cells. A standard device configuration: ITO/PEDOT:PSS/**P3HT**:PA/LiF/Al was used to fabrication the all-PSCs. The J-V characteristics of both **P1** and **P2** are shown in Figure 2-12. As preliminary results,

the devices based on **P1** achieved quite high PCEs up to 2.56% while the device based on **P2** achieved the best PCE at 2.14%. As preliminary optimization, we tuned the D/A ratio for **P1:P3HT** to improve the device performance. As shown in Figure 2-13 and Table 2-3, the optimal D/A ratio was determined to be 1:1.5, where the best PCE of 3.38% was realized. To our best knowledge, this is the highest PCE that has been obtained from P3HT-based all-PSCs by far.[120–122] EQE spectrum for the same cell was shown in Figure 2-13. Owing to the complementary absorption of these two polymers to each other, the spectrum showed full coverage over the visible region as well as part of the NIR region (up to 1000 nm). However, the EQE is much lower those of the **P3HT:PCBM** cells (up to 60%)[48] and NDI polymer based all-PSCs (usually 45% to 55%)[66,97], indicating blend morphology is probably suboptimal. The calculated J_{SC} from the EQE spectrum is 8.2 mA/cm^2, which is within 5% error of the measured value.

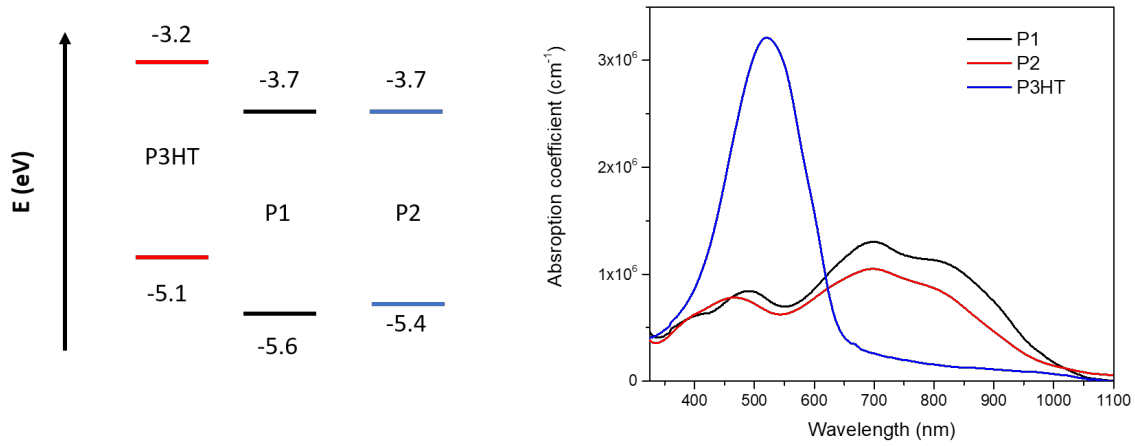

Figure 2-11 The comparison of the HOMO/LUMOs of **P3HT**, **P1** and **P2** as well as their absorption coefficients.

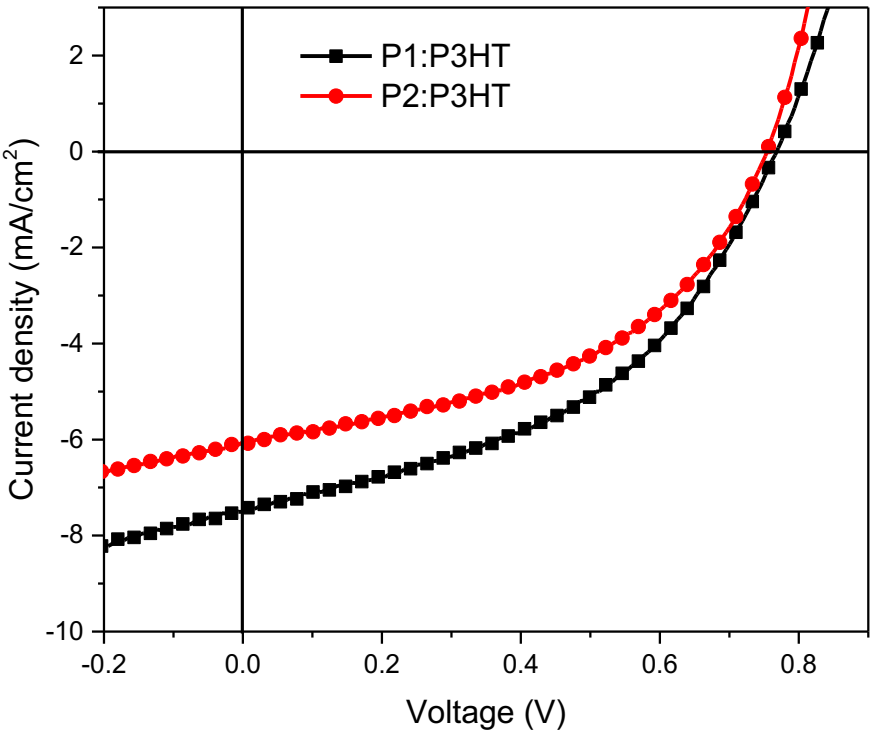

Figure 2-12 The J-V characteristics of the devices based on **P1** and **P2** under AM 1.5G illumination. The blend film (1:1 wt ratio) was spin-coated at 2000 rpm using a solution (12.5 mg/mL) in CF.

Table 2-2 The summary of the all-PSC device performance for **P1** and **P2**.

Acceptor	J_{SC} (mA/cm^2)	V_{OC} (V)	FF	PCE (%)
P1	7.47	0.77	0.44	2.56 (2.32)
P2	6.04	0.76	0.46	2.14 (1.95)

All devices used **P3HT** as the donor and the same device configuration: ITO/PEDOT:PSS/Polymer blend/LiF/Al. The active layer thickness is around 130 nm. The numbers in the parenthesis are average values for 4 devices on the same substrate.

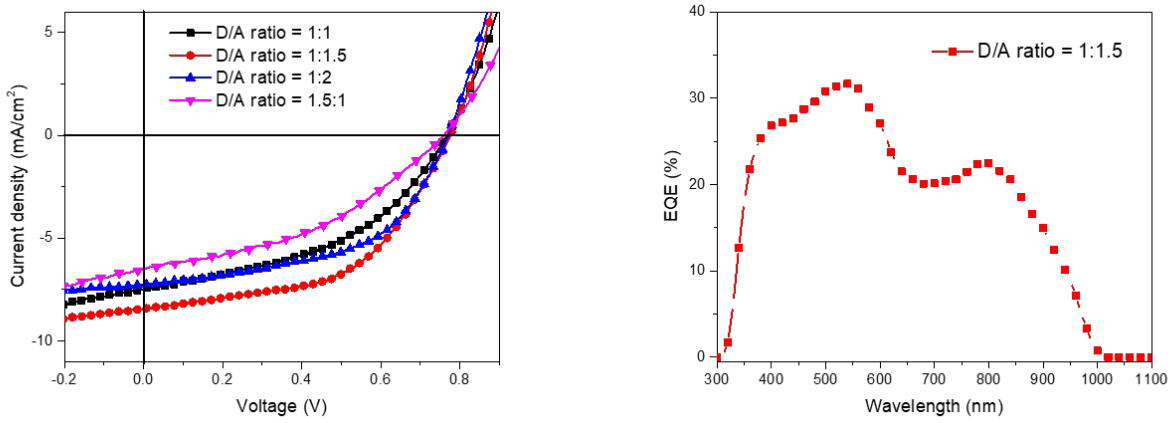

Figure 2-13 The J-V characteristics of the devices based on **P1**:**P3HT** with different weight ratio under AM 1.5G illumination and the EQE spectrum of the cell with 1:1.5 D/A ratio that showed the best PCE.

Table 2-3 The D/A optimization of the **P1:P3HT** blend in all-PSC devices

D/A ratio	J_{SC} (mA/cm^2)	V_{OC} (V)	FF	PCE (%)
1:1	7.47	0.77	0.44	2.56 (2.32)
1:1.5	8.43	0.77	0.52	3.38 (3.08)
1:2	7.26	0.77	0.52	2.93 (2.70)
1.5:1	5.90	0.76	0.41	1.82 (1.55)

All devices used **P3HT** as the donor and the same device configuration: ITO/PEDOT:PSS/Polymer blend/LiF/Al. The active layers were spin-coated under the same conditions (2000 rpm and 12.5 mg/mL). The numbers in the parenthesis are average values for 4 devices on the same substrate.

Table 2-4 The comparison of different polymer acceptor in all-PSCs using with P3HT as the donor.

Blend	J_{SC} (mA/cm^2)	V_{OC} (V)	FF	PCE (%)
PIBDPBT:P3HT[a]	8.43	0.77	0.52	**3.38 (3.08)**
N2200:P3HT[b]	3.77	0.56	0.65	1.4
PDPP2TzT:P3HT	7.8	0.65	0.61	3.0

[a,b]Data is from the references.[122,123]

2.3 Summary and Future Direction

In conclusion, a novel electron deficient building block, IBDP, is designed, synthesized, and incorporated into D–A polymers. With lactam groups replacing the lactone groups, IBDP gets two extra side chains to yield good solution processability, which is requisite for the fabrication of OSCs. On the other hand, the donating effect of lactam groups has raised the LUMO levels of **P1** and **P2** to ~-3.7 eV from -4.0 eV of those IBDF-based polymers. With a raised LUMO level, the electron injection barrier now is higher and electron transport will become less favourable.[124,125] Therefore IBDP-based polymers exhibited balanced ambipolar semiconductor performance in OTFTs with high electron (up to 0.10 cm^2 V^{-1} s^{-1}) and hole (up to 0.19 cm^2 V^{-1} s^{-1}) mobility. Both polymers showed enhanced absorption with absorption coefficient as high as 1.3×10^6 cm^{-1} and a broad absorption up to 1100 nm according to the UV-Vis-NIR absorption spectra. The high absorption coefficient and broad absorption range in Visible and NIR region are extremely desired for OSC application. On the other hand, the relatively deep HOMO levels and high LUMO levels would also help to increase the V_{OC} of the resultant solar cells. Given these features, these two IBDP-based polymers were used as acceptor for all-PSCs in combination with regioregular **P3HT** as donor, which has suitable HOMO/LUMO levels. Initially all-PSC device based on **P1** exhibited better PCEs up to 2.56% than 2.14% from the cell based on **P2**. We furthered our study by optimizing the D/A ratio of **P1**:**P3HT**. A PCE of 3.38% was obtained from the cell with a D/A ratio of 1:1.5, which is the highest value that has been obtained from **P3HT**-based all-PSCs. The EQE spectrum of the same cell showed a full coverage over the Vis-NIR region (up to 1000 nm) due to the complementary absorption. Further study is limited by the available amount of materials. For future direction, the synthesis of the IBDP monomers need to be optimized to achieve

higher yield and cleaner chemistry (thiophenol was used in the synthesis). Second of all, the extended absorption into NIR may enable the photo-detection applications such as phototransistor in NIR region, which has been rarely explored and believed to be a useful technology in various fields.[126–128] What is more, these IBDP polymers can be also used in ternary organic solar cells, which is also a new direction for the development of OSCs. In a nutshell, the preliminary results demonstrated that IBDP is a promising electron acceptor building block for constructing ambipolar type of polymer semiconductors, which can bring strong and broad absorption in OSC applications.

2.4 Experimental

2.4.1 Materials and Characterization

All chemicals were purchased from commercial sources and used without further purification unless specified. 6-Bromo-1-(2-decyltetradecyl)indoline-2,3-dione[98] and (*E*)-1,2-bis(5-(trimethylstannyl)thiophen-2-yl)ethene[129] were synthesized according to the literature. Computational simulations were performed using density function theory (DFT) calculation with the 6-311G+(d,p) basis set and all the orbital pictures were obtained using GaussView 5.0 software. GPC measurements were performed on a Waters SEC system using 1,2,4-trichlorobezene as eluent and polystyrene as standards at 140°C. TGA measurements were carried out on a TA Instruments SDT 2960 at a scan rate of 10°C min^{-1} under nitrogen. The UV-Vis-IR absorption spectra of polymers were recorded on a Thermo Scientific model GENESYS™ 10S VIS spectrophotometer. Cyclic voltammetry (CV) data were obtained on a CHI600E electrochemical analyser using an Ag/AgCl reference electrode and two Pt disk electrodes as the working and counter electrodes in a 0.1 M tetrabutylammonium

hexafluorophosphate solution in acetonitrile at a scan rate of 100 mV s^{-1}. Ferrocene was used as the reference, which has a HOMO energy value of -4.8 eV.[130] NMR data was recorded with a Bruker DPX 300 MHz spectrometer with chemical shifts relative to tetramethylsilane (TMS, 0 ppm). Transmission XRD measurements were carried out on a Bruker Smart 6000 CCD 3-circle D8 diffractometer with a Cu RA (Rigaku) X-ray source (λ = 0.15406 nm) and the polymer flakes stacked between two Mylar substrates. Atomic force microscopy (AFM) images were taken on polymer thin films spin-coated on the DDTS-modified SiO_2/Si substrates with a Dimension 3100 scanning probe microscope.

2.4.2 Fabrication and Characterization of OTFT devices

The bottom-contact, bottom-gate configuration was used for all OTFT devices. The preparation procedure of the substrate and device is as follows. A heavily n-doped SiO_2/Si wafer with ~300 nm-thick SiO_2 was patterned with gold source and drain pairs by conventional photolithography and thermal deposition. Then the substrate was treated with air plasma, followed by cleaning with acetone and isopropanol in an ultra-sonic bath. Subsequently, the substrate was placed in a solution of DDTS in toluene (3 % in toluene) at room temperature for 20 min. the substrate was washed with toluene and dried under a nitrogen flow. Then a polymer solution in chloroform (5 mg mL^{-1}) was spin-coated onto the substrate at 3000 rpm for 60s to give a polymer film (~40 nm), which was further subject to thermal annealing at different temperatures for 20 min in a glove box. All the OTFT devices have a channel length (L) of 30 μm and a channel width (W) of 1000 μm, and were characterized in the same glove box using an Agilent B2912A Semiconductor Analyser.

2.4.3 Fabrication and Characterization of all-PSC devices

All all-PSC devices were fabricated using the conventional configuration ITO/PEDOT:PSS/**PTB7-Th**:PA/LiF/Al. ITO glass substrates were sonicated in water, acetone and IPA. Then the substrates were treated with plasma cleaning. A thin layer of PEDOT:PSS (Al 4083) was deposited through spin-coating at 4000 rpm and dried subsequently at 150 °C for 20 min in air. Then the substrates were transferred to a nitrogen glove box, where the polymer blend layer (~140 nm) was spin-coated onto the PEDOT:PSS layer. The active layer was formed using a chloroform solution of **P3HT**:PA (1:1). Finally, a thin layer of LiF (1 nm) and a layer of Al (100 nm) electrode were deposited in vacuum onto the substrate at P $\approx 5.0 \times 10^{-6}$ Pa. The active area is 0.07 cm^2. The current density–voltage (J – V) characteristics of the all-PSCs were measured on an Agilent B2912A Semiconductor Analyser with a ScienceTech SLB300-A Solar Simulator. A 450 W xenon lamp and an air mass (AM) 1.5 filter were used as the light source.

2.4.4 Synthetic Procedures

Synthesis of *N*,*N*'-didodecylbenzene-1,4-diamine (1)

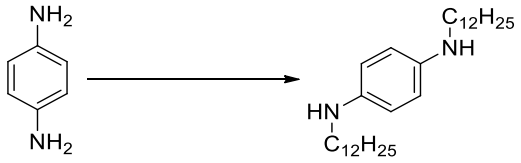

1

To a solution of *p*-phenylenediamine (4.33 g, 40.0 mmol) in ethanol (120 mL), 1-bromododecane (19.94 g, 80.0 mmol) was added. The reaction mixture was stirred under reflux for 24 h. Upon cooling

to room temperature, the reaction mixture was filtered. The filter cake was washed with ethanol and then dried in vacuo to give **1**. Yield: 4.45 g (25%). Compound **1** was used immediately for the next step without further purification due to its very poor stability in air. ^{1}H-NMR (300 MHz, DMSO-d_6) δ 6.90 (s, 4H), 3.07 (t, J = 7.0 Hz, 4H), 1.60 – 1.48 (m, 4H), 1.24 (br, 36H), 0.85 (t, J = 6.4 Hz, 6H).

Synthesis of *N*,*N*'-(1,4-phenylene)bis(N-dodecyl-2-hydroxyacetamide) (2)

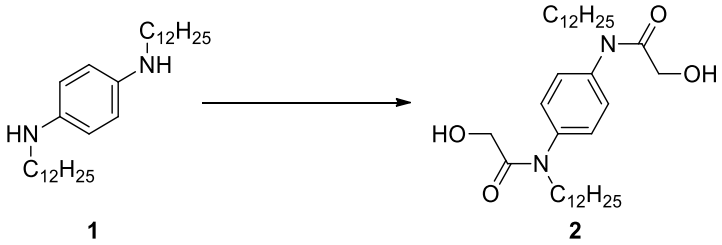

1 **2**

To a solution of **1** (4.45 g, 10.0 mmol) and triethylamine (5.2 mL) in CH_2Cl_2 (50 mL), acetoxyacetyl chloride (2.4 mL, 22.3 mmol) was added dropwise at 0°C. Then the reaction mixture was allowed to warm to room temperature and stirred for 15 h. Then the reaction was quenched with saturated $NaHCO_3$ aqueous solution. The organic phase was further washed with brine twice and dried over anhydrous Na_2SO_4. Upon removal of solvent in vacuo, the intermediate acetoxy amide was dissolved in a mixture solvent of THF (50 mL), methanol (45 mL), and water (5 mL) before K_2CO_3 (13.8 g, 100 mmol) was added. The reaction mixture was stirred at room temperature for 24 h. The solid was then filtered off and washed with CH_2Cl_2. The combined filtrate was washed with brine, dried over Na_2SO_4 and concentrated in vacuo to give the crude product, which was further purified by silica gel column chromatography with hexane : ethyl acetate (1:1) to give **2**. Yield: 3.04 g (54%). ^{1}H-NMR (300 MHz,

DMSO-d_6) δ 7.36 (s, 4H), 4.58 (t, J = 5.7 Hz, 2H), 3.71 (s, 4H), 3.63 (t, J = 7.0 Hz, 4H), 1.45 – 1.30 (m, 4H), 1.21 – 1.19 (m, 36H), 0.85 (t, J = 6.4 Hz, 6H). ^{13}C-NMR (75 MHz, $CDCl_3$) δ 171.35, 140.12, 129.83, 60.57, 49.77, 31.89, 29.60, 29.54, 29.32, 27.72, 26.69, 22.67, 14.11. HR-ESI-MS $(M + H)^+$ calc. for $C_{34}H_{61}N_2O_4^+$: 561.4631; found: 561.4611.

Synthesis of 1,5-didodecyl-3,7-bis(phenylthio)-5,7-dihydropyrrolo[2,3-*f*]indole-2,6(1*H*,3*H*)-dione (3)

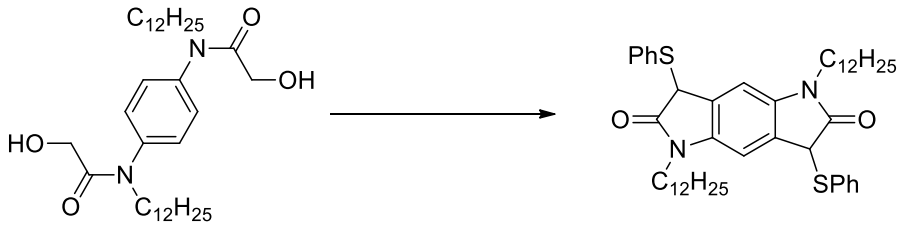

2 **3**

To a solution of oxalyl chloride (0.85 mL, 9.80 mmol) in CH_2Cl_2 (30 mL) at -78°C, was added dimethyl sulfoxide (DMSO) (1.3 mL, 18.3 mmol) in CH_2Cl_2 (10 mL) dropwise. After stirring for 30 min, a solution of **2** (2.50 g, 4.46 mmol) in CH_2Cl_2 (10 mL) was added dropwise. The reaction mixture was stirred for another hour, and then triethylamine (6.0 mL, 43.0 mmol) was added and the solution was allowed to warm to room temperature. After stirring for another 1.5 h, CH_2Cl_2 (100 mL) and saturated $NaHCO_3$ aqueous solution (150 mL) were added. The organic phase was separated and washed with saturated $NaHCO_3$ aqueous solution twice and dried over anhydrous Na_2SO_4. Upon removal of solvent, the crude intermediate was used immediately without further purification. To a solution of the crude intermediate in CH_2Cl_2 (50 mL), thiophenol (0.91 mL, 8.92 mmol) was added. After stirring at room temperature for 15 h, trifluoroacetic acid (TFAA) (5.7 mL, 40.2 mmol) was added. After stirring for

another hour, $BF_3 \bullet Et_2O$ (2.8 mL, 22.0 mmol) was added. The reaction mixture was stirred for another 6 h and quenched by saturated $NaHCO_3$ aqueous solution cautiously. The organic phase was separated and washed with saturated $NaHCO_3$ aqueous solution three times and dried over anhydrous Na_2SO_4. Removing solvent in vacuo gave the crude product **3**, which was used for the next step without further purification. Yield: 0.89 g (28%). ^{1}H-NMR (300 MHz, $CDCl_3$) δ 7.35 – 7.17 (m, 10H), 6.68 (s, 2H), 4.55 – 4.51 (m, 2H), 3.73 – 3.37 (m, 4H), 1.35 – 1.26 (br, 40H), 0.87 (t, J = 6.4 Hz, 6H).

Synthesis of 1,5-didodecylpyrrolo[2,3-*f*]indole-2,3,6,7(1*H*,5*H*)-tetraone (4)

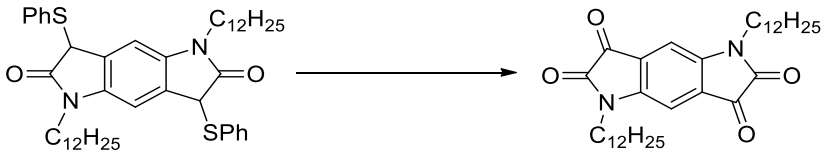

3 **4**

To a solution of **3** (1.40 g, 1.89 mmol) in a solvent of THF (50 mL) and water (8.5 mL), ammonium cerium nitrate (8.28 g, 15.1 mmol) was added. The reaction mixture was stirred at room temperature for 24 h. The solution was then concentrated in vacuo and the residue was purified by silica gel column chromatography with hexane : ethyl acetate (2:1) to give **4**. Yield: 0.491 g (47%). ^{1}H-NMR (300 MHz, $CDCl_3$) δ 7.16 (s, 2H), 3.73 (t, J = 7.4 Hz, 4H), 1.70 – 1.66 (m, 4H), 0.88 (t, J = 6.3 Hz, 6H). ^{13}C-NMR (75 MHz, $CDCl_3$) δ 183.35, 156.63, 147.33, 123.13, 106.81, 40.84, 31.92, 29.54, 29.48, 29.35, 29.20, 27.10, 26.88, 22.70, 14.14. HR-ESI-MS $(M + H)^+$ calc. for $C_{34}H_{53}N_2O_4^+$: 553.4005; found: 553.4003.

Synthesis of 6-bromo-3,3-dichloro-1-(2-decyltetradecyl)indolin-2-one (5)

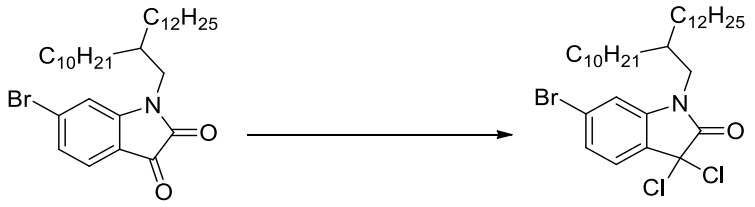

6-bromo-1-(2-decyltetradecyl)indoline-2,3-dione **5**

To a solution of 6-bromo-1-(2-decyltetradecyl)indoline-2,3-dione (1.13 g, 2.0 mmol) in toluene (15 mL), was added anhydrous PCl_5 (0.92 g, 4.4 mmol). The reaction mixture was stirred at room temperature for 24 h. Then a saturation $NaHCO_3$ aqueous solution was added to quench the reaction and the organic layer was washed with brine three times and dried over anhydrous Na_2SO_4. Removing solvent in vacuo gave the unstable **5**, which was used for the next step without further purification.

Synthesis of 6-bromo-1-(2-decyltetradecyl)indolin-2-one (6)

5 **6**

To a solution of the intermediate in acetic acid (10 mL), zinc powder (0.29 g, 4.4 mmol) was added portion-wise. After the resultant mixture was stirred at room temperature for 20 minutes the excess zinc powder was filtered off and washed with dichloromethane. The combined organics was washed brine and saturation $NaHCO_3$ aqueous solution. The solution was then concentrated in vacuo and purified by silica gel column chromatography with hexane : ethyl acetate (10:1) to give **5**. Yield: 0.86 g (78%). ^{1}H-NMR (300 MHz, $CDCl_3$) δ 7.16 – 7.07 (q, 2H), 6.92 (s, 2H), 3.54 (d, J = 7.5 Hz, 2H), 3.46 (s, 2H), 1.83

(m, 1H), 1.38 – 1.25 (br, 40H), 0.88 (t, J = 6.4 Hz, 6H). ^{13}C-NMR (75 MHz, $CDCl_3$) δ 175.05, 146.47, 125.58, 124.80, 123.39, 121.29, 111.97, 44.63, 35.88, 35.34, 31.94, 31.48, 30.01, 29.67, 29.38, 26.38, 22.72, 14.15. HR-ESI-MS $(M + H)^+$ calc. for $C_{32}H_{55}BrNO^+$: 548.3467; found: 548.3468.

Synthesis of (3*E*,7*E*)-3,7-bis(6-bromo-1-(2-decyltetradecyl)-2-oxoindolin-3-ylidene)-1,5-didodecyl-5,7-dihydropyrrolo[2,3-*f*]indole-2,6(1*H*,3*H*)-dione (7)

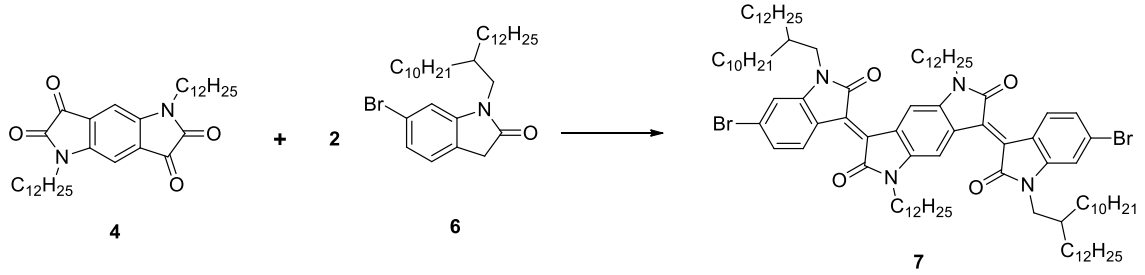

To a solution of **4** (0.25 g, 0.45 mmol) and **5** (0.50 g, 0.50 mmol) in acetic acid (6 mL), was added concentrated HCl aqueous solution (0.05 mL). The reaction mixture was heated to reflux and stirred for 24 h. Upon cooling to room temperature, the precipitate was filtered off from the reaction mixture and was further purified by silica gel column chromatography with chloroform : hexane (1:1) to give **6**. Yield: 0.232 g (32%). ^{1}H-NMR (300 MHz, $CDCl_3$) δ 9.14 (d, J = 8.4 Hz, 2H), 8.82 (s, 2H), 7.15 (d, J = 8.4 Hz, 2H), 6.86 (s, 2H), 3.82 (t, J = 6.9 Hz, 2H), 3.62 (d, J = 6.9 Hz, 2H), 1.87 (m, 2H), 1.72 (m, 4H), 1.40 – 1.24 (m, 116H), 0.88 – 0.84 (m, 18H). ^{13}C-NMR (75 MHz, $CDCl_3$) δ 168.16, 167.44, 146.57, 140.44, 133.82, 133.25, 131.54, 127.12, 125.20, 125.02, 120.65, 111.63, 109.71, 44.67, 40.44, 36.24, 32.08, 31.68, 31.67, 29.85, 29.51, 27.51, 27.38, 27.23, 26.54, 22.85, 14.28. HR-ESI-MS (M^+) calc. for $C_{98}H_{156}Br_2N_4O_4^+$: 1612.0572; found: 1612.0491.

Synthesis of P1

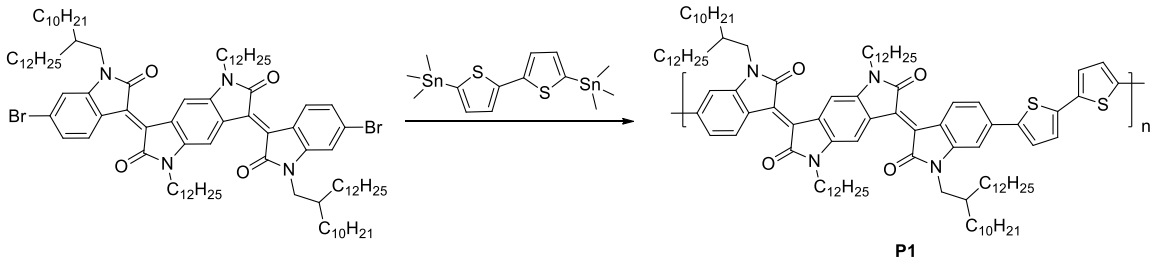

To a 25 mL Schlenk flask, **6** (68.4 mg, 0.0424 mmol), 5,5'-bis(trimethylstannyl)-2,2'-bithiophene (20.8 mg, 0.0424 mmol) and tri(*o*-totyl)phosphine (1.0 mg, 0.00330 mmol, 8mol%) were charged. After degassing and refilling argon three times, chlorobenzene (5 mL) and tris(dibenzylideneacetone)-dipalladium (0.8 mg, 0.0008 mmol, 2mol%) were added. The reaction mixture was stirred at 120 °C for 72 h. Upon cooling to room temperature, the reaction mixture was poured into methanol (100 mL). The precipitate was collected by filtration and subject to Soxhlet extraction with acetone and hexanes successively. The residual was dissolved in chloroform and give **P1** upon removal of solvent in vacuo. Yield: 56.2 mg (82%).

Synthesis of P2

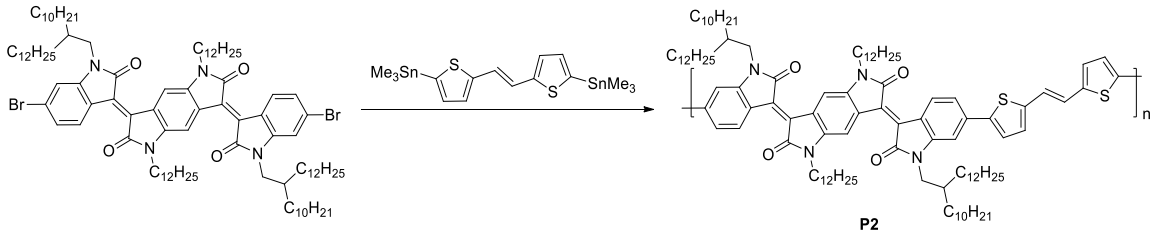

P2 was synthesized with **6** (67.0 mg, 0.0415 mmol) and (*E*)-1,2-bis(5-(trimethylstannyl)thiophen-2-yl)ethene (21.6 mg, 0.0415 mmol), according to a similar synthetic procedure that was used for **P1**. Yield: 67.2 mg (98%).

Chapter 3. Side Chain Engineering for IBDF-based Polymers

Part of this chapter was published in Yinghui He, Chang Guo, Bin Sun, Jesse Quinn and Yuning Li, *Polym. Chem.*, 2015, 6, 6689–6697.

3.1 Introduction

So far for development of novel n-type materials, most efforts have been directed to the development of novel electron deficient building blocks,[14,93,131] particularly fused ring acceptor building blocks[132] such as IBDF, (3*E*,8*E*)-3,8-bis(2-oxoindolin-3-ylidene)naphtho-[1,2-*b*:5,6-*b'*]difuran-2,7(3*H*,8*H*)-dione (INDF) and thiophene-*S*,*S*-dioxidized indophenine (IDTO). In general, sufficiently long branched alkyl side chains (Scheme 3-1) are required to offset the strong aggregation tendency of polymer main chains to render these D-A polymers soluble. Mei *et al*. reported a siloxane-terminated side chain and used it to solubilise an isoindigo-based polymer, achieving much improved hole mobility of up to 2.48 $cm^2 V^{-1} s^{-1}$ compared with the alkyl-substituted polymer.[133] We previously found that branched acetal groups (Scheme 3-1) could be used as solubilising side chains for D-A polymers.[134,135]

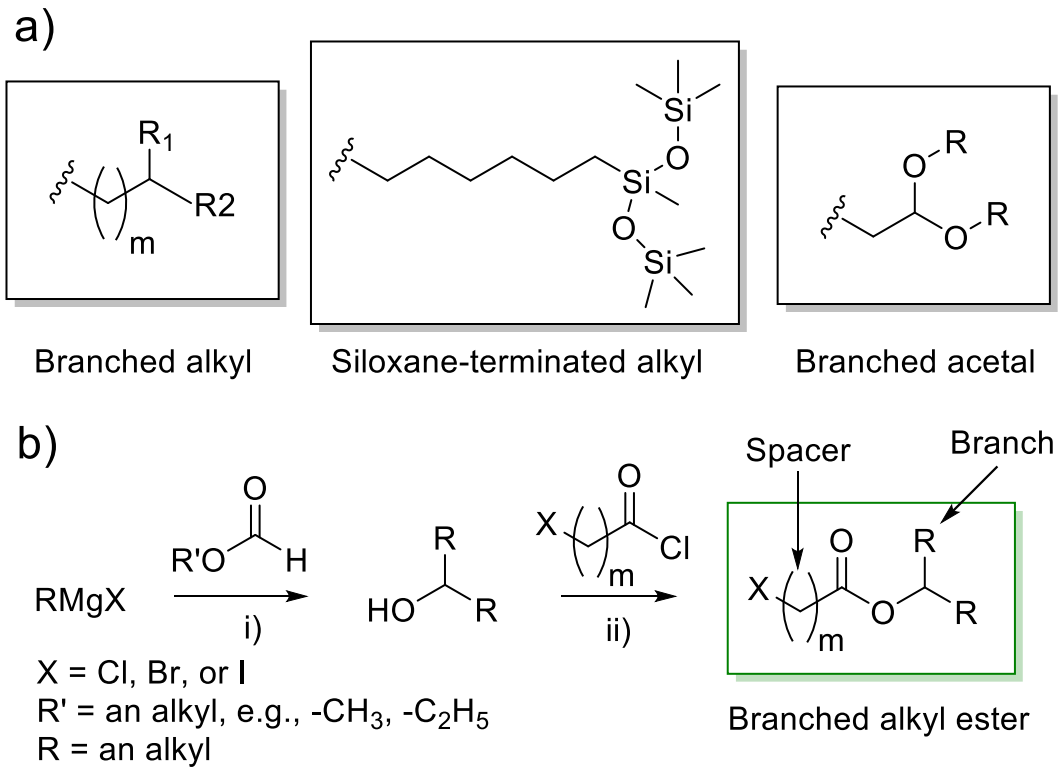

Scheme 3-1 (a) Side chains used for solubilising D-A polymers. (b) An exemplary synthetic route to the halogenated branched alkyl esters: i) r.t./ether; ii) 0 °C/THF.

Several other studies have shown that engineering of alkyl side chains has significant impacts on chain packing, film morphology and hence charge transport properties.[104,118,136] For example, Lei *et al.* conducted a study on the branching position of the branched alkyl chains on the copolymers of isoindigo (IID) and bithiothene (BT).[118] They found that π-π stacking was hindered by the side chains as the spacer group between the IID unit and the branching point of the side chain was CH_2 or C_2H_4 (simply, C1 or C2) (m = 1 or 2 in Scheme 3-1). When the branching position was moved away further, the backbone became more exposed so that the π-π stacking distance was reduced, which led to improved charge transport property. The copolymer (IIDDT-C3, Figure 3-1) with a spacer group of C3 (m = 3)

achieved the highest OTFT performance. We also found that the side chain length and the branching position greatly influenced the crystallinity, morphology, as well as the π-π stacking distance of a DPP-based polymer, PDQT (Figure 3-1).[119] By increasing the size of the side chain from 2-octyldodecyl (C20) to 2-decyltetradecyl (C24), the crystallinity of the polymer improved, resulting an increase in mobility from 2.10 $cm^2 V^{-1} s^{-1}$ to 3.37 $cm^2 V^{-1} s^{-1}$. When the distance of the branching point from the backbone was increased from C1 (for 2-octyldodecyl) to C3 (for 4-decylhexadecyl), the π-π distance decreased from 0.386 nm to 0.368 nm, leading to further improved mobility up to 6.90 $cm^2 V^{-1} s^{-1}$.

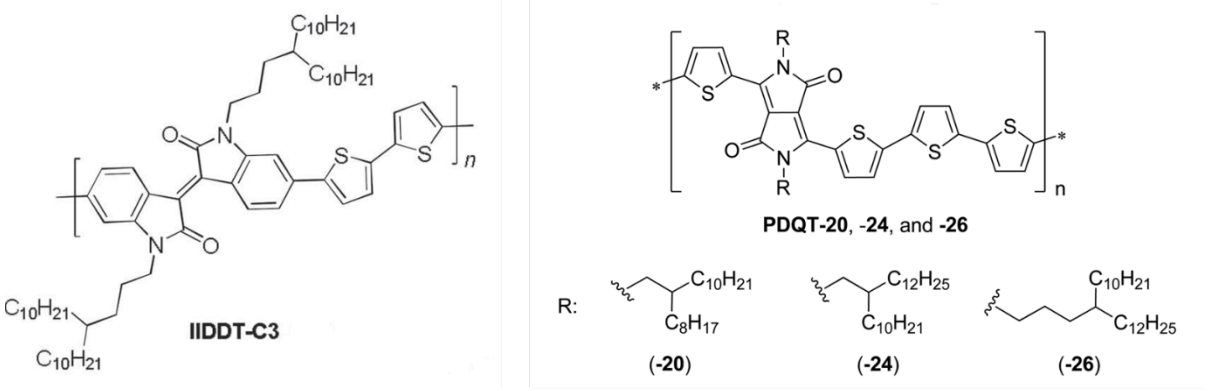

Figure 3-1 The chemical structures of IIDT-C3 and PDQT polymers.

Previously we have found the copolymer of C24-substituted IBDF and bithiophene (BT), PIBDFBT-24, was completely insoluble in any solvent and could not be processed into any device due to the very strong intermolecular interaction.[98] Later, Lei *et al* used a giant 4-octadecyldocosyl (C40) group as the side chain to render the IBDF-BT copolymer, **PIBDFBT-40** (Figure 3-2), solution-processable.[99] High electron mobility up to 1.74 $cm^2 V^{-1} s^{-1}$ was achieved for this polymer in top-gate bottom-contact (TGBC) devices. (The electron mobility is 0.13 $cm^2 V^{-1} s^{-1}$ in the BGBC devices, somehow lower than in the TGBC devices.) The same group also studied the branching point position of a series of side chains, C38-C43, and found that the side chain (C40) with a C3 spacer gave the best charge transport

performance.[104] However, these giant alkyl side chain precursors, alkyl iodide or bromide compounds, are not commercially readily available[137] and the synthesis of these compounds is very tedious,[138] which would limit their use in large-scale application. We also synthesized **PIBDFBT-40** and found that even with such large side chains this polymer still showed poor solubility in common solvents (see below).

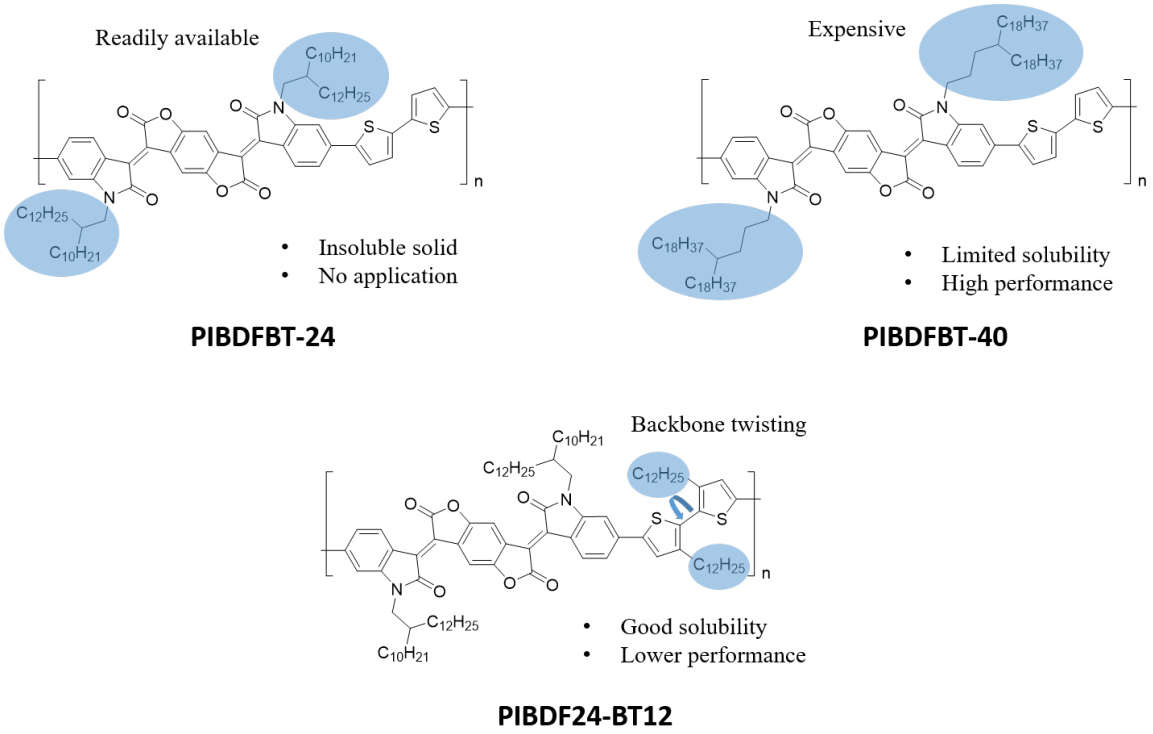

Figure 3-2 The comparison of three different types of IBDF-BT copolymers.

In this regard, we propose to use halogenated branched alkyl ester compounds as precursors to substitute IBDF to form soluble IBDF-BT copolymers. These halogenated branched alkyl esters can be conveniently prepared using an exemplary two-step route shown in Scheme 3-2. The branching point position and the branch length can be varied by using different commercially readily available starting

materials. A C3 spacer was chosen for this series of ester side chains since it has been found optimal for achieving high charge transport performance. We synthesized three PIBDFBT polymers with these new branched alkyl ester side chains with different branch length (-$C_{14}H_{29}$, -$C_{16}H_{33}$ and -$C_{18}H_{37}$), which are named **P-33**, **P-37** and **P-41** respectively. These polymers will be first fully characterized with several techniques. Then the charge transport properties will be evaluated in OTFTs and finally these polymers will be used as acceptor in all-PSCs with **PTB7-Th** as donor and the structure-property relationship will be investigated using several techniques such as AFM, XRD and SCLC.

3.2 Results and Discussion

The syntheses of all four polymers having branched alkyl ester side chains, **P-33**, **P-37** and **P-41** are outlined in Scheme 3-2. Three branched alkyl ester bromides (**8a-c**) were conveniently synthesized by reacting respective secondary alcohols with 4-bromobutyryl chloride, which was prepared *in situ* by using 4-bromobutyric acid and thionyl chloride. The two-step yields were around 65%. **8a-c** were then reacted with 6-bromoisatin to form the branched alkyl ester-substituted 6-bromoisatins **9a-c**. Condensation of 3,7-dihydrobenzo[1,2-*b*:4,5-*b*']difuran-2,6-dione with two equivalents of **9a-c** produced the IBDF monomers **10a-c**. Finally three copolymers **P-33**, **P-37**, and **P-41** were synthesized *via* the Stille coupling polymerization following a similar procedure reported previously.[98] The yields for **P-33**, **P-37**, and **P-41** are 98%, 95% and 92% respectively, after purification by Soxhlet extraction. We tested the solubility of the polymers (**P-33**, **P-37**, **P-41** and **PIBDFBT-40**) in various common organic solvents including 1,1,2,2-tetrachloroethane (TCE), chlorobenzene (CB), *o*-dichlorobenzene (DCB), chloroform (CF), dichloromethane (DCM), toluene (TL), and *m*-xylene (XL) at room temperature (Table 3-1). **P-41** with the largest side chains can be easily dissolved in all above solvents. **P-37** is less soluble, but can still be dissolved in CF, TCE, CB, and DCB. **P-33** with the smallest side

chains is only soluble in TCE among the solvents tested. We also tested solubility of **PIBDFBT-40**, which has branched C40 alkyl side chains. This polymer can only be dissolved in TCE and DCB. Compared to the C40 branched alkyl side chain, the C37 branched alkyl side chain with the similar size appears to have stronger solubilizing ability. High temperature-gel permeation chromatography (HT-GPC) was used to evaluate the molecular weights of these polymers. The column temperature was set at 140 °C and 1,2,4-trichlorobenzene was used as the eluent. **P-33** has a rather low number average molecular weight (M_n) of 16 kDa, which is probably due to its poor solubility in the polymerization medium (CB as the solvent). The molecular weights of **P-37** and **P-41** are much higher with M_n of 40 kDa and 39 kDa, respectively, owing to their better solubility enabled by their larger side chains. **PIBDFBT-40** has a similar M_n of 40 kDa, but the polydispersity (PDI) is extremely large (8.4), which is thought to be caused by the strong polymer chain aggregation or poorer solubility even at such as high temperature (Figure 3-3). The thermal stability of the polymers was characterized by thermogravimetric analysis (Figure 3-4). The 5% weight loss temperatures ($T_{-5\%}$) are 290 °C, 300 °C and 300 °C for **P-33**, **P-37** and **P-41**, respectively, indicating their decent thermal stability. However, these polymers started to decompose at lower temperatures compared to that of **PIBDFBT-40** ($T_{-5\%}$ = ~380 °C) probably due to the less thermally stable ester groups.

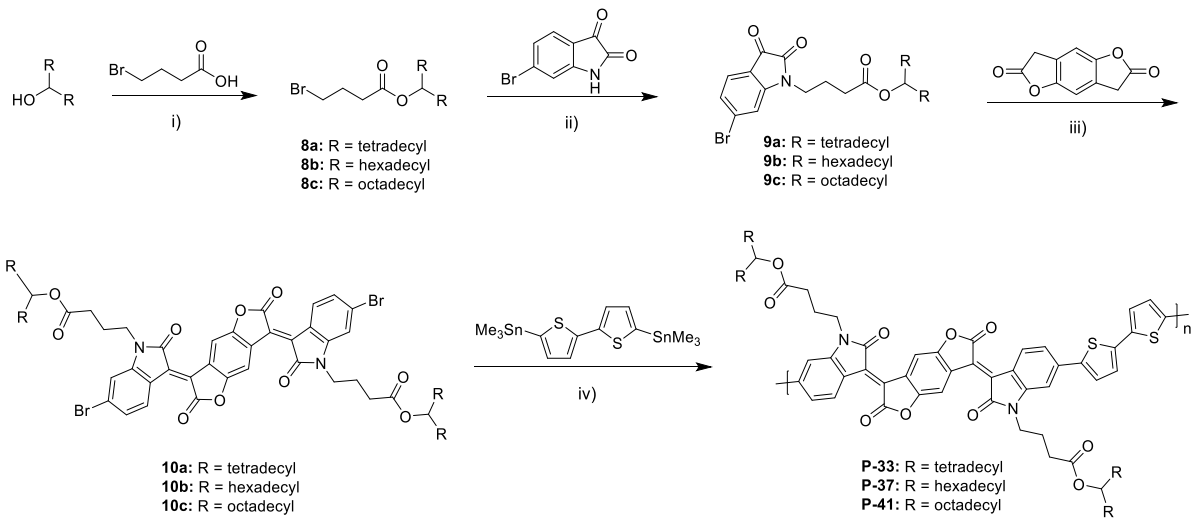

Scheme 3-2 Synthetic route to branched ester-substituted IBDF polymers **P-33**, **P-37** and **P-41**. Reaction conditions: i) $CH_2Cl_2/SOCl_2$/0 °C to r.t., THF/reflux, 60-70%; ii) DMF/K_2CO_3/50 °C, 50-60%; iii) AcOH/*p*-toluenesulfonic acid/115 °C, 30-40%; iv) chlorobenzene/P(*o*-tolyl)$_3$/$Pd_2(dba)_3$/130 °C, 90-98%.

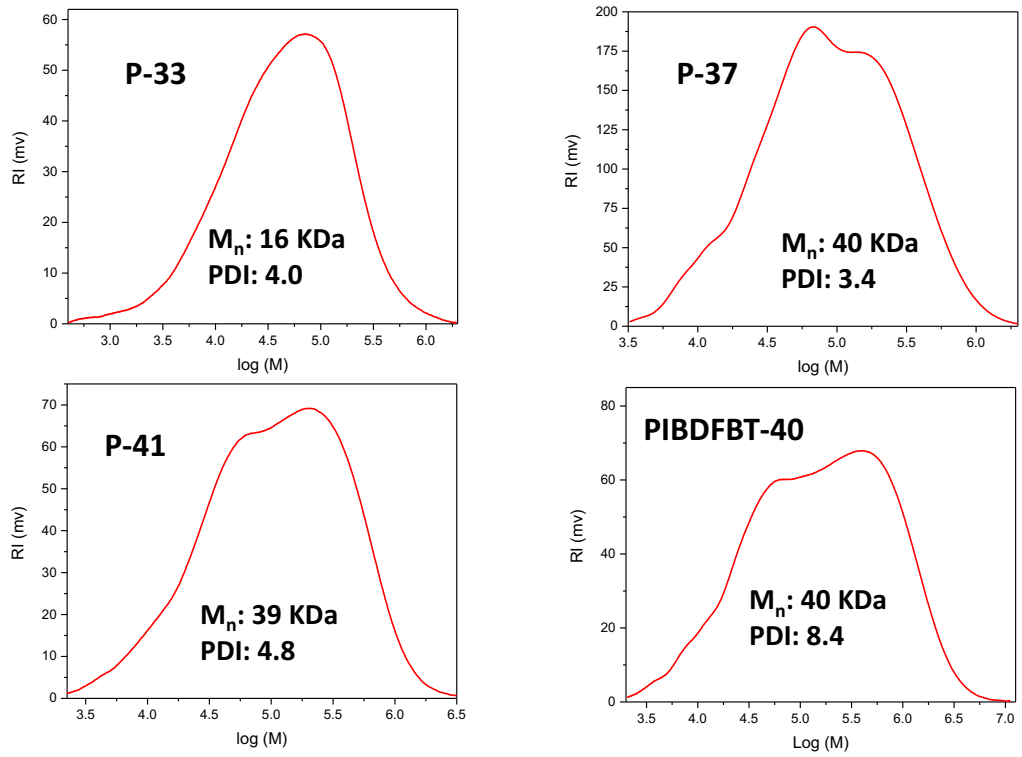

Figure 3-3 The molecular weight distribution of **P-33, P-37, P-41** and **PIBDEFBT-40** obtained with HT-GPC.

Table 3-1 The summary of properties of polymers.

Polymer	Solubility testing[a]	M_n (kDa)	PDI	$\lambda_{max}^{sol/film}$ (nm)	E_g^{opt} (eV)	E_{HOMO}/E_{LUMO} (eV)
P-33	TCE	16	4.0	847/847	1.31	-5.68/-3.85
P-37	TCE, CB, DCB, CF	40	3.4	847/847	1.31	-5.72/-3.87

P-41	TCE, CB, DCB, CF, DCM, TL, XL	39	4.8	840/840	1.31	-5.73/-3.85
PIBDFBT-40	TCE, CB	40	8.4	780/782[c]	1.31[c]	-5.70/-3.90[c]

[a] Solubility testing was conducted by dissolving the polymer in a solvent (~5 mg/mL) at room temperature (sometimes with an aid of heating before cooling to room temperature). [b] Solvent in which the polymer can be completely dissolved. TCE: 1,1,2,2-tetrachloroethane, CF: chloroform; DCM: dichloromethane; CB: chlorobenzene; DCB: *o*-dichlorobenzene; TL: toluene; XL: xylene. [c] The data can be found in the reference.[99]

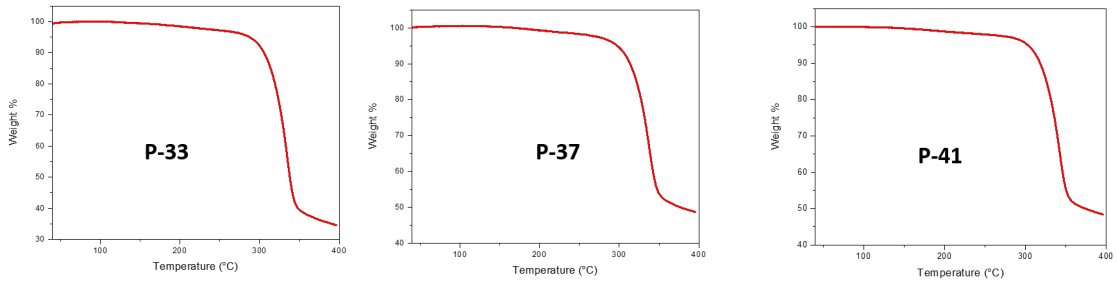

Figure 3-4 The TGA diagrams for **P-33, P-37, P-41** and **PIBDFBT-40** obtained in nitrogen.

The optical properties of the polymers in dilute solutions and thin films are characterized by UV-Vis-NIR absorption spectroscopy (Figure 3-5 and Table 3-1). All three polymers showed a significant red-shift in the maximum absorption (λ_{max}) compared to that of **PIBDFBT-40** in solutions and films[99]. These results suggest that the ester side chains have an impact on the backbone conjugation. **P-41** showed a λ_{max} at ~840 nm in solution and the solid state, which is blue-shifted compared to those of **P-33** and **P-37**. This implies that the backbone of **P-41** is less coplanar than those of **P-33** and **P-37**, likely

caused by the stronger interactions of its larger side chains with solvent molecules in solution and between themselves in the film to make the backbone slightly more twisted.[119,139] All polymers showed vibronic splitting adsorption peaks at ~750 nm in both dilute solutions and films. In solution, the vibronic splitting adsorption for **P-33** is much weaker compared to the other two polymers, which might be due to its low molecular weight. In films, the vibronic splitting adsorption peaks for all polymers became more resolved as compared to those in the solution spectra. This could be attributed to the exitonic-vibronic coupling induced by interchain aggregation in the solid state[140], indicating a more ordered packing of chains. The optical bandgaps were estimated using the onset absorption wavelengths to be ~1.31 eV for all three polymers, which is the same as that of **PIBDFBT-40**[99]. It is worth noting that all IBDF-based polymers showed considerable absorption from 350 nm to 600 nm, which can be idea complementary absorption to **PTB7-Th** in the same region. The absorption coefficient for these polymers (**P-33, P-37** and **P-41**) were determined to be 7.4×10^5 cm^{-1}, 7.1×10^5 cm^{-1} and 6.6×10^5 cm^{-1}, respectively. Cyclic voltammetry (CV) was used to study the electrochemical properties of the polymers (Figure 3-6 and Table 3-1). All polymers showed both the reductive and oxidative peaks. The highest occupied molecular orbital and lowest unoccupied molecular orbital (HOMO and LUMO) levels were estimated using the onset oxidation and reduction potentials. All three polymers have similar HOMO levels (ranging from -5.68 eV to -5.73 eV) and LUMO levels (ranging from -3.85 eV to -3.87 eV). The similar HOMO and LUMO levels of these polymers indicate that side chains have minimal impacts on the electrochemical properties of the polymers. The frontier orbital levels of these polymers fall in the ranges where n-type dominant ambipolar charge transport performance might be observed.[141,142] Moreover, we measured electrochemical characteristic of **PTB7-Th** with CV as well. With the HOMO/LUMO being -5.36 eV and -3.55 eV respectively,[143]

the HOMO and LUMO offsets between the IBDF-based polymers (**P-33**, **P-37** and **P-41**) and **PTB7-Th** are larger than 0.3 eV, which made them suitable active layer materials in all-PSCs.[26]

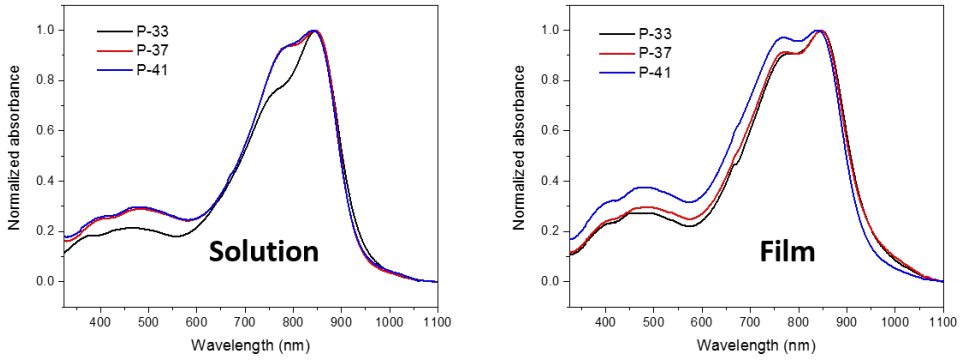

Figure 3-5 The UV-Vis-NIR adsorption spectra in solution (chloroform) and in film.

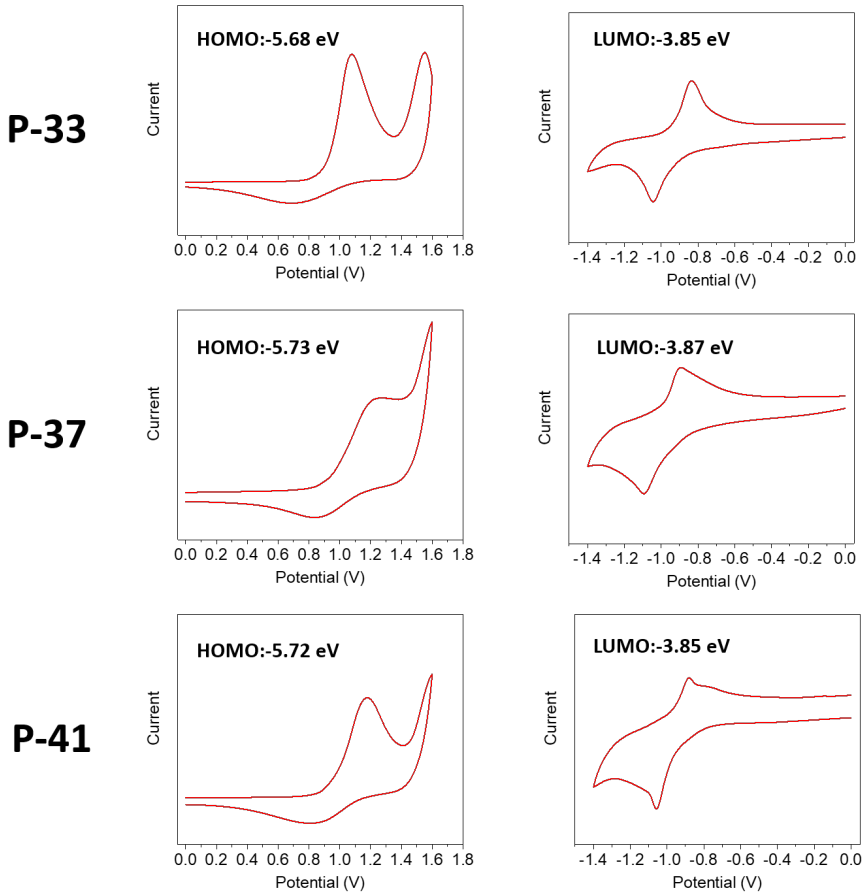

Figure 3-6 the CV diagrams for **P-33, P-37** and **P-41**.

To probe how the length of the alkyl branch (R) will impact the charge transport, these polymers were used as channel semiconductor materials in BGBC OTFT devices using SiO_2/Si wafer as the substrate. All three polymers showed n-type dominant ambipolar charge transporting characteristics (Table 3-2). When the annealing temperature was increased from 100 °C to 200 °C, the carrier mobility improved gradually for all devices. However, it was found that further increasing the annealing temperature to 250 °C led to performance degradation. Among three polymers, **P-37** with $C_{16}H_{33}$ as the branch showed the best device performance with the average electron mobility of 0.32 $cm^2\ V^{-1}\ s^{-1}$ and hole mobility of

0.15 $cm^2 V^{-1} s^{-1}$ when the films were annealed at 200 °C (Figure 3-7). **P-33** showed the average electron and hole mobilities of 0.10 $cm^2 V^{-1} s^{-1}$ and 0.051 $cm^2 V^{-1} s^{-1}$, respectively, for the films annealed at 200 °C. The lower performance of **P-33** is considered due to its lower molecular weight as well as its poorer thin film morphology (see below). The best performance for **P-41** was obtained for the films annealed at 200 °C, with average electron mobility of 0.072 $cm^2 V^{-1} s^{-1}$ and hole mobility of 0.027 $cm^2 V^{-1} s^{-1}$. The poorest charge transport performance of **P-41** among three polymers is probably the result of its more twisted back bone as previously discussed (UV-Vis-NIR absorption spectra) and its poor film morphology (see below). To compare the ester chains with alkyl side chains, we also tested **PIBDFBT-40** as channel semiconductor in BGBC devices under the same conditions. Ambipolar charge transport was also observed for the devices based on **PIBDFBT-40** (Table 3-2). For the devices annealed at 200 °C, the average electron mobility was 0.39 $cm^2 V^{-1} s^{-1}$ and the average hole mobility was 0.22 $cm^2 V^{-1} s^{-1}$, which are slightly higher than those of **P-37**. Our results indicate that ester side chains can be used as solubilizing chains for D-A polymers and the resulting polymers can achieve comparable charge transporting properties to those with alkyl side chains in BGBC OTFTs.

Table 3-2 OTFT device performance of the polymers annealed at different annealing temperatures.

Polymer	Annealing temperature (°C)	μ_e ($cm^2 V^{-1} s^{-1}$)		μ_h ($cm^2 V^{-1} s^{-1}$)	
		avg	*max*	*avg*	*max*
P-33	100	0.081±0.005	0.089	0.034±0.012	0.050
	150	0.092±0.010	0.11	0.050±0.011	0.065
	200	0.10±0.015	0.12	0.051±0.010	0.065

	100	0.24±0.022	0.28	0.096±0.009	0.11
P-37	150	0.27±0.025	0.30	0.10±0.010	0.12
	200	0.32±0.023	0.35	0.15±0.037	0.20
	100	0.041±0.003	0.045	0.023±0.004	0.028
P-41	150	0.054±0.004	0.058	0.023±0.004	0.029
	200	0.072±0.003	0.074	0.027±0.002	0.030
PIBDFBT-40	200[a]	0.39±0.032	0.43	0.17±0.043	0.24

[a] The annealing temperature was chosen for the best performance according to the references.

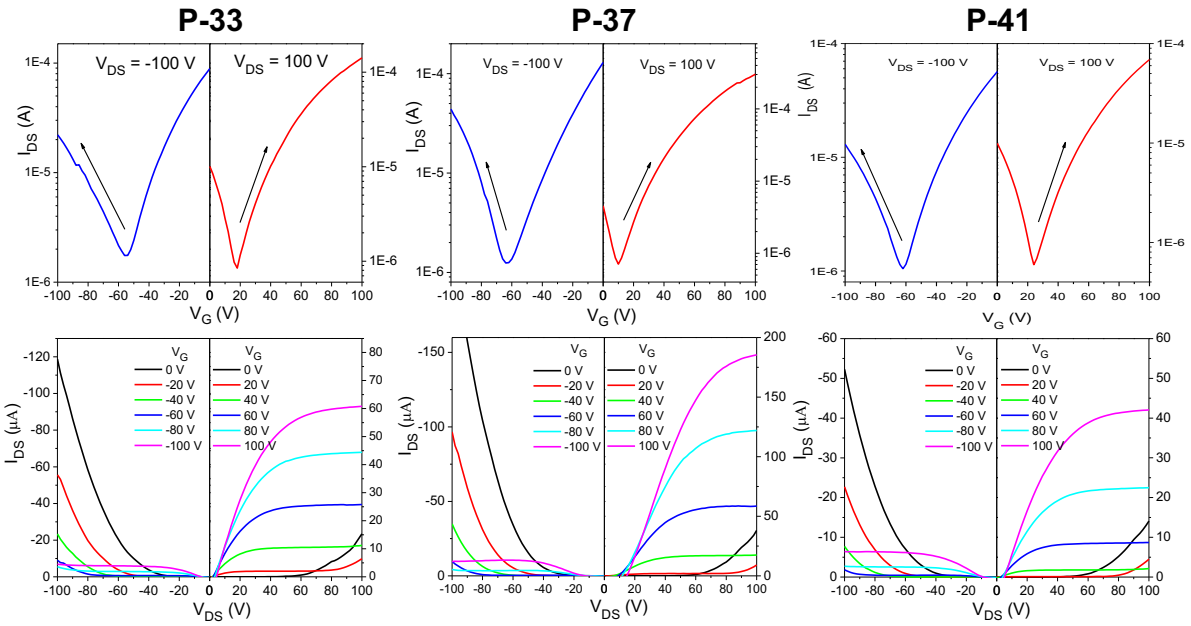

Figure 3-7 Transfer (top) and output (bottom) curves of BGBC OTFT devices with 200 °C-annealed **P-33**, **P-37** and **P-41** films. Device dimensions: channel length (L) = 30 μm; channel width (W) = 1000 μm.

To further understand why **P-37** showed better charge transport property than **P-33** and **P-41**, we characterized the microstructures of the polymer thin films with atomic force microscopy (AFM, Figure 26) and X-ray diffraction (XRD, Figure 3-8). The thin film samples were prepared under the same conditions as those used for the OTFT devices. In the AFM images of the **P-33** films, very smooth surfaces with low root mean squared roughness (R_q) of 1.3 nm were observed. However only small grains with poor interconnections can be seen, which might be due to the low molecular weight of **P-33**. For the **P-37** films, well-interconnected large fibre-like domains are observed, which is regarded to be beneficial for the charge transport.[144]. The as-spun **P-41** films showed very large grains and grain boundaries with R_q of 23 nm. With increasing annealing temperature, the film morphology slightly improved, but the films are still very rough. The very poor film morphology might be another reason for the poor charge transport performance of **P-41**. Reflective mode XRD was employed to investigate the chain packing of these polymers in spin-coated thin films (Figure 3-9). The as-spun **P-33**, **P-37** and **P-41** films showed the primary diffraction peaks at 2θ = 3.37°, 2.97° and 2.90°, which correspond to their inter-lamellar d-spacing distances of 2.62 nm, 2.97 nm and 3.04 nm, respectively, agreeing with the increasing size of their side chains. Since there are no diffractions corresponding to the co-facial π-π-distance (normally at 2θ = ~20-25°), the polymer chains presumably adopted an edge-on orientation motif with respect to the substrate.[145,146] As the annealing temperature was increased, the intensity of the primary diffraction peaks increased and the secondary diffraction peaks became more visible, indicating that longer range ordering was achieved. That explains why the carrier mobility increased

with increasing annealing temperature. The 200 °C-annealed **P-37** film showed the strongest diffraction peaks and thus the most ordered chain packing, which is also accounted for its best charge transport performance among three polymers.

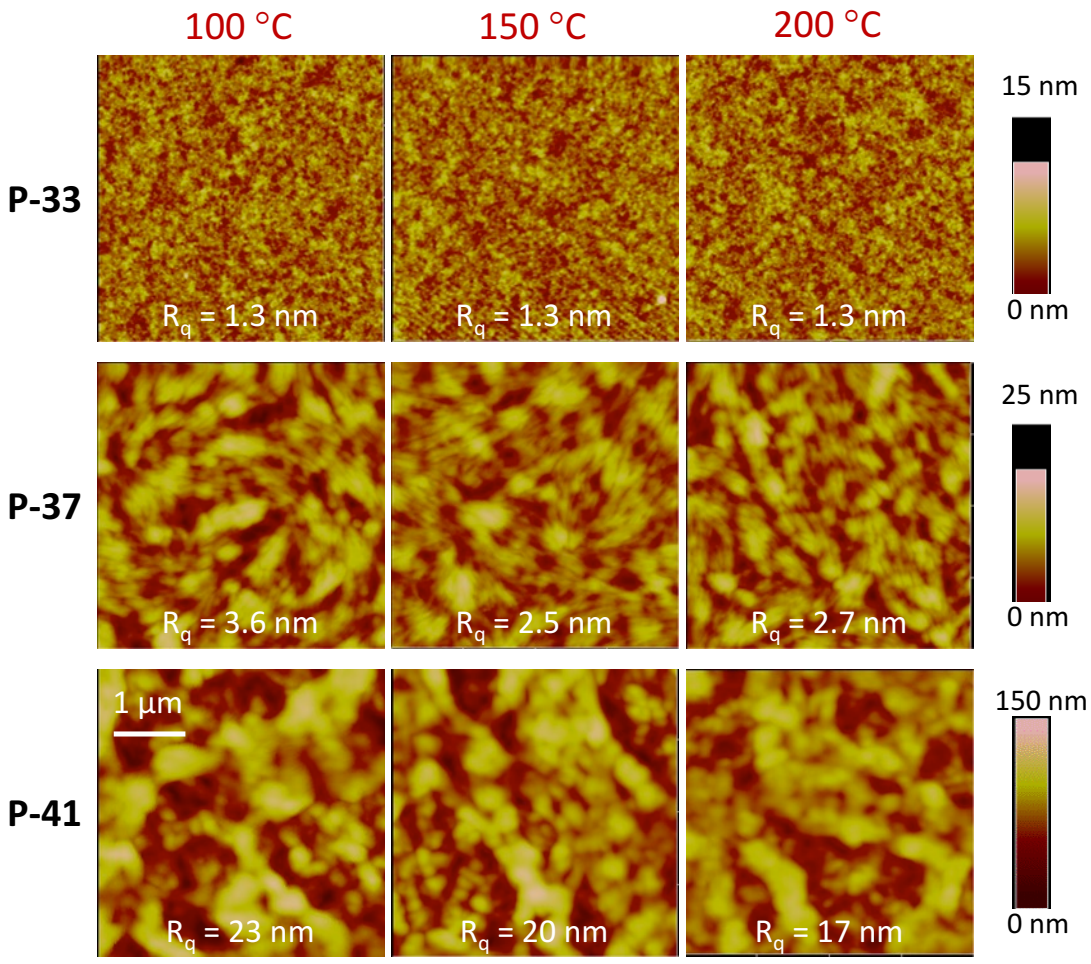

Figure 3-8 AFM height images (4µm × 4µm) of polymer films annealed at different temperatures.

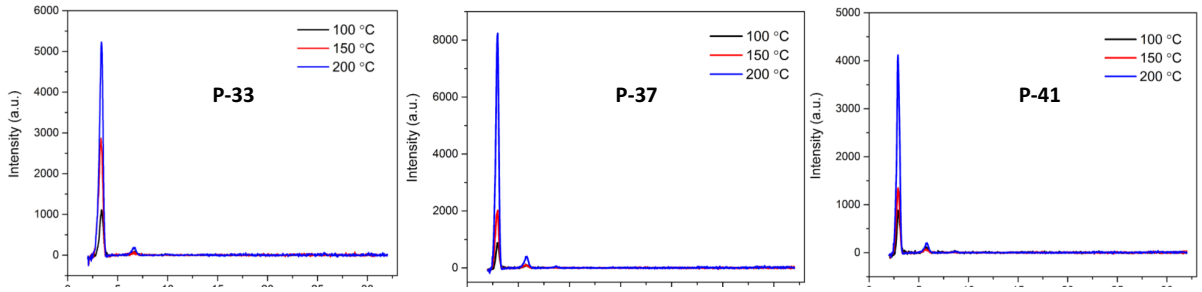

Figure 3-9 Reflective XRD patterns of **P-33**, **P-37** and **P-41** films annealed at different temperatures.

Given that LUMO/HOMO offsets ($E_{LUMO,D}$ - $E_{LUMO,A}$ and $E_{HOMO,D}$ – $E_{HOMO,A}$) between these polymers and **PTB7-Th** are larger than 0.3 eV (Figure 3-10), these three polymers were used as electron acceptor with **PTB7-Th** as electron donor to fabricate all-PSC devices. The device configuration was ITO/PEDOT:PSS/**PTB7-Th**:PA/LiF/Al. The active layer was spin-coated from the blend of the two polymers (1:1 wt ratio) in a chlorobenzene solution (10 mg/mL). Due to the poor solubility of **P-33** in chlorobenzene, we were unable to process **P-33:PTB7-Th** into a uniform thin film. Figure 3-11 shows the J–V characteristics of the devices measured under AM 1.5G illumination (100 mW cm $^{-2}$). The devices based on **P-37** exhibited on average the V_{OC} of 0.72 V, J_{SC} of 1.2 mA cm $^{-2}$, and FF of 0.39, corresponding to a PCE of 0.34%. The devices based on **P-41** exhibited on average the V_{OC} of 0.57 V, J_{SC} of 0.54 mA cm $^{-2}$, and FF of 0.37, corresponding to a PCE of 0.11%. We can clearly tell the low PCEs mainly resulted from the extremely low Jsc and relatively low FF.

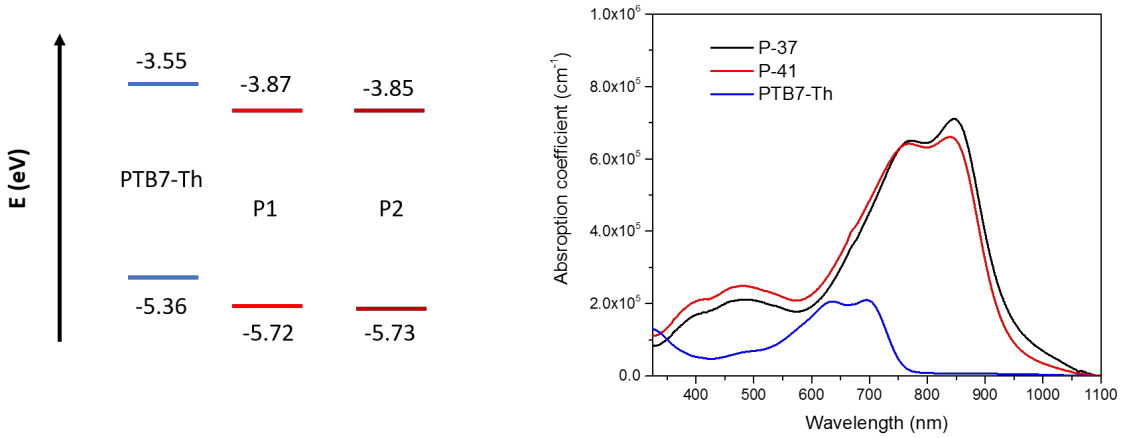

Figure 3-10 The energy level alignment and adsorption coefficient spectra of the IBDF-polymers and **PTB7-Th**.

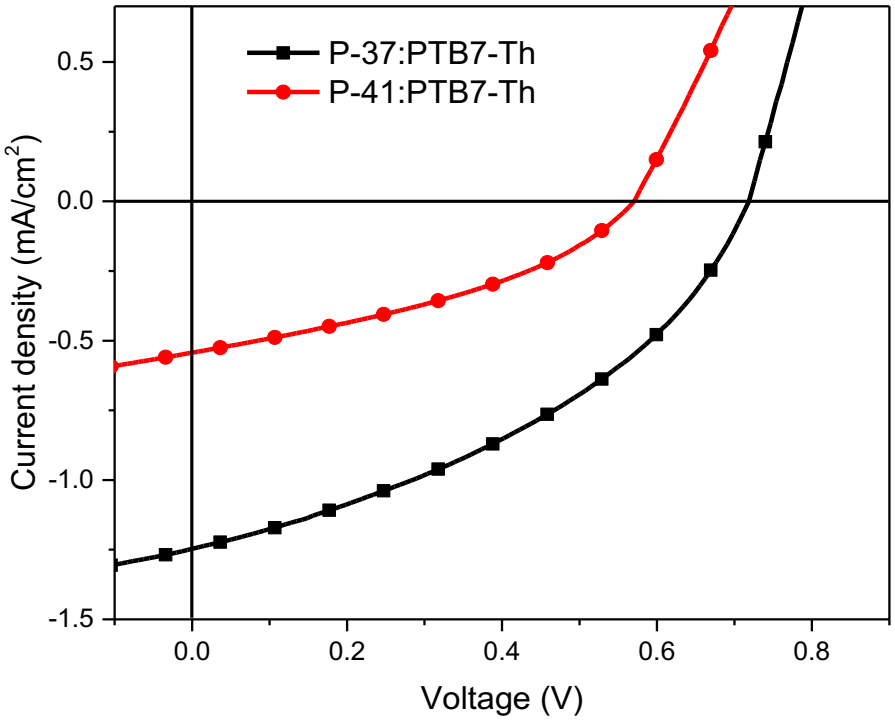

Figure 3-11 The J-V characteristics of the devices based on **P-37** and **P-41** under AM 1.5G illumination. The blend film (~90 nm) was spin-coated at 1500 rpm using a solution in chlorobenzene with a total concentration of 10 mg/mL.

Table 3-3 The summary of all-PSC devices and SCLC devices based on **P-37**, **P-41** and **N2200**.

Acceptor	J_{SC} (mA/cm^2)	V_{OC} (V)	FF	PCE (%)	μ_h (cm^2 V^{-1} s^{-1})	μ_e (cm^2 V^{-1} s^{-1})
P-37	1.21	0.72	0.39	0.34 (0.29)	2.54×10^{-4}	7.24×10^{-6}
P-41	0.54	0.57	0.37	0.11 (0.09)	1.75×10^{-4}	4.39×10^{-6}

N2200	8.4	0.80	0.47	3.2 (3.0)

All devices used **PTB7-Th** as the donor and the same device configuration: ITO/PEDOT:PSS/Polymer blend/LiF/Al. The active layer thickness is around 90 nm. The numbers in the parenthesis are average values for 4 devices on the same substrate.

To understand why these devices have such poor performance, we investigated the morphology of the **PTB7-Th**:PA blend by AFM (Figure 3-12). The samples were prepared under the same conditions to emulate the solar cell devices. Both samples showed pretty rough film morphology with root mean squared roughness of 4.3 nm for **P-37** blend and 5.5 nm for **P-41** blend respectively. In addition, large-size and poorly defined fabril structures can be observed in the AFM images with size over 1μm. Similar observation has been previous reported in literature and usually correlated to large phase separation.[70,81,147] For example, Fabino *et al*. found the blend of **P3HT:P(NDI2OD-T2)** processed from *o*-DCB exhibited extremely low J_{SC} (~0.4 mA/cm^2) and PCE (~0.1%) in all-PSCs.[70] The AFM image (Figure 3-13a) of the blend showed large polymer fabrils indicating large phase separation. Later, Schubert *et al.* used a mixture of *p*-xylene and 1-CN as the processing solvent for the same blend and achieved significantly improved PCE of 1.4% with a J_{SC} of 3.77 mA/cm^2.[81] The AMF image (Figure 3-13b) of the blend showed a well-mixed morphology of the two polymers. Therefore, the large phase separation between the IBDF polymers and **PTB7-Th** has greatly limited the exciton dissociation at the D-A interface because the exciton diffusion length in organic semiconductors is usually around or below 10 nm.[147]

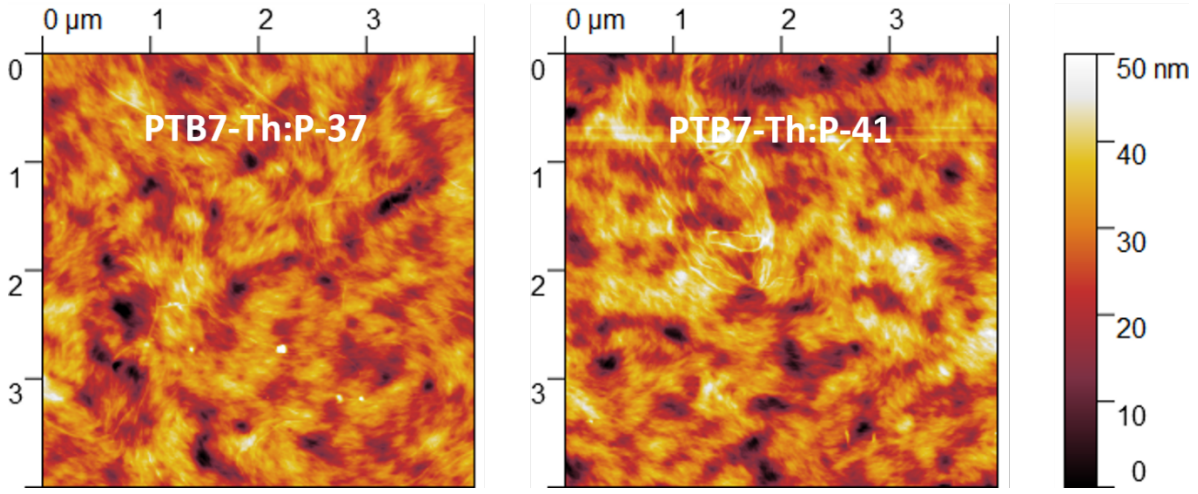

Figure 3-12 AFM height images (4µm × 4µm) of polymer blend films spin-coated on PEDOT:PSS/ITO substrates.

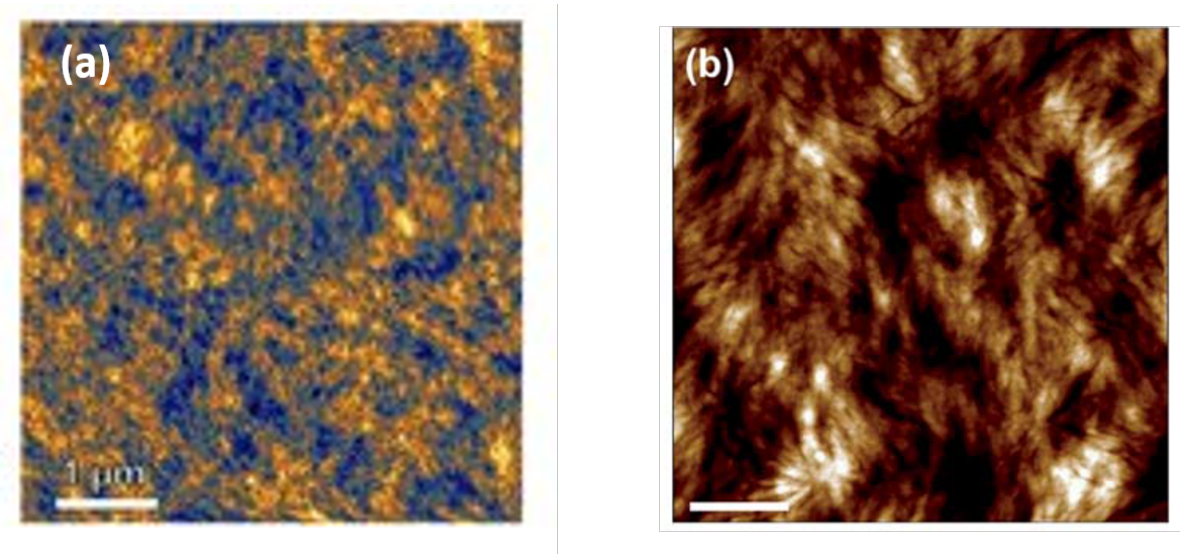

Figure 3-13 AFM height images (4µm × 4µm) of P(NDI2OD-2T):**P3HT** blend films: processed with *p*-xylene:1-CN (a)[122] and *o*-DCB (b)[148].

In addition, we fabricated the electron-only (ITO/ZnO/polymer blend/LiF/Al) and hole-only (ITO/PEDOT:PSS/polymer blend/MoO_3/Ag) devices for **PTB7-Th:P-37** and **PTB7-Th:P-41** and measured the space-charge-limited current versus voltage characteristic (Figure 3-14). We calculated the charge carrier mobility using the following equation:

$$J = \frac{9}{8}\mu\varepsilon\varepsilon_0\frac{V^2}{L^3}$$

Where ε is approximately 3 for organic semiconductors and L is the thickness of the semiconductor films. The electron mobilities for **P-37** and **P-41** were determined to be 7.24×10^{-6} cm^2 V^{-1} s^{-1} and 4.39×10^{-6} cm^2 V^{-1} s^{-1}, which are orders lower than those of **PCBM** ($\sim10^{-3}$ cm^2 V^{-1} s^{-1}) and **P(NDI2OD-T2)** ($\sim10^{-4}$ cm^2 V^{-1} s^{-1}) in literature.[78,97] On the other hand, the calculated hole mobilities for **PTB7-Th** were 2.54×10^{-4} cm^2 V^{-1} s^{-1} and 1.75×10^{-4} cm^2 V^{-1} s^{-1} in **PTB7-Th:P-37** and **PTB7-Th:P-41** respectively, which are in good agreement with previous reports.[72,75,76] The poor electron transport properties has led to unbalanced charge transport in the polymer blend, which is known to have negative impact on FF and J_{SC} according previous studies.[57,149,150] This may partially explain why the FFs of these cells have such low values (<0.4). We also tested the neat films of **P-37** and **P-41**. Similar electron mobilities were found for **P-37** (8.36×10^{-6} cm^2 V^{-1} s^{-1}) and **P-41** (3.91×10^{-6} cm^2 V^{-1} s^{-1}) while hole mobilities were 6.88×10^{-7} cm^2 V^{-1} s^{-1} and 1.33×10^{-7} cm^2 V^{-1} s^{-1} for **P-37** and **P-41** respectively. These results show that the low electron mobilities for bulk charge transport result from the polymers themselves and the hole transport is mainly undertaken by the **PTB7-Th**. To investigate the polymer molecular packing in solid state, we performed thin film XRD on the polymer neat films for **P-37** and **P-41** (Figure 3-15). The samples were prepared by spin-coating the polymer films on SiO_2/Si wafer substrates. XRD patterns of both the **P-37** and **P-41** neat films showed almost completely amorphous morphology. A weak (100) at diffraction peak 2θ = ~3.10 ° was observed for **P-37**,

corresponding to a d-spacing of 2.84 nm, indicating the presence of edge-on oriented chains on the substrate. The amorphous morphology of these two polymers is likely because the bulky side chains have imposed a large hindrance for the polymer chain to form order packing, this has also been observed by previous studies.[151–154] The intrinsic disordered packing property of these polymers may explain why low SCLC electron mobilities were observed in the electron-only devices on both the blend films and neat films.

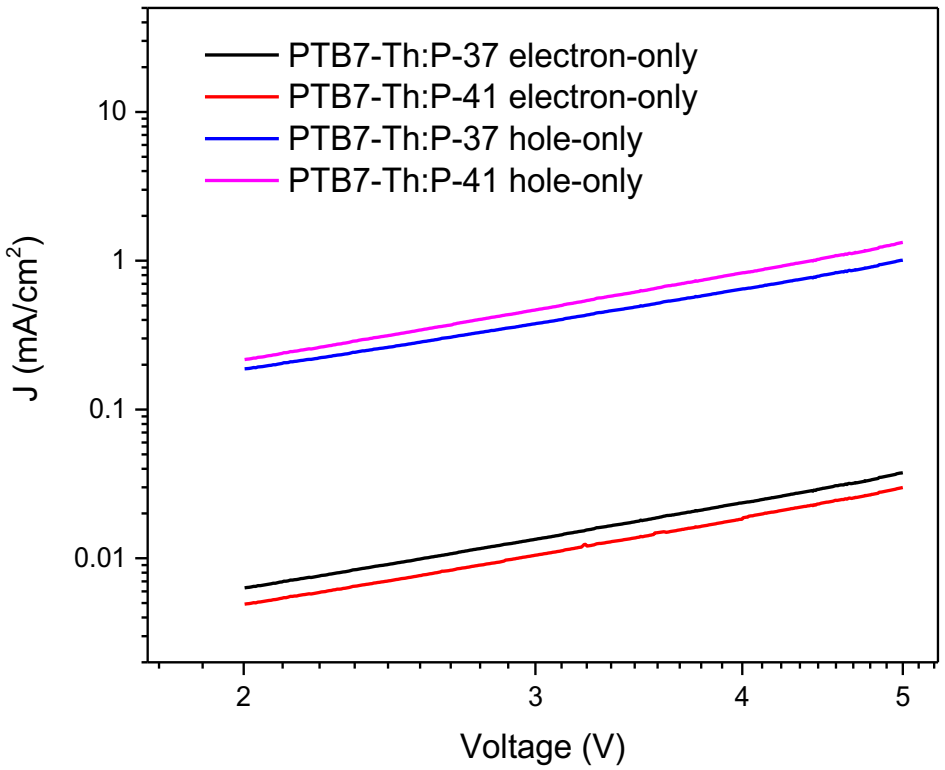

Figure 3-14 The J-V characteristics of the electron-only and hole-only devices for **PTB7-Th:P-37** and **PTB7-Th:P-41**.

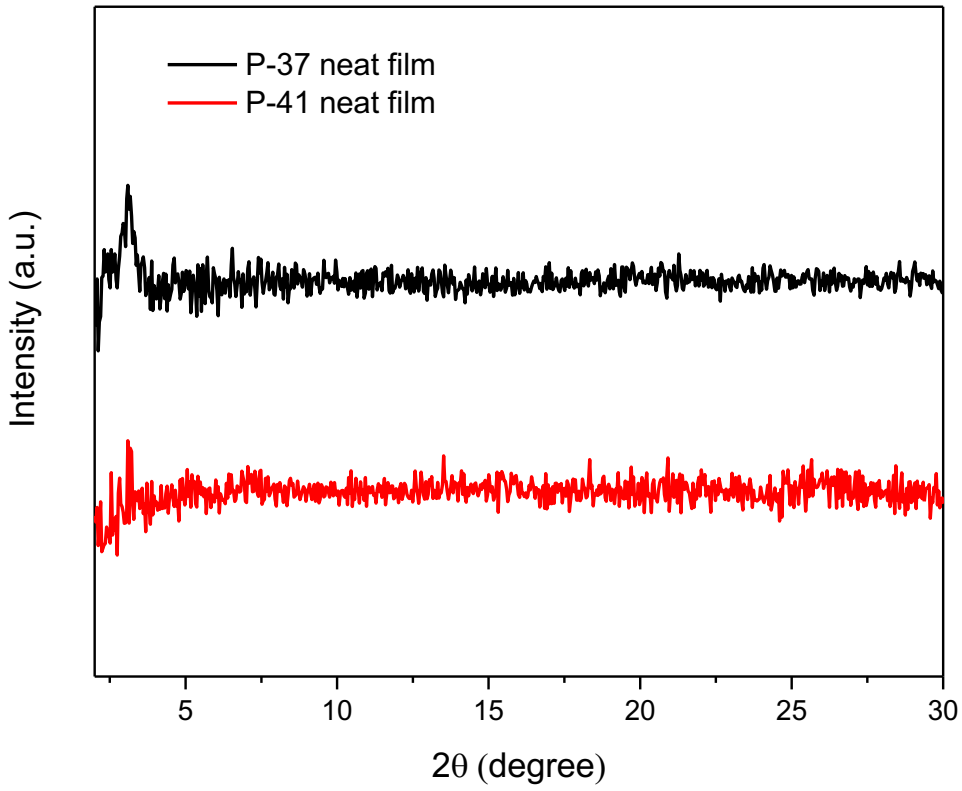

Figure 3-15 The XRD patterns of **P-37** and **P-41** on ZnO/ITO fabricated under the same conditions as the electron-only devices.

3.3 Summary and Future Direction

In conclusion, a series of ester side chains have been developed and used as solubilizing side chains for the copolymers of IBDF and BT. Three IBDF-BT polymers were synthesized and demonstrated

excellent solubility, suitable HOMO/LUMO levels and excellent charge transport properties in OTFTs with electron mobility up to 0.35 cm^2 V^{-1} s^{-1}. When the polymers were incorporated in all-PSCs in conjunction with **PTB7-Th**, all devices showed very poor performance (PCEs <0.4% with J_{SC} < 1 mA/cm^2 and FF<0.4). AFM images suggested there were large polymer fabrils (>1000 nm) present in the polymer blends, indicating a large phase separation for the blends. This has limited the charge generation that happens at the D-A interface, and led to a very low J_{SC}. In addition, SCLC measurement of the blends exhibited quite low electron mobilities (~10^{-6} cm^2 V^{-1} s^{-1}) and led to unbalanced charge transport in the polymer blend, which could be one of the reasons why the devices showing low FFs. Through XRD and SCLC studies, we found the spin-coated polymer thin films were intrinsically amorphous and the bulky side chains seemed to disrupt the chain packing, which might have caused the poor bulk electron charge transport in the solar cell devices. To further improve the performance of IBDF-based polymers as acceptor in organic solar cells, large phase separation needs to be avoided. This will take a comprehensive consideration of various measures such as reducing the side chain's length[155,156], introducing a twisted backbone[157,158] and tuning the backbone structures[74,77,159] to improve the miscibility of the acceptor polymer and donor polymer. A good balance between crystallinity (charge transport) and solubility/miscibility (blend morphology) must be realized to achieve considerable solar cell performance.

3.4 Experimental

3.4.1 Materials and Characterization

All chemicals were obtained from commercial sources and used as received. Nonacosan-15-ol,[160] tritriacontan-17-ol,[160] heptatriacontan-19-ol,[161] 3,7-dihydrobenzo[1,2-*b*:4,5-

b']difuran-2,6-dione[105] and **PIBDFBT-40**[99] were prepared according to the literature methods. High-temperature gel permeation chromatography (HT-GPC) measurements were performed on a Malvern 350 HT-GPC system using 1,2,4-trichlorobenzene as eluent and polystyrene as standards at a column temperature of 140 °C. Thermogravimetric analysis (TGA) was carried out on a TA Instruments SDT 2960 at a scan rate of 10 °C min^{-1} under nitrogen. The UV-Vis absorption spectra of polymers were recorded on a Thermo Scientific model GENESYS™ 10S VIS spectrophotometer. Cyclic voltammetry (CV) data were obtained on a CHI600E electrochemical analyser using an Ag/AgCl reference electrode and two Pt disk electrodes as the working and counter electrodes in a 0.1 M tetrabutylammonium hexafluorophosphate solution in acetonitrile at a scan rate of 50 mV s^{-1}. Ferrocene was used as the reference, which has a HOMO energy value of -4.8 eV.[162] NMR spectra were recorded with a Bruker DPX 300 MHz spectrometer with chemical shifts relative to tetramethylsilane (TMS, 0 ppm). Reflective XRD measurements were carried out on a Bruker D8 Advance diffractometer with Cu Ka radiation (λ = 0.15406 nm) using polymer films spin coated on SiO_2/Si substrates. Atomic force microscopy (AFM) images were taken with a Dimension 3100 scanning probe microscope.

3.4.2 Fabrication and Characterization of OTFT devices

The bottom-contact bottom-gate (BGBC) configuration was used for all OTFT devices. The preparation procedure of the substrate and device is as follows. A heavily n-doped Si wafer with ~300 nm-thick SiO_2 layer was patterned with gold source and drain pairs by conventional photolithography and thermal deposition. Then the substrate was treated with air plasma, followed by cleaning with acetone and isopropanol in an ultrasonic bath. Subsequently, the substrate was placed in a 3%

dodecyltrichlorosilane (DDTS) solution in toluene at room temperature for 20 min. The substrate was washed with toluene and dried under a nitrogen flow. Then a polymer solution in chloroform (5 mg mL^{-1}) or 1,1,2,2-tetrachloroethane (TCE) (10 mg mL^{-1}) was spin-coated onto the substrate at 3000 rpm for 60 s to give a polymer film (~40 nm), which was further subjected to thermal annealing at different temperatures for 20 min in a glove box. All OTFT devices were characterized in the same glove box using an Agilent B2912A Semiconductor Analyser. The hole and electron mobilities are calculated in the saturation regime according to the following equation:

$$I_{DS} = \frac{\mu C_i W}{2L}(V_G - V_T)^2$$

where I_{DS} is the drain-source current, μ is charge carrier mobility, C_i is the gate dielectric layer capacitance per unit area (~ 11.6 nF cm^{-2}), V_G is the gate voltage, V_T is the threshold voltage, L is the channel length (30 μm), and W is the channel width (1000 μm).

3.4.3 Fabrication and Characterization of all-PSC devices

All all-PSC devices were fabricated using the conventional configuration ITO/PEDOT:PSS/**PTB7-Th**:PA/LiF/Al. ITO glass substrates were sonicated in water, acetone and IPA. Then the substrates were treated with plasma cleaning. A thin layer of PEDOT:PSS (Al 4083) was deposited through spin-coating at 4000 rpm and dried subsequently at 150 °C for 20 min in air. Then the substrates were transferred to a nitrogen glove box, where the polymer blend layer (~90 nm) was spin-coated onto the PEDOT:PSS layer. The active layer was formed using a chlorobenzene solution of **PTB7-Th**:PA (1:1). Finally, a thin layer of LiF (1 nm) and a layer of Al (100 nm) electrode were deposited in vacuum onto the substrate at P $\approx 5.0 \times 10^{-6}$ Pa. The active area is 0.07 cm^2. The current density–voltage (J – V) characteristics of the all-PSCs were measured on an Agilent B2912A Semiconductor Analyser with a

ScienceTech SLB300-A Solar Simulator. A 450 W xenon lamp and an air mass (AM) 1.5 filter were used as the light source.

3.4.4 Synthetic Procedures

General procedure for the synthesis of brominated branched alkyl esters 8a~8c

To a solution of 4-bromobutyric acid (8.4 g, 50 mmol) in dichloromethane (50 mL) under ice/water bath, thionyl chloride (8.3 g, 70 mmol) was added. The solution was stirred at room temperature for 4 h. Then solvent and the excess thionyl chloride were removed under reduced pressure and then the residual was dissolved by tetrahydrofuran (THF) (50 mL). The solution was added drop wise to a suspension of a secondary alcohol (40 mmol) (nonacosan-15-ol for **8a**, tritriacontan-17-ol for **8b**, and heptatriacontan-19-ol for **8c**) in THF (200 mL) at 0 °C. After addition, the reaction mixture was gradually heated to reflux. After 12 h, the reaction mixture was cooled down in an ice/water bath and water was added to quench the reaction. Diethyl ether was added to extract the product. The separated organic phase was washed with saturated $NaHCO_3$ aqueous solution and brine. After removal of solvent under reduced pressure, the crude product was purified by column chromatography using hexanes/ethyl acetate as the eluent, affording **8** as a white solid.

Nonacosan-15-yl 4-bromobutanoate (8a). Yield: 15.1 g, 66%. ^{1}H-NMR (300 MHz, $CDCl_3$) δ 4.92 – 4.84 (m, 1H), 3.46 (t, J = 6.4 Hz, 2H), 2.48 (t, J = 7.2 Hz, 2H), 2.22 – 2.15 (m, 2H), 1.53 – 1.50 (m, 4H), 1.25 (br, 48H), 0.88 (t, J = 6.6 Hz, 6H).

Tritriacontan-17-yl 4-bromobutanoate (8b). Yield: 21.3 g, 85%. ^{1}H-NMR (300 MHz, $CDCl_3$) δ 4.90 – 4.84 (m, 1H), 3.46 (t, J = 6.8 Hz, 2H), 2.48 (t, J = 7.0 Hz, 2H), 2.21 – 2.12 (m, 2H), 1.53 – 1.45 (m, 4H), 1.25 (br, 56H), 0.88 (t, J = 6.3 Hz, 6H).

Heptatriacontan-19-yl 4-bromobutanoate (8c). Yield: 15.4 g, 56%. ^{1}H-NMR (300 MHz, $CDCl_3$) δ 4.92 – 4.84 (m, 1H), 3.46 (t, J = 6.4 Hz, 2H), 2.48 (t, J = 7.2 Hz, 2H), 2.22 – 2.12 (m, 2H), 1.52 – 1.50 (m, 4H), 1.25 (br, 64H), 0.88 (t, J = 6.8 Hz, 6H).

General procedure for the synthesis of 9a~9c

To a two-neck round bottom flask, 6-bromoisatin (1.13 g, 5 mmol), potassium carbonate (1.38 g, 10 mmol), **1** (5 mmol) and *N,N'*-dimethylformamide (40 mL) were added. The reaction mixture was then stirred at 50 °C for 18 h. The solvent was removed and the residual was dissolved in dichloromethane and washed with water. After removal of solvent, the crude product was purified by column chromatography using a mixture of hexanes and ethyl acetate as the eluent, affording **9** as an orange solid.

Nonacosan-15-yl 4-(6-bromo-2,3-dioxoindolin-1-yl)butanoate (9a). Yield: 2.55 g, 71%. ^{1}H-NMR (300 MHz, $CDCl_3$) δ 7.46 (d, J = 7.8 Hz, 1H), 7.28 (dd, J = 8.1 Hz, 1.5 Hz, 1H), 7.23 (d, J = 1.5 Hz, 1H), 4.94 – 4.86 (m, 1H), 3.77 (t, J = 7.5 Hz, 2H), 2.42 (t, J = 6.9 Hz, 2H), 2.05 – 1.96 (m, 2H), 1.54 - 1.52 (m, 4H), 1.25 (br, 48H), 0.88 (t, J = 6.6 Hz, 6H).

Tritriacontan-17-yl 4-(6-bromo-2,3-dioxoindolin-1-yl)butanoate (9b): Yield: 2.56 g, 66%. ^{1}H-NMR (300 MHz, $CDCl_3$) δ 7.46 (d, J = 7.8 Hz, 1H), 7.28 (dd, J = 8.1 Hz, 1.4 Hz, 1H), 7.23 (d, J = 1.4

Hz, 1H), 4.94 – 4.86 (m, 1H), 3.77 (t, J = 7.4 Hz, 2H), 2.42 (t, J = 6.9 Hz, 2H), 2.05 – 1.95 (m, 2H), 1.55 - 1.51 (m, 4H), 1.25 (br, 56H), 0.88 (t, J = 6.9 Hz, 6H).

Heptatriacontan-19-yl 4-(6-bromo-2,3-dioxoindolin-1-yl)butanoate (9c). Yield: 2.45 g, 59%. ^{1}H-NMR (300 MHz, $CDCl_3$) δ 7.46 (d, J = 7.8 Hz, 1H), 7.28 (dd, J = 8.1 Hz, 1.5 Hz, 1H), 7.23 (d, J = 1.5 Hz, 1H), 4.94 – 4.86 (m, 1H), 3.77 (t, J = 7.4 Hz, 2H), 2.42 (t, J = 6.9 Hz, 2H), 2.05 – 1.98 (m, 2H), 1.55 - 1.51 (m, 4H), 1.25 (br, 64H), 0.88 (t, J = 6.9 Hz, 6H).

General procedure for the synthesis of 10a~10c

To a two-neck round bottom flask, **9** (2 mmol), *p*-toluenesulfonic acid (53 mg, 0.28 mmol), 3,7-dihydrobenzo[1,2-*b*:4,5-*b*']difuran-2,6-dione (0.19 g, 1 mmol) and acetic acid (10 mL) were added. The reaction mixture was stirred at 115 °C for 24 h. Upon cooling to room temperature, the reaction mixture was filtered and the filter cake was washed with methanol. The crude product was then purified by column chromatography using a mixture of hexanes and chloroform as the eluent, affording **10** as a black solid.

Di(nonacosan-15-yl) 4,4'-((3*E*,3'*E*)-(2,6-dioxobenzo[1,2-*b*:4,5-*b*']difuran-3,7(2*H*,6*H*)-diylidene)bis(6-bromo-2-oxoindoline-1-yl-3-ylidene))dibutyrate (10a). Yield: 0.56 g, 35%. ^{1}H-NMR (300 MHz, CDCl3) δ 9.06 (s, 2H), 8.90 (d, J = 8.4 Hz), 7.19 (dd, J = 5.1 Hz, 1.6 Hz, 2H), 7.06 (d, J = 1.5 Hz, 2H), 4.94 – 4.90 (m, 2H), 3.83 (t, J = 7.2 Hz, 4H), 2.44 (t, J = 6.9 Hz, 4H), 2.05 – 2.01 (m, 4H), 1.53(br, 4H), 1.23 (br, 96H), 0.87 (t, J = 6.8 Hz, 12H). ^{13}C-NMR (75 MHz, $CDCl_3$) δ 172.57,

167.19, 151.96, 146.76, 135.74, 131.74, 129.47, 127.11, 126.72, 126.07, 126.02, 119.89, 112.10, 112.23, 75.22 39.76, 34.02, 32.12, 31.60, 29.89, 29.75, 29.57, 25.58, 22.89, 14.30.

Di(tritriacontan-17-yl) 4,4'-((3*E*,3'*E*)-(2,6-dioxobenzo[1,2-*b*:4,5-*b*']difuran-3,7(2*H*,6*H*)-diylidene)bis(6-bromo-2-oxoindoline-1-yl-3-ylidene))dibutyrate (10b). Yield: 0.44 g, 26%. ^{1}H-NMR (300 MHz, CDCl3) δ 9.09 (s, 2H), 8.93 (d, J = 8.7 Hz), 7.22 (dd, J = 5.1 Hz, 1.6 Hz, 2H), 7.08 (d, J = 1.5 Hz, 2H), 4.94 – 4.90 (m, 2H), 3.84 (t, J = 7.2 Hz, 4H), 2.44 (t, J = 6.9 Hz, 4H), 2.06 – 2.01 (m, 4H), 1.53(br, 4H), 1.23 (br, 112H), 0.87 (t, J = 6.6 Hz, 12H). ^{13}C-NMR (75 MHz, $CDCl_3$) δ 172.57, 167.19, 151.96, 146.75, 135.74, 131.74, 129.47, 127.01, 126.72, 126.07, 126.02, 119.89, 112.10, 111.20, 75.22 39.76, 34.26, 32.12, 31.60, 29.89, 29.75, 29.57, 25.58, 22.89, 14.30.

Di(heptatriacontan-19-yl) 4,4'-((3*E*,3'*E*)-(2,6-dioxobenzo[1,2-*b*:4,5-*b*']difuran-3,7(2*H*,6*H*)-diylidene)bis(6-bromo-2-oxoindoline-1-yl-3-ylidene))dibutyrate (10c). Yield: 0.44 g, 24%. ^{1}H-NMR (300 MHz, $CDCl_3$) δ 9.10 (s, 2H), 8.94 (d, J = 8.7 Hz, 2H), 7.25 (d, J = 7.8 Hz, 2H), 7.09 (s, 2H), 4.92 (m, 2H), 3.84 (t, J = 6.8 Hz, 4H), 2.44 (t, J = 6.8 Hz, 4H), 2.05 – 2.03 (m, 4H), 1.51 - 1.24 (br, 132H), 0.87 (t, J = 6.4 Hz, 12H). ^{13}C-NMR (75 MHz, $CDCl_3$) δ 172.56, 167.19, 151.97, 146.76, 135.77, 131.72, 129.46, 127.03, 126.75, 126.13, 126.01, 119.90, 112.06, 111.19, 75.21 39.70, 34.26, 32.12, 31.59, 29.90, 29.76, 29.57, 25.57, 22.89, 14.32.

General procedure for the synthesis of P-33, P-37, and P-41.

To a Schlenk flask, **10** (0.0453 mmol), 5,5'-bis(trimethylstannyl)-2,2'-bithiophene (22.6 mg, 0.0453 mmol), tri(*o*-tolyl)phosphine (1.1 mg, 3.6 μmol), tris(dibenzylideneacetone)dipalladium (0.8 mg, 0.9 μmol) and anhydrous chlorobenzene (4 mL) were added under argon atmosphere. The reaction mixture

was then stirred at 130 °C for 48 h. Upon cooling to room temperature, the reaction mixture was poured into methanol and the precipitate was collected by filtration, followed by Soxhlet extraction.

P-33: This polymer was purified by Soxhlet extraction using acetone, hexanes, chloroform and TCE. Yield: 71 mg, 98% (from the TCE fraction).

P-37: This polymer was purified by Soxhlet extraction using acetone, hexanes and chloroform. Yield: 74 mg, 95% (from the chloroform fraction).

P-41: This polymer was purified by Soxhlet extraction using acetone, hexanes and chloroform. Yield: 76 mg, 92% (from the chloroform fraction).

Chapter 4. Unipolar N-type NDIO-based Polymers

4.1 Introduction

Nowadays one of the most widely studied n-type conjugated polymers are the ones based on the strong electron-deficient building block, naphthalene diimide (NDI) (Figure 4-1).[72,163–168] For example, the copolymer of NDI-20 and bithiophene (Figure 4-1), namely **P(NDI2OD-T2)**, was found to show excellent electron charge transport property back in 2009 by He *et al.*, used as channel material in OTFTs, showing electron mobility between 0.45 and 0.85 $cm^2 V^{-1} s^{-1}$[94], while at that time, the other n-type organic semiconductors were only showing electron mobility around 0.01 $cm^2 V^{-1} s^{-1}$.[169–171] With such a huge breakthrough, this polymer was commercialized by Polyera and became the benchmark n-type polymer semiconductor for OTFTs.[95,129,167] Meanwhile researchers also attempted to use **P(NDI2OD-T2)** to replace **PCBM** as acceptor material in all-PSCs given the promising electron transport properties. Due the immiscibility and energy level mismatch between **P(NDI2OD-T2)** and the donor materials such as **P3HT**, the PCEs of these all-PSCs were all below 2%.[122,148,172] It was not until 2014 when Mori *et al.* introduced the donor polymer, **PTB7-Th**, in all-PSCs and achieved high PCE up to 5.7%[72] that **P(NDI2OD-T2)** gained considerable attention in the field of fullerene-free solar cell. Since then, numerous efforts were made to further improve the performance of **P(NDI2OD-T2)**-based all-PSCs, including using different donor building blocks for the polymer backbone[73,74,77], side chain engineering[76,82], using different donor materials[13,83,165,173] for the solar cells and fabrication optimization[74,81,174]. For instance, Fan *et al*. reported the optimization by choosing the processing solvent judiciously, controlling the molecular weight of **P(NDI2DT-T2)** and optimizing the active layer thickness. A record high PCE of

9.16% was realized[174], which is already approaching the high PCEs of fullerene-based OSCs.[24,53,54,56]

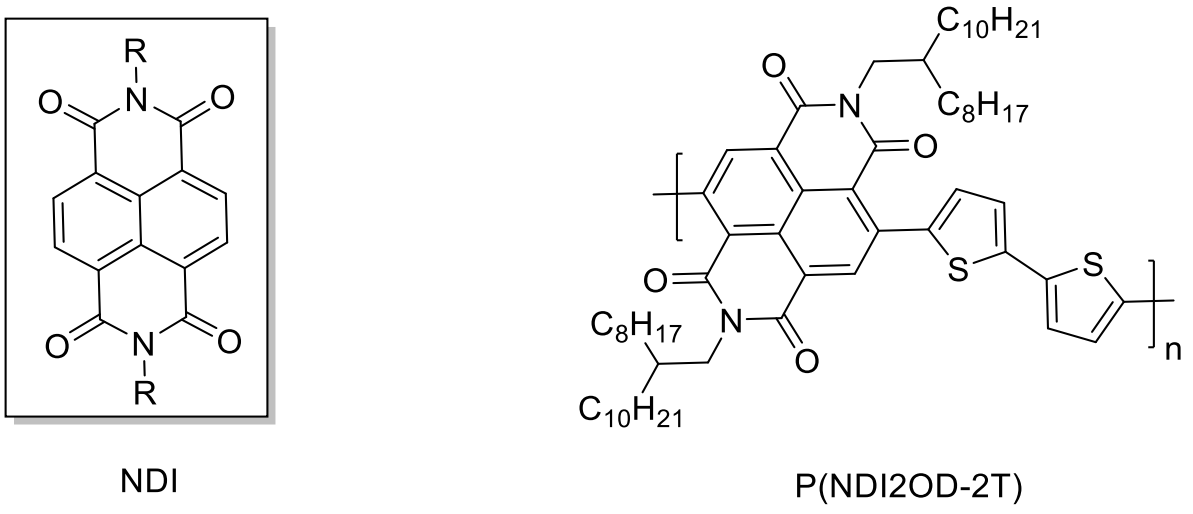

Figure 4-1 The chemical structures of NDI and P(NDI2OD-2T).

Despite all these advancements in tuning the performance of NDI-based polymers in all-PSCs, the FF (0.40-0.55) and J_{SC} (<12 mA cm^{-2})[78,122,173,175] of these solar cells are still significantly behind those (0.7-0.8 for FF and ~20 mA cm^{-2} for J_{SC}) of high-performance fullerene based OSCs.[24,56] It is generally believed the FF of all-PSCs is limited due to three main causes: relatively low bulk charge carrier mobilities, imbalanced charge transport and bimolecular recombination. Realizing a high FF requires simultaneously improvement on these three aspects. Jung *et al.* used a fluoro-substituted bithiophene units on the backbone of an n-type NDI polymer backbone to increase the electron affinity and electron transport. The resultant polymer, **P(NDI2OD-FT2)**, demonstrated a deeper HOMO level of -5.9 eV and a high PCE of 6.29% was obtained by the fluoro-substituted polymer compared to 5.21% of **P(NDI2OD-T2)** under the same conditions.[75] Their success was mainly attributed to the enhancement of charge generation and less bimolecular recombination, leading to the raised short-

circuit current density (J_{SC}) and fill factor (FF), and PCE. On the other hand, a number of studies have shown that the NDI-based polymers generally adopted an mixture of edge-on and face-on molecular orientations in solid state while **PTB7-Th** is completely face-on orientated.[122,176–178] The suboptimal orientation match leads to less efficient exciton dissociation at the D-A interface and higher germinate recombination than fullerene/polymer BHJ, which are believed to be one of the main causes for inferior J_{SC} and FF in all-PSCs, respectively. Their studies have triggered the thought that chemically modifying the NDI moiety to enhance the bulk electron transport and improve the energy level matchup is of significance for achieving high performance all-PSCs.

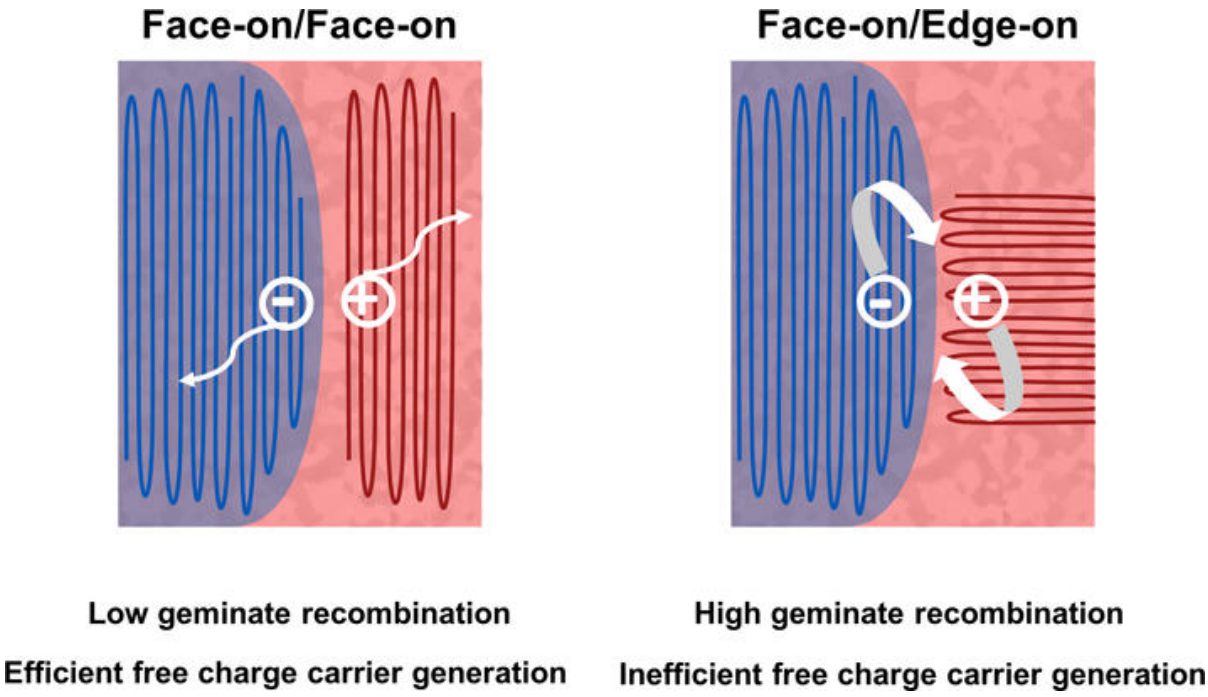

Figure 4-2 The importance of molecular orientation control at the D−A Interface of all-PSCs.[66]

In this chapter, we report for the first time the use of a new electron deficient building block, NDIO, in π-conjugated polymers. We synthesized a promising unipolar n-type NDIO-based polymers, **PNDIOT**, which feature the addition of an alkoxyl chain to the nitrogen atoms of the NDI moiety (Figure 4-3)

with the intention of lowering the HOMO and LUMO levels to facilitate the electron transport properties and improve the resultant solar cell performance. Previously, Kantchev *et al*. reported the structure of NDIO. They found with the alkoxy substitution, the NDIO moieties showed a deeper LUMO and HOMO levels.[179] Furthermore, the π-π interaction between the NDIO molecules were predicted to be stronger due to the stabilized flat conformation. Herein, we managed to brominate NDIO and used it to form a D-A polymer, **PNDIOT**, whose backbone is comprised of NDIO and thiophene (T). The polymer will be first fully characterized with several techniques. Then the charge transport properties will be evaluated in OTFTs in both glovebox and air to assess the performance robustness in ambient conditions. Finally, the polymer will be used as acceptor in all-PSCs with **PTB7-Th** and the structure-property relationship will be investigated by using AFM, XRD and SCLC.

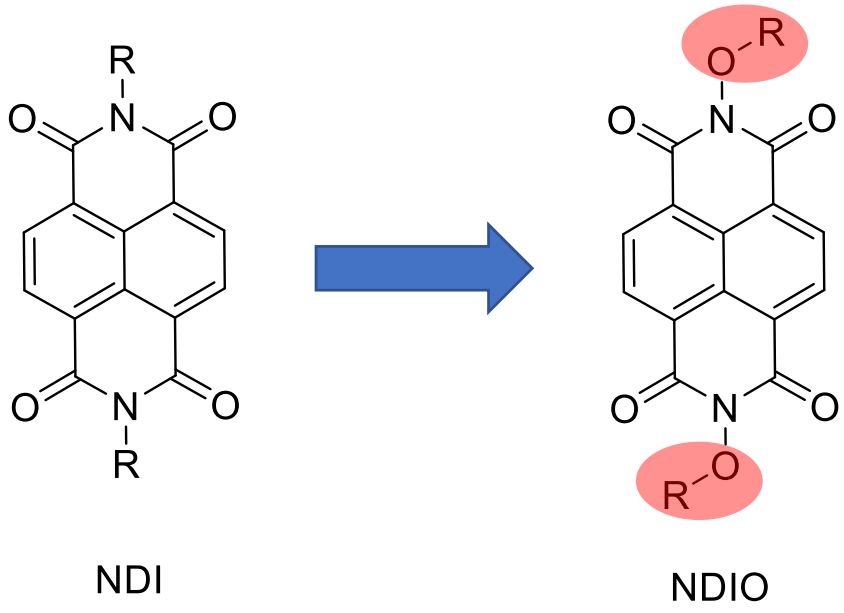

Figure 4-3 The chemical structure of NDIO moiety.

4.2 Results and Discussion

We started our synthesis with the monomer, NDIO20-Br (R = 2-octyldodecyl), which was provided by our collaborator. At first, bithiophene was chosen as the donor building block. The polymerization was conducted via Stille coupling using the toluene/$Pd(PPh_3)_2Cl_2$ system. The resultant polymer, PNDIOBT (Scheme 4-1), showed very poor solubility in chlorobenzene. Soxhlet extraction with chlorobenzene only yielded 15% of the crude polymer, with the remaining as insoluble solid. The dissolved polymer fraction was subject to HT-GPC measurement to confirm the molecular weight. M_n of 22.3 kDa was found with a PDI of 6.2. In previous studies, the NDI analogue, **P(NDI2DT-2T)**, demonstrated good solubility and processability in chlorobenzene even with a high M_n of 91.7 kDa. Such a dramatic difference implies that NDIO based polymers have a stronger π-π interaction among polymer chains than the NDI-based polymers, which is due to large spacer group between the alkyl branches and the NDI core. The stronger π-π interaction can bring the polymer chains closer to each other and favor the interchain charge hopping and the overall charge transport performance.[43,104,118,119] To improve the solubility of the polymer, thiophene was used as the donor building block instead to form **PNDIOT** (Scheme 4-1), which was synthesized by reacting NDIO20-Br with 2,5-bis(trimethylstannyl)thiophene via. The crude polymer was precipitated in methanol and then subject to Soxhlet extraction with acetone, hexanes and chloroform. The chloroform fraction was dried under vacuum to afford **PNDIOT** as a purple solid in a yield of 94%. The molecular weight was determined by HT-GPC using 1,2,4-trichlorobenzene at 140 °C (Figure 4-4). The number average molecular weight (M_n) was found to be 68.5 kDa with a PDI of 2.3. The thermal stability of the polymer was characterized by TGA (Figure 4-5). A 5% weight loss was observed at 370 °C for **PNDIOT**, indicating good thermal stability of this

polymer. We also conducted DSC on **PNDIOT**. However, no noticeable endo- or exothermic transitions were observed in the range of -20 °C and 300 °C (Figure 4-6).

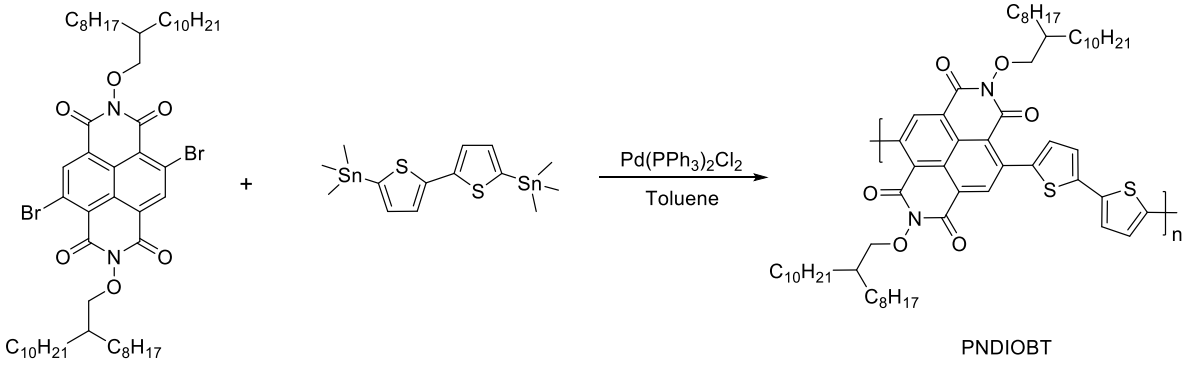

NDIO20-Br PNDIOBT

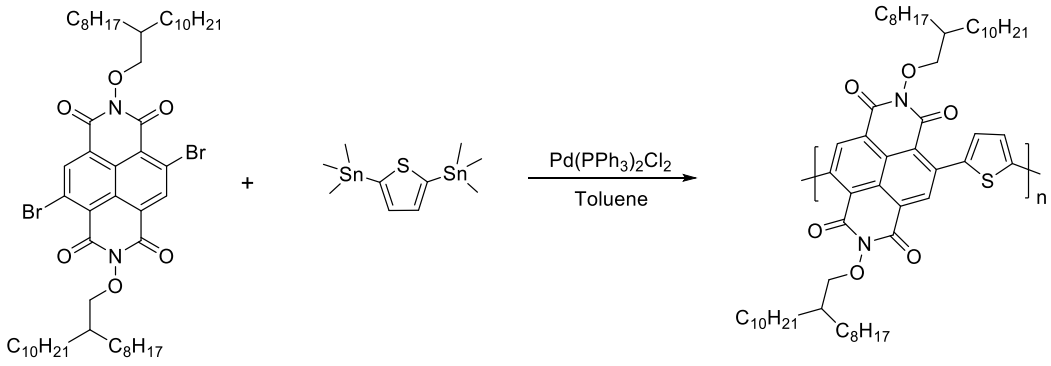

NDIO20-Br PNDIOT

Scheme 4-1 The reaction formulas for Stille coupling polymerization using NDIO20-Br. Reaction conditions: toluene/ $Pd(PPh_3)_2Cl_2$/110 °C, 48 h, 15% for PNDIOBT and 94% for PNDIOT.

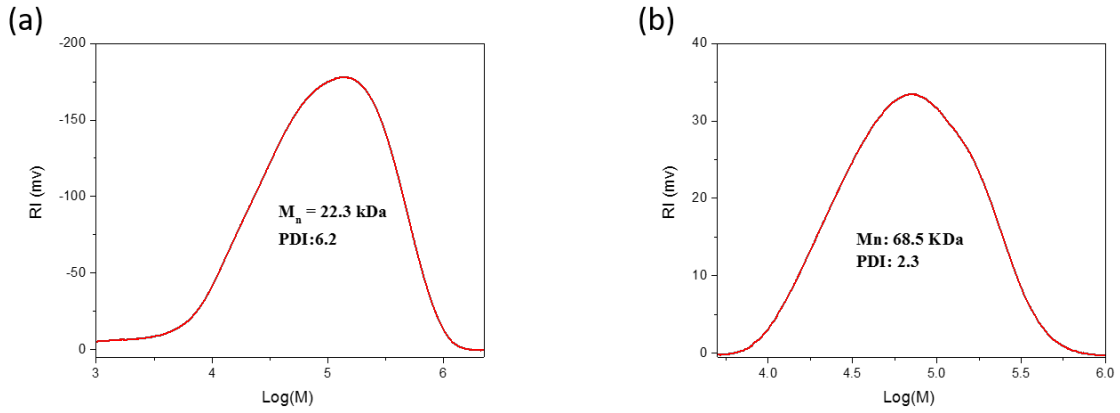

Figure 4-4 The molecular weight distribution for **PNDIOBT (a)** and **PNDIOT (b)** obtained by HT-GPC.

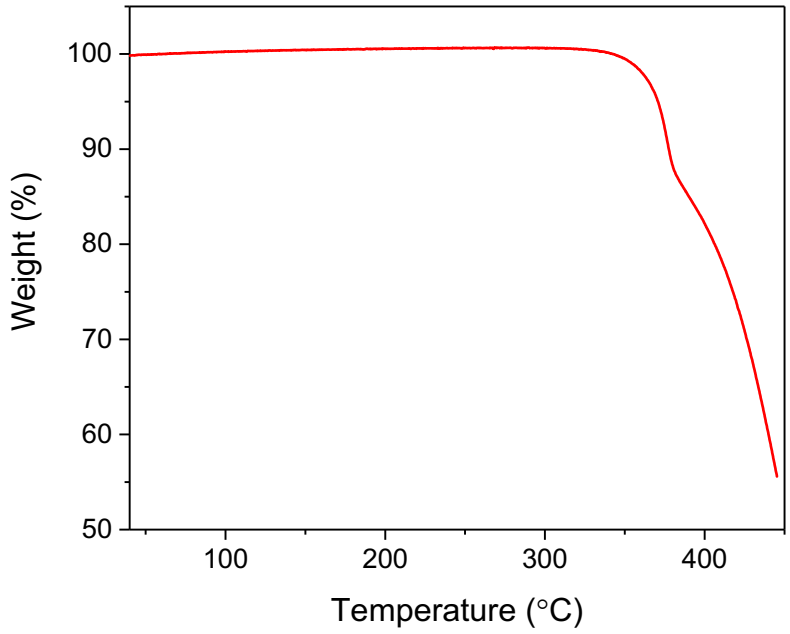

Figure 4-5 The TGA diagrams for **PNDIOT** conducted under nitrogen.

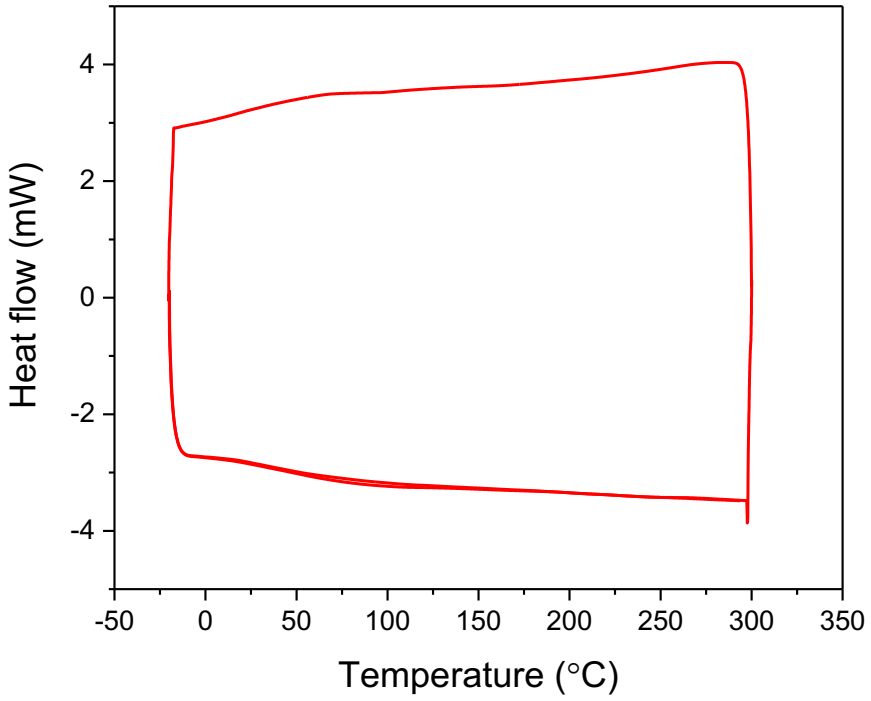

Figure 4-6 The DSC diagram for **PNDIOT** obtained at 20 °C/min.

Figure 4-7 shows the UV–vis-IR absorption spectra of **PNDIOT** for both the dilute solution (~10^{-6} M in chloroform) $CHCl_3$ and as-spun film. Both spectra show two distinctive absorption peaks, the π–π* transition peak and the intramolecular charge transfer (ICT) peak. Compared to the solution absorption, both peaks of thin film absorption were red-shifted from 336 nm to 341 nm and 588 nm to 598 nm. This red-shifting is attributed to the chain packing in the solid state that makes the backbone more coplanar and reduces the bandgap. It is interesting that the ICT peak has become stronger in thin film absorption, which implies potentially better visible light harvesting for the all-PSC devices. The absorption coefficient (α) of the as-spun thin film was determined to be ~2.7×10^4 cm^{-1}, comparable to those of **PNDIT** ($3\sim5\times10^4$ cm^{-1}).[72] The optical bandgap of the thin film was estimated to be 1.89

eV by using the absorption onset. As shown in Figure 4-8, cyclic voltammograms of **PNDIOT** exhibited a strong reversible reduction process and no noticeable oxidation peak in the range of 0 and 1.4 V. Based on the onset reduction and oxidation potentials (reduction onset = −0.72 V), the LUMO level is estimated to be −4.08 eV. Due to absence of oxidation peak, the HOMO was calculated by subtracting the optical bandgap from the LUMO level, giving a HOMO level of -5.98 eV. Comparing to the HOMO/LUMO levels (-5.77 eV/-4.0 eV)[73] of the NDI analogue, **PNDIT**, **PNDIOT**'s HOMO/LUMO levels were lowered by 0.08 eV and 0.21 eV due to the electron withdrawing effect from the alkoxy side groups. The LUMO and HOMO offsets of **PTB7-Th** and **PNDIOT** are up to 0.58 eV and 0.62 eV, which are much larger than the empirical value of 0.3 eV required for charge separation[26]. As we will see later, the large offsets are very adequate for charge separation. We also noticed **PNDIOT** has a larger optical bandgap than **PNDIT** while it has a larger M_n. One possible reason is that the alkoxy side chains have increased the dielectric constant of the polymer, which led to a smaller binding energy and larger optical bandgap for **PNDIOT**. A similar study was reported in literature.[180]

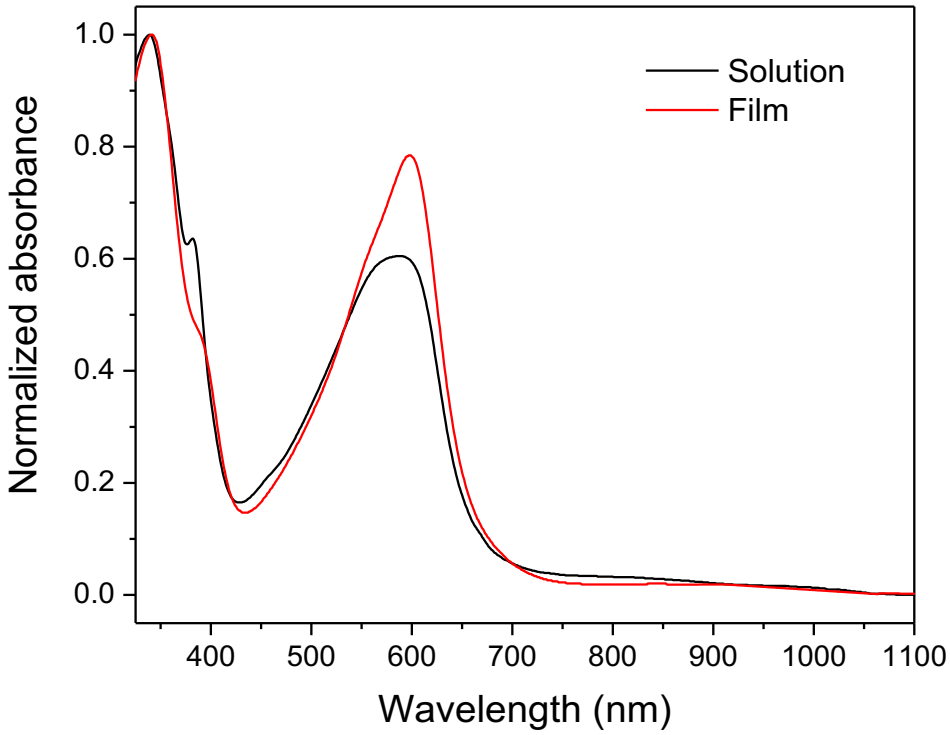

Figure 4-7 The absorption profile of in **PNDIOT** solution (chloroform) and thin film.

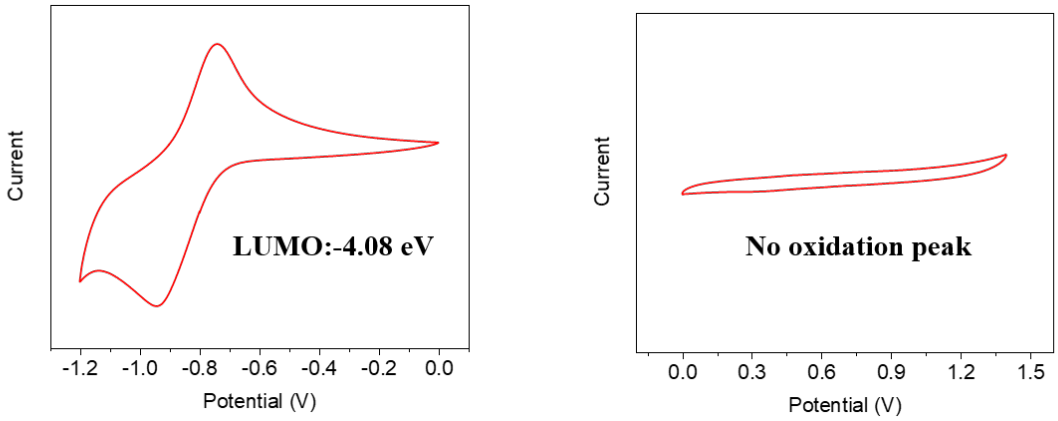

Figure 4-8 The cyclic voltammetry diagrams for **PNDIOT**: reduction process (a) and oxidation process (b).

Table 4-1 Molecular Weight, thermal stability, electrochemical and photophysical properties of **PNDIOT** and **PNDIT.**

Polymer	M_n (kDa)	PDI	T_d (°C)	HOMO/LUMO (eV)	E_g (eV)	λ_{max}^{film} (nm)	λ_{max}^{sol} (nm)
PNDIOT	68.5	2.3	370	-5.98/-4.08	1.89	341, 598	336, 588
PNDIT[a]	23.9	1.3	430	-5.77/-4.0	1.77	341,598	326, 542

[a] The numbers can be found in the reference.[73]

The charge transport property of **PNDIOT** was investigated by fabricating the OTFTs. The BGBC OTFT device was fabricated on SiO_2/Si wafer with Au electrode pairs as the source and drain contacts. The polymer film was spin-coated using a chloroform solution (5 mg/mL) and then subject to different annealing temperatures (100 °C, 150 °C and 200 °C) in a nitrogen filled glovebox. The devices were tested in the same glovebox. All devices showed unipolar n-type charge transport characteristics (Table 3). The best performance was achieved at annealing temperature of 150 °C, where the devices showed electron mobility up to 5.4×10^{-3} cm^2 V^{-1} s^{-1} with an average of 4.1×10^{-3} cm^2 V^{-1} s^{-1}. With PNDIT's FET mobility only being on the order of 10^{-4} to 10^{-5} cm^2 V^{-1} s^{-1},[73,163] our result represents a significant enhancement in electron charge transport performance, which can be attributed to the stronger π-π interaction and higher electron affinity. Under the same conditions, previously, several n-type polymer OTFTs were reported to show stable or decently stable operation under ambient conditions. For instance, the fluorinated **PIBDFBT-40**, **F_4-BDOPV-2T**, showed excellent electron charge transport property in air, with electron mobility up to 14.9 cm^2 V^{-1} s^{-1}.[181] Zhang *et al*. showed long term stability of the IBDF polymer based OTFT in air. They found the OTFT device was still able to show 0.65 cm^2 V^{-1} s^{-1} electron mobility and 10^4 on/off current ratio after exposed in air for 70 days.[100] It

is worth noting that all these OTFT devices were in a top-gate bottom-contact device configuration, in which the conductive channel is protected by the dielectric and gate contact layers. Herein, we tested the air stability of the BGBC devices in an ambient environment with RH of ~50%. For the **PNDIOT** based devices, the electron mobility was able to remain 65% of what it was in the glovebox, with an electron mobility of 2.8×10^{-3} cm^2 V^{-1} s^{-1} on average and 3.9×10^{-3} cm^2 V^{-1} s^{-1} at maximum. On the other hand, we also fabricated the OTFTs using **P(NDI2OD-T2)** as the channel material under the same conditions. In the glovebox, the best performance of **P(NDI2OD-T2)**-based devices was achieved at 150 °C annealing temperature. The highest electron mobility observed was up to 0.013 cm^2 V^{-1} s^{-1} with an average of 1.1×10^{-2} cm^2 V^{-1} s^{-1}. In the air, however, **P(NDI2OD-T2)**-based devices showed significant decrease in the electron mobility with only 2.2×10^{-3} cm^2 V^{-1} s^{-1} on average and 3.4×10^{-3} cm^2 V^{-1} s^{-1} at maximum, leading to an 80% drop from what it was in glovebox. It is clear that **PNDIOT** is a much more robust n-type semiconductor in the air than **P(NDI2OD-T2)**, which can be attributed to the deep-lying LUMO level (~-4.1 eV). Moreover, the p-type charge transport in **P(NDI2OD-T2)** has become quite prominent leading to a ambipolar charge transport characteristic, while the charge transport in **PNDIOT** remained unipolar n-type characteristic. The enhanced p-type charge transport in air was also reported by previous studies. Lei *et al*. found that the oxygen in the air would p-doped the HOMO level of PIBDFBT-40 and led to occurrence of p-type charge transport characteristic. **P(NDI2OD-T2)** has a similar HOMO level with PIBDFBT-40 (both around -5.7 eV)[75,99] and therefore **P(NDI2OD-T2)** showed a similar behaviour in the air. While **PNDIOT** has a HOMO level of ~6.0 eV, it seems that the HOMO is deep enough to resist the oxygen doping and the polymer can maintain unipolar n-type charge transport characteristic. Finally, we stored the device in the air over a period of 24 days and monitored the device performance. In the first two weeks, the electron mobility

slowly dropped to around 1.6×10^{-3} cm^2 V^{-1} s^{-1} and after that the electron mobility seemed to stabilize at around 1.6×10^{-3} cm^2 V^{-1} s^{-1}. Our results showed that **PNDIOT** with deep-lying LUMO and HOMO levels is robust n-type semiconductor and suitable for n-type OTFT operation in the air.

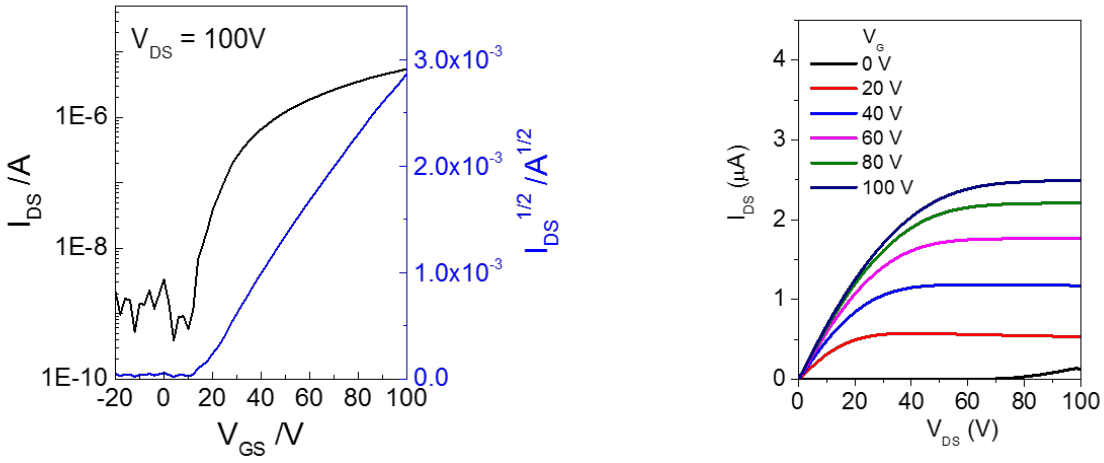

Figure 4-9 Transfer and output curves of BGBC OTFT devices annealed at 150 °C for **PNDIOT** films tested in a glovebox. Device dimensions: channel length (L) = 30 μm; channel width (W) = 1000 μm.

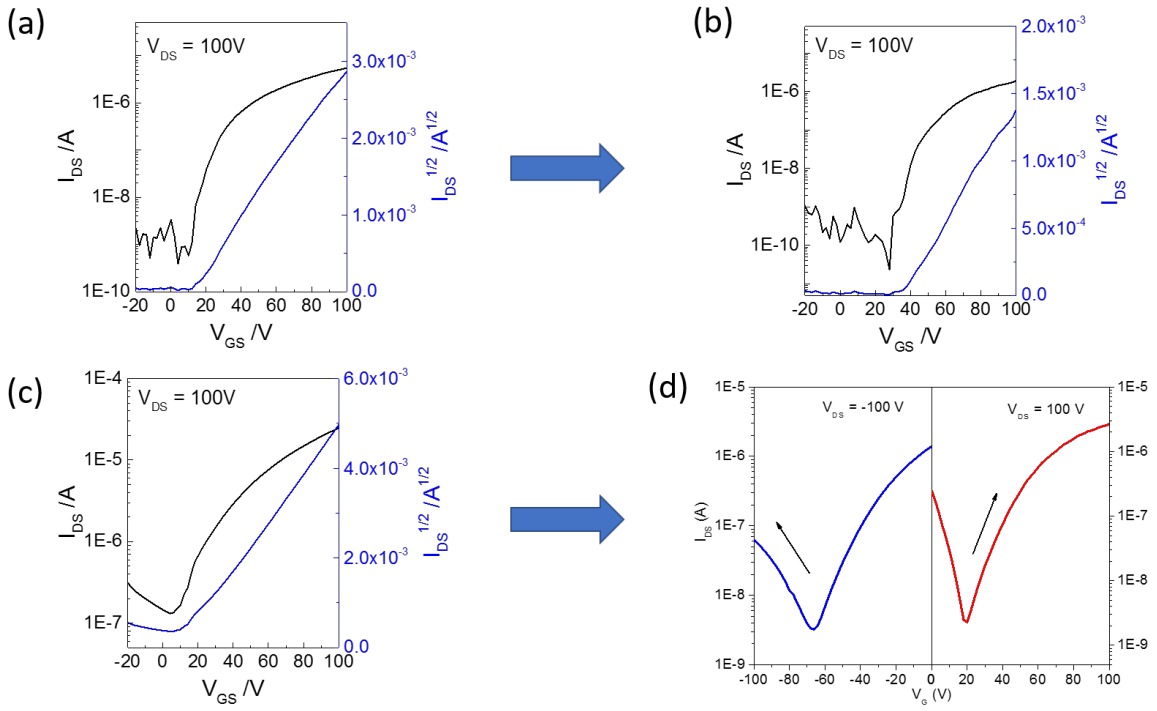

Figure 4-10 Transfer curves of BGBC OTFT devices annealed at 150 °C and tested in nitrogen or air: **PNDIOT**, in a glovebox (a) and air (b); **P(NDI2OD-T2)**, in nitrogen (c) and air (d). Device dimensions: channel length (L) = 30 μm; channel width (W) = 1000 μm.

Table 4-2 A summary of the OTFT performance **of PNDIOT** and **P(NDI2OD-T2).**

Polymer	Environment	T_{Ann} (°C)	$\mu_{e,avg}$ (std) ($cm^2\ V^{-1}\ s^{-1}$)	V_{th} (V)	I_{on}/I_{off}	$\mu_{h,avg}$ (std) ($cm^2\ V^{-1}\ s^{-1}$)	V_{th} (V)	I_{on}/I_{off}
PNDIOT	Nitrogen	100	0.0020 (0.0005)	15	~10^3			
		150	0.0041 (0.0009)	13	~10^4			
		200	0.0016 (0.0002)	21	~10^3			

P(NDI2OD-T2)	Air	150	0.0028 (0.0008)	33	~10^4			
		100	0.0087 (0.001)	10	~10^3			
	Nitrogen	150	0.011 (0.002)	9	~10^3			
		200	0.010 (0.001)	11	~10^3			
	Air	150	0.0022 (0.0008)	20	~10^3	2.6×10^{-4} (1.0×10^{-4})	-65	10

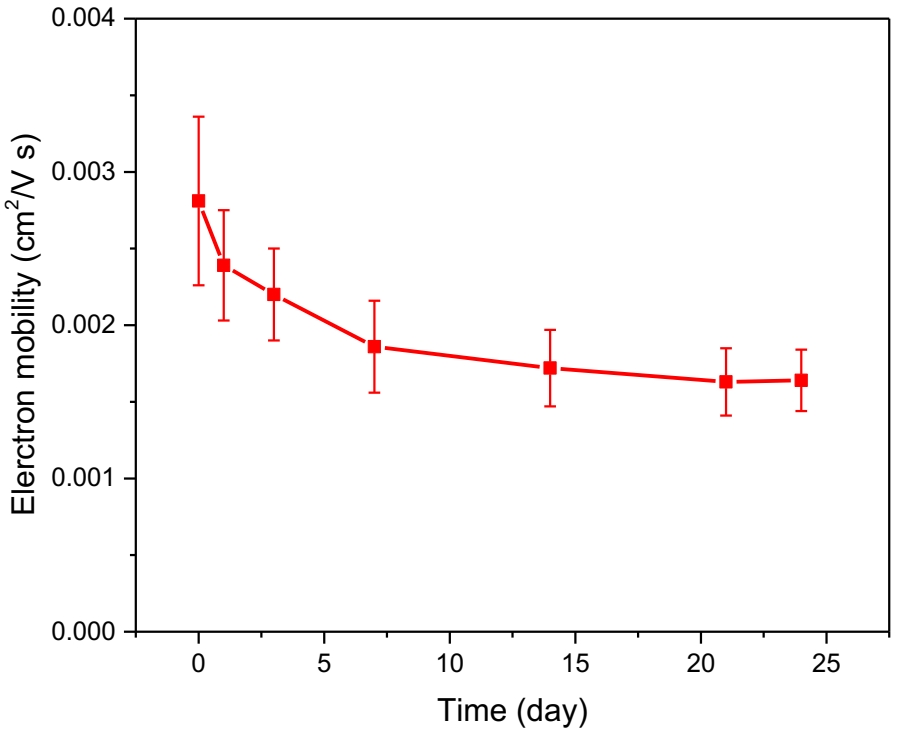

Figure 4-11 The long-term stability of **PNDIOT**-based OTFT device in ambient conditions.

We used **PNDIOT** as electron acceptor and **PTB7-Th** as electron donor to fabricate all-PSC devices. The device configuration was ITO/PEDOT:PSS/**PTB7-Th**:**PNDIOT**/LiF/Al. Chlorobenzene was chosen as the processing solvent for the active layer since both polymers demonstrated excellent solubility in chlorobenzene (>10 mg/mL). Initially, the optimal donor/acceptor ratio and active layer thickness were determined to be 1:1 and 113±5 nm (Table 4-4 & 4-5). Fabricated under these optimal conditions, the best device exhibited a promising PCE of 2.92% (V_{OC} = 0.75 V, J_{SC} = 6.73 mA cm^{-2}, and FF = 0.59) with an average PCE of 2.68%. Previously solvent annealing was reported to have a positive effect on the device performance.[182–184] We tried the solvent annealing treatment for 15 and 30 minutes on the polymer blend. However, they only led to a slight decrease in performance with the highest PCE of 2.73% and average PCE of 2.55% (Table 4-6). Furthermore, we tried aging the film before the anode deposition to improve the device performance. After the film aged in the glovebox for 24 hours, the PCE improved up to 3.25% (Figure 4-12 & Table 4-6) (V_{OC} = 0.75 V, J_{SC} = 7.11 mA cm^{-2}, and FF = 0.61) with an average PCE of 3.03%, which is superior to the NDI analogue in the same device configuration[77] and slightly lower than the devices based on **P(NDI2OD-T2)** under the same device configuration [81]. We also tried using 1,8-diiodooctane (DIO) as additive in the solvent to improve the morphology. However, both 0.5 vol% and 1 vol% DIO in CB led to a significant drop in performance (Table 4-7). The J_{SC} value was well matched (within 10% error) with the integrated J_{SC} values obtained from the EQE spectrum (Figure 4-12). EQE spectrum showed two peaks with EQEs around 40% at 710 nm and 370 nm, respectively, which can be attributed to the absorption of **PTB7-Th** and **PNDIOT**. The relatively low EQE values (~40%) for the **PNDIOT**-based device was found to be caused by the unfavourable charge dissociation at the interface (discussion below). The relatively low J_{SC} seems to originate from the poor light harvesting in the region of 400 nm to 600 nm. This can

be further improved by modifying the backbone structure to boost the absorption[175,185] or using an donor that has complementary absorption.[173]

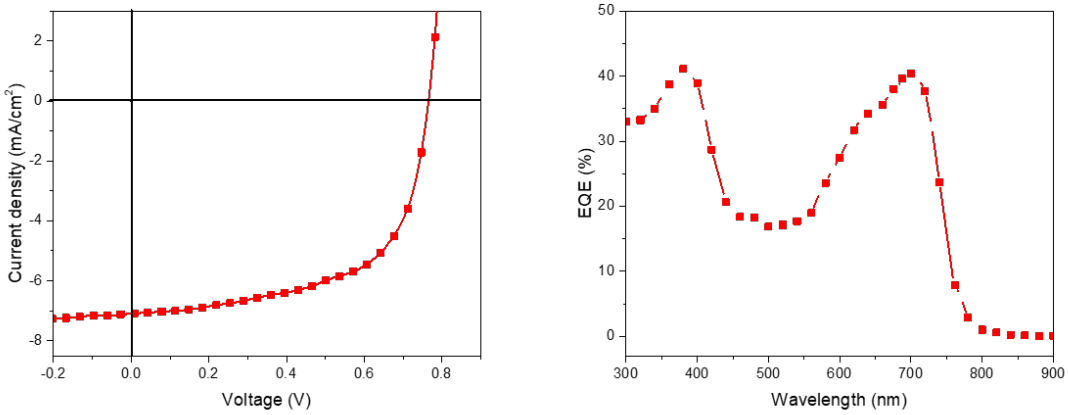

Figure 4-12 The J-V characteristic and EQE spectrum for the solar cell device based on **PNDIOT**:**PTB7-Th**. The active layer (1:1 wt ratio) was spin-coated using a solution (11 mg/mL) in chlorobenzene at 1300 rpm and aged for 24 hrs.

Table 4-3 A summary of all-PSCs based on different acceptors

Acceptor	J_{SC} (mA/cm^2)	V_{OC} (V)	FF	PCE (%)	μ_e (cm^2 V^{-1} s^{-1})	μ_h (cm^2 V^{-1} s^{-1})
PNDIOT	7.11	0.75	0.61	3.25 (3.03)[a]	6.93×10^{-5}	1.35×10^{-4}
P(NDI2OD-T2)[b]	9.4	0.81	0.49	3.70 (3.40)[a]	2.0×10^{-3}	2.0×10^{-4}
PNDIT[c]	8.84	0.80	0.43	3.03 (2.87)[a]	6.7×10^{-6}	2.0×10^{-4}

All devices used **PTB7-Th** as the donor and the same device configuration: ITO/PEDOT:PSS/Polymer Blend/LiF/Al; [a] The average value was obtained from a batch of 4 devices; [b] The numbers can be found from the reference.[81] [c] The numbers can be found from the reference.[77]

Table 4-4 The optimization of D/A ratio in the active layer

D/A ratio	Thickness (nm)	J_{SC} (mA/cm^2)	V_{OC} (V)	FF	PCE (%)
1:1	98 ± 6	5.89	0.75	0.59	2.61 (2.50)[a]
1.5:1	92 ± 5	6.06	0.75	0.48	2.18 (2.02)[a]
1:1.5	97 ± 5	4.12	0.74	0.52	1.58 (1.39)[a]

A solution with a total concentration of 11 mg/mL and a spin speed of 1500 rpm were used for spin-coating the active layer for these solar cells. [a] The average value was obtained from a batch of 4 devices.

Table 4-5 The optimization of active layer thickness

D/A ratio	Thickness (nm)	J_{SC} (mA/cm^2)	V_{OC} (V)	FF	PCE (%)
1:1	98 ± 6	5.89	0.75	0.59	2.61 (2.50)[a]
1:1	113 ± 5	6.73	0.75	0.59	2.92 (2.68)[a]
1:1	127 ± 8	6.14	0.75	0.56	2.59 (2.44)[a]

The active layers were formed by using a blend solution (11 mg/mL) at different spin speeds (1500 rpm, 1300 rpm and 1000 rpm). [a] The average value was obtained from a batch of 4 devices.

Table 4-6 Device performance optimization through post-treatment

Post-treatment	Duration	J_{SC} (mA/cm^2)	V_{OC} (V)	FF	PCE (%)
None	N/A	6.73	0.75	0.59	2.92 (2.68)[a]

Solvent-annealing	15 min	6.77	0.74	0.55	2.73 (2.55)[a]
	30 min	6.09	0.74	0.51	2.30 (2.04)[a]
Film-aging	24 hrs	7.11	0.75	0.61	3.25 (3.03)[a]
	72 hrs	6.88	0.75	0.61	3.15 (3.00)[a]

The active layers were formed by using a blend solution (D/A ratio 1:1, 11 mg/mL) at 1300 rpm. [a] The average value was obtained from a batch of 4 devices. Solvent annealing was performed in a Petri dish at room temperature and film aging was performed by storing the device in a glovebox.

Table 4-7 Device performance optimization by using DIO as additive

DIO content	J_{SC} (mA/cm^2)	V_{OC} (V)	FF	PCE (%)
0.5 vol%	4.12	0.75	0.56	1.73 (1.56)[a]
1 vol%	3.67	0.75	0.53	1.46 (1.20)[a]

The active layers were formed by using a blend solution (D/A ratio 1:1, 11 mg/mL) at 1300 rpm. [a] The average value was obtained from a batch of 4 devices.

It was worth noting that the FF of 0.61 for the **PNDIOT**-based device is much higher than those of the **P(NDI2OD-T2)** or **PNDIT** devices, for which the FF is usually between 0.40 to 0.55. The improved FF can be related to the suppressed bimolecular recombination (see below) and balanced hole and electron mobilities (1.35×10^{-4} cm^2 V^{-1} s^{-1} for hole and 6.93×10^{-5} cm^2 V^{-1} s^{-1} for electron), which were obtained from the SCLC measurement of the hole-only device and electron-only device (Figure 4-13) mentioned in the previous chapter. The light intensity dependence of the J–V characteristics was investigated to probe the bimolecular recombination that affects the device performance. It has been

reported that the correlation between J_{SC} and illumination intensity (P) can be addressed by $J_{SC} \propto P^{\alpha}$ where α should be unity when the bimolecular recombination is negligible (maximum carrier swept out). We investigated the relationship between J_{SC} and P and found the α for the solar cell based on **PTB7-Th: PNDIOT**. The higher α value of the device based on **PTB7-Th: PNDIOT** (0.945) than that of **PTB7-Th: P(NDI2OD-T2)** (0.886)[75] clearly indicates that bimolecular recombination is significantly suppressed when **PNDIOT** was used as the electron acceptor, which is probably due to the larger dielectric constant in the **PNDIOT**. All these results prove that NDIO polymers is a promising class of n-type semiconductors for high-performance all-PSCs, and with further material optimization[175,186] they can achieve an excellent photovoltaic performance.

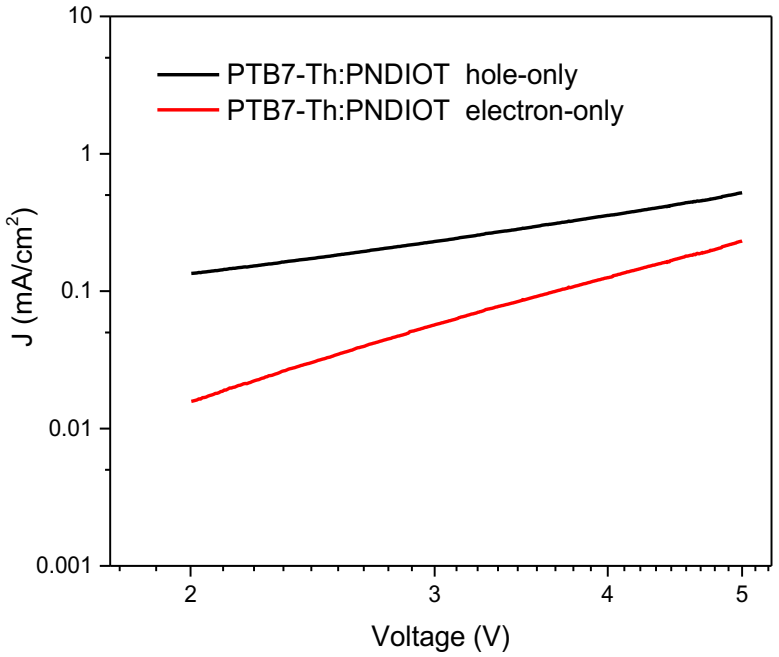

Figure 4-13 The J-V characteristics for the hole-only and electron-only devices for **PTB7-Th**:**PNDIOT** blend.

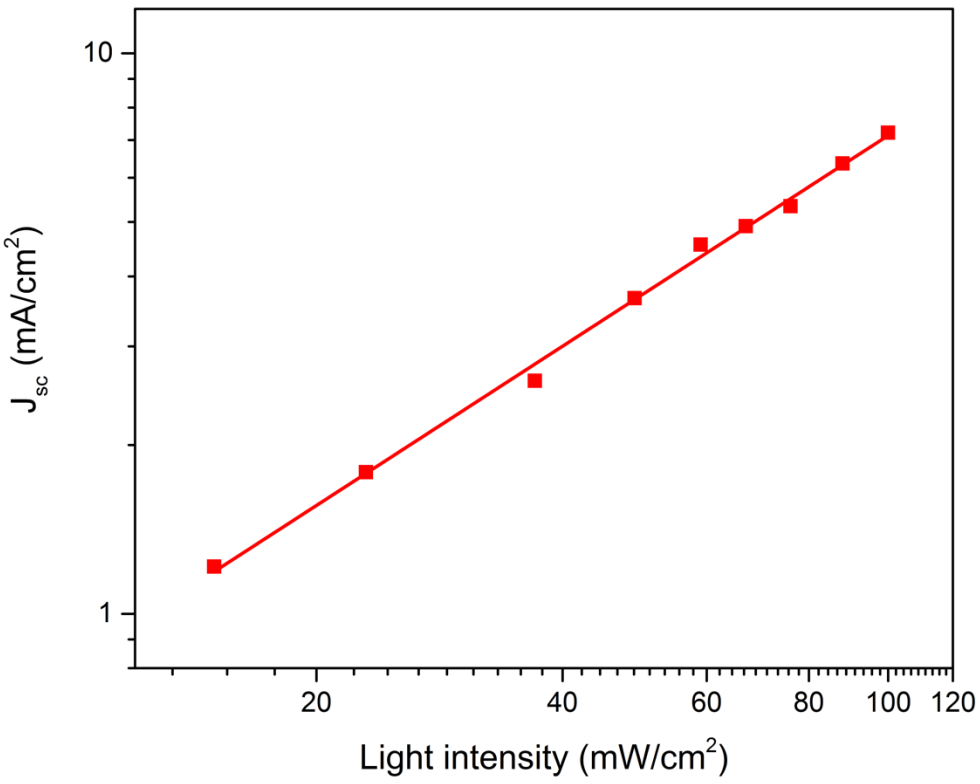

Figure 4-14 The J_{SC} dependence on light intensity for the **PNDIOT**-based solar cell.

Another important factor that has a great impact on the performance of all-PSCs lies on the appropriate nanoscale phase-separated morphology. For bulk heterojunction solar cells, the ideal blend morphology will be the bi-continuous interpenetration network with a phase dimension around 20 nm. Since the charge transport in polymer semiconductor is highly anisotropic. Therefore, the molecular orientations of the donor polymer and acceptor polymer should match in order to for efficient exciton dissociation and charge generation. The atomic force microscopy (AFM) topographical image of the **PTB7-**

Th:PNDIOT blend film is shown in Figure 4-15. Nanostructures with fine phase-separated domains (~100 nm) was clearly observed in the blend film with a RMS of 1.01 nm. Such blend morphology is considered beneficial for exciton dissociation and charge generation. Further, the molecular orientation of the polymer blend film and individual neat films were investigated by using the reflective X-ray diffraction technique (Figure 4-15 and 4-16). The **PTB7-Th** neat film only showed a (010) diffraction peak at 2θ = 22.5 °, indicating **PTB7-Th** intrinsically prefers a face-on orientation. This is in good agreement with previous studies.[74,76,77,79,187] On the other hand, **PNDIOT** neat film showed a strong (100) peak at 2θ = 3.84 ° and a very weak (010) at 2θ = 23.6 °, indicating **PNDIO** prefers the edge-on orientation over the face-on orientation. The d-spacing of (010) for **PNDIOT** was 0.376 nm, which is significantly reduced compare to that of **PNDIT** reported in literature (0.420 nm).[73] This has consolidated the stronger π-π interaction of **PNDIOT** owing to the alkoxy side chain. The blend film of **PTB7-Th** and **PNDIOT** exhibited both the (100) at and (010) diffractions for the polymer crystallines, indicating a mixed edge-on and face-on orientation of the polymer crystallites, which can be attributed to the **PNDIOT** and **PTB7-Th**, respectively, based on the results obtained from the neat films. The orientation mismatch between **PTB7-Th** (face-on) and **PNDIOT** (edge-on) is probably one of the reasons that the all-PSC devices showed relatively low EQE and J_{SC}. Jung *et al.* synthesized a series of **P(NDI2OD-T2)** polymers with different molecular weights, namely, high molecular weight (P_H), medium molecular weight (P_M) and low molecular weight (P_L).[80] They found P_H showed mix of face-on and edge-on molecular orientation while P_L showed merely edge-on orientation. As the resultant all-PSC devices, the device based on P_H exhibited much higher PCE, J_{SC} and EQE than the device based on P_L and P_M, which is correlated to the beneficial molecular orientation.

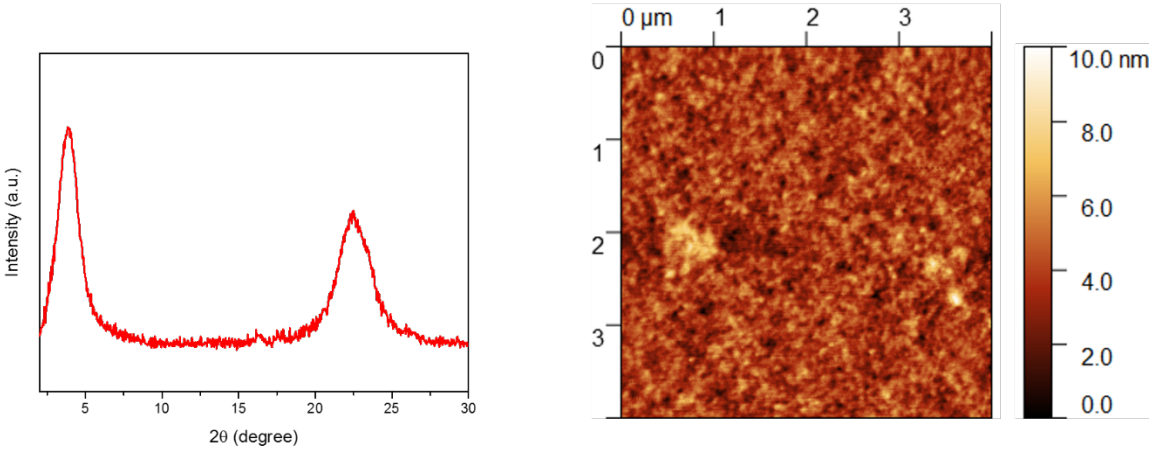

Figure 4-15 The XRD pattern and AFM image of the **PTB7-Th**:**PNDIOT** blend on PEDOT:PSS/ITO substrate.

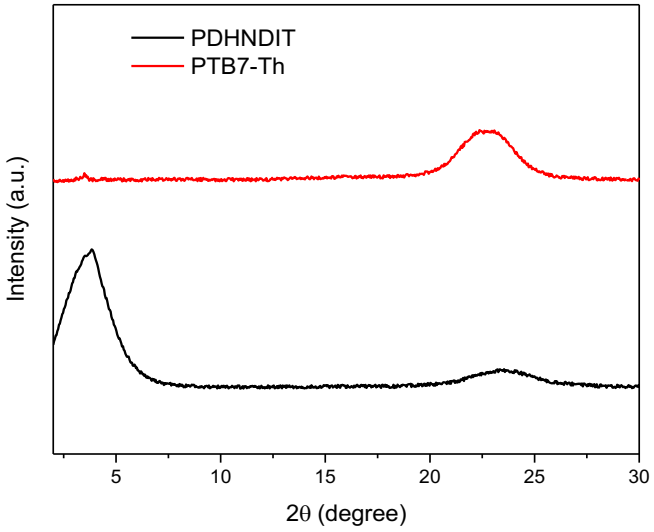

Figure 4-16 The XRD patterns of the **PTB7-Th** and **PNDIOT** neat films on PEDOT:PSS/ITO substrate.

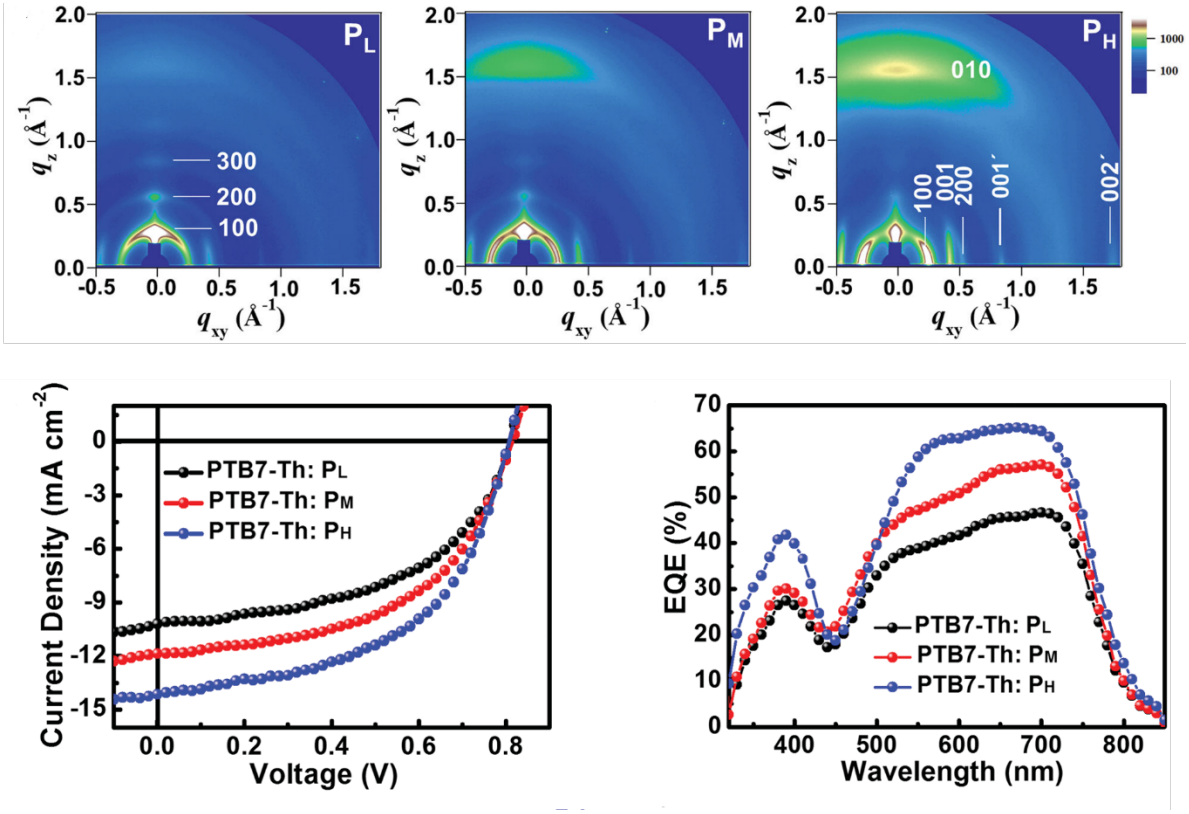

Figure 4-17 The correlation between molecular orientation and device performance for the blend of **PTB7-Th** and **P(NDI2OD-T2)**.[80]

4.3 Summary and Future Direction

In conclusion, we reported the use of NDIO in D-A polymer for the first time and we synthesized a copolymer of NDIO and thiophene, **PNDIOT**. The HOMO/LUMO levels of **PNDIOT** were determined to be -5.97 eV/-4.08 eV, significantly lower than the those of NDI analogue. As the channel semiconductor in BGBC OTFTs, **PNDIOT** exhibited unipolar n-type charge transport characteristic with an electron mobility up to 5.9×10^{-3} cm^2 V^{-1} s^{-1}, an order higher than the NDI analogue. In addition, the BGBC OTFTs still maintained unipolar n-type charge transport characteristic with an electron mobility of 3.9×10^{-3} cm^2 V^{-1} s^{-1} under ambient conditions, indicating the good device performance

robustness. Moreover, the electron mobility of the BGBC OTFT devices showed decent long-term stability when stored in air for up to 24 days. Finally, **PNDIOT** was used as acceptor in all-PSCs with **PTB7-Th** as donor. PCE as high as 3.25% was realized in the standard device configuration. In particular, the FF (0.61) of the **PNDIOT**-based devices is much higher than those of the NDI polymer based all-PSCs. This is due to the balanced charge transport in the polymer blend and the suppressed bimolecular recombination. Our preliminary results suggested that NDIO polymers represent a class of promising n-type semiconductors for air-stable OTFTs and high-performance organic solar cells.

For future work on the NDIO-based materials, the focus should be placed on the backbone structure optimization. For high performance OTFTs, bithiophene (BT) or thiophene-vinylene-thiophene (TVT) is proven to be a better donor building block for D-A polymers. The reason is being that BT and TVT will bring higher symmetry into the polymer backbone, leading to a higher crystallinity for better charge transport. In addition, BT and TVT can provide larger spacer between two NDIO units to avoid the steric effect, which helps to improve the coplanarity of the backbone and intramolecular charge transport. It was also reported that the increase of coplanarity and crystallinity may help turn the molecular orientation from edge-on to face-on.[78] For OSCs, the current hurdles are the poor absorption in the visible region (1ow absorption coefficient and narrow coverage) and undesired molecular orientation. Using BT and TVT in the backbone can improve the ICT efficiency and lower the bandgap for better light harvesting. On the other hand, the increase of crystallinity will lower the solubility and affect the processability of the material. Therefore, a sweet balance between the crystallinity and solubility needs to be reached by tuning the side chain and molecular weight of the polymer to achieve the higher performance in OSCs than the NDI polymers and fullerene.

4.4 Experimental

4.4.1 Materials and Characterization

All chemicals were obtained from commercial sources and used as received. 4,9-dibromo-2,7-bis((2-octyldodecyl)oxy)benzo[lmn][3,8]phenanthroline-1,3,6,8(2*H*,7*H*)-tetraone (NDIO20-Br) was provided by our collaborator. High-temperature gel permeation chromatography (HT-GPC) measurements were performed on a Malvern 350 HT-GPC system using 1,2,4-trichlorobenzene as eluent and polystyrene as standards at a column temperature of 140 °C. Thermogravimetric analysis (TGA) was carried out on a TA Instruments SDT 2960 at a scan rate of 10 °C min^{-1} under nitrogen. The UV-Vis absorption spectra of polymers were recorded on a Thermo Scientific model GENESYS™ 10S VIS spectrophotometer. Cyclic voltammetry (CV) data were obtained on a CHI600E electrochemical analyser using an Ag/AgCl reference electrode and two Pt disk electrodes as the working and counter electrodes in a 0.1 M tetrabutylammonium hexafluorophosphate solution in acetonitrile at a scan rate of 50 mV s^{-1}. Ferrocene was used as the reference, which has a HOMO energy value of -4.8 eV.[162] NMR spectra were recorded with a Bruker DPX 300 MHz spectrometer with chemical shifts relative to tetramethylsilane (TMS, 0 ppm). Reflective XRD measurements were carried out on a Bruker D8 Advance diffractometer with Cu Ka radiation (λ = 0.15406 nm) using polymer films spin coated on PEDOT:PSS/ITO substrates. Atomic force microscopy (AFM) images were taken with a Dimension 3100 scanning probe microscope on the samples prepared the same way.

4.4.2 Fabrication and Characterization of OTFT devices

The bottom-contact bottom-gate (BGBC) configuration was used for all OTFT devices. The preparation procedure of the substrate and device is as follows. A heavily n-doped Si wafer with ~300 nm-thick SiO_2 layer was patterned with gold source and drain pairs by conventional photolithography and thermal deposition. Then the substrate was treated with air plasma, followed by cleaning with acetone and isopropanol in an ultrasonic bath. Subsequently, the substrate was placed in a 3% dodecyltrichlorosilane (DDTS) solution in toluene at room temperature for 20 min. The substrate was washed with toluene and dried under a nitrogen flow. Then a polymer solution in chloroform (5 mg mL^{-1}) was spin-coated onto the substrate at 3000 rpm for 60 s to give a polymer film (~40 nm), which was further subjected to thermal annealing at different temperatures for 20 min in a glove box. All OTFT devices were characterized in the same glove box using an Agilent B2912A Semiconductor Analyser. The hole and electron mobilities are calculated in the saturation regime according to the following equation:

$$I_{DS} = \frac{\mu C_i W}{2L}(V_G - V_T)^2$$

where I_{DS} is the drain-source current, μ is charge carrier mobility, C_i is the gate dielectric layer capacitance per unit area (~ 11.6 nF cm^{-2}), V_G is the gate voltage, V_T is the threshold voltage, L is the channel length (30 μm), and W is the channel width (1000 μm).

4.4.3 Fabrication and Characterization of all-PSC devices

All all-PSC devices were fabricated using the conventional configuration ITO/PEDOT:PSS/**PTB7-Th**:PA/LiF/Al. ITO glass substrates were sonicated in water, acetone and IPA. Then the substrates were treated with plasma cleaning. A thin layer of PEDOT:PSS (Al 4083) was deposited through spin-

coating at 4000 rpm and dried subsequently at 150 °C for 20 min in air. Then the substrates were transferred to a nitrogen glove box, where the polymer blend layer (~90 nm) was spin-coated onto the PEDOT:PSS layer. The active layer was formed using a chlorobenzene solution of **PTB7-Th**:PA (1:1). Finally, a thin layer of LiF (1 nm) and a layer of Al (100 nm) electrode were deposited in vacuum onto the substrate at P $\approx 5.0 \times 10^{-6}$ Pa. The active area is 0.07 cm^2. The current density–voltage (J – V) characteristics of the all-PSCs were measured on an Agilent B2912A Semiconductor Analyser with a ScienceTech SLB300-A Solar Simulator. A 450 W xenon lamp and an air mass (AM) 1.5 filter were used as the light source.

Chapter 5. Conclusions and Future Direction

5.1 Conclusions

Organic semiconductors are under rapid development in the last two decades for their distinguished merits: light weight, low cost and solution processability. It is believed that organic electronics will bring the next generation of electronics, for example, flexible electronics. The development of n-type organic semiconductors is very challenging due to the lack of electron-deficient moieties for the polymer backbone. This thesis presents the synthesis and characterization of several n-type or ambipolar polymer semiconductors that were used for OTFTs and all-PSCs, which demonstrated promising performance.

In chapter 2, a novel electron-accepting building block, IBDP, is designed, synthesized, and incorporated into D–A polymers. With lactam groups replacing the lactone groups, IBDP gets two extra side chains to yield good solution processability, which is requisite for the fabrication of OSCs. On the other hand, the donating effect of lactam groups has raised the LUMO levels of **P1** and **P2** to ~-3.7 eV from -4.0 eV of those IBDF-based polymers. With a raised LUMO level, the electron injection barrier now is higher and electron transport will become more unstable.[124,125] Therefore the electron transport is supressed and the IBDP-based polymers exhibited balanced ambipolar semiconductor performance in OTFTs. Since both polymers exhibited high hole mobility up to 0.19 $cm^2 V^{-1} s^{-1}$ and electron mobility up to 0.10 $cm^2 V^{-1} s^{-1}$, these two IBDP-based polymers was used as acceptor material in combination with **P3HT** as donor. As preliminary results, the devices based on **P1** exhibited a high PCE of 3.38%. To our best knowledge, this is the highest PCE that has been obtained from P3HT-based all-PSCs. Besides, both IBDP-based polymers demonstrate a broad absorption up to 1100 nm according to the UV-Vis-NIR absorption spectra. This may enable the photo-detection applications such as

phototransistor in NIR region, which has been rarely explored and believed to be a useful technology in various areas[188–192].

In chapter 3, a series of ester side chains have been developed and used as solubilizing side chains for the copolymers of IBDF and BT. Three IBDF-BT polymers were synthesized and demonstrated excellent solubility, suitable HOMO/LUMO levels and excellent charge transport properties in OTFTs with electron mobility up to 0.35 $cm^2 V^{-1} s^{-1}$. When the polymers were incorporated in all-PSCs in conjunction with **PTB7-Th**, all devices showed very poor performance (PCES < 0.4% with J_{SC} < 1 mA/cm^2 and FF < 0.4). AFM images suggested there were large polymer fabrils (>1000 nm) present in the polymer blends, indicating a large phase separation for the blends. This has limited the charge generation that happens at the D-A interface, and led to a very low J_{SC}. In addition, SCLC measurement of the blends exhibited quite low electron mobilities (~10^{-6} $cm^2 V^{-1} s^{-1}$) and led to unbalanced charge transport in the polymer blend, which could be one of the reasons why the devices showing low FF. Through XRD and SCLC studies, we found the spin-coated polymer thin films were intrinsically amorphous and the bulky side chains seemed to disrupt the chain packing, which might have caused the poor bulk electron charge transport in the solar cell devices.

In chapter 4, we reported the use of NDIO in D-A polymer for the first time and we synthesized a copolymer of NDIO and thiophene, **PNDIOT**. The HOMO/LUMO levels of **PNDIOT** were determined to be -5.97 eV/-4.08 eV, significantly lower than those of NDI analogue. As the channel semiconductor in BGBC OTFTs, **PNDIOT** exhibited unipolar n-type charge transport characteristic with an electron mobility up to 5.9×10^{-3} $cm^2 V^{-1} s^{-1}$, an order higher than the NDI analogue. In addition, the BGBC OTFTs still maintained unipolar n-type charge transport characteristic with an electron mobility of 3.9×10^{-3} $cm^2 V^{-1} s^{-1}$ under ambient conditions, indicating the good device performance

robustness. Moreover, the electron mobility of the BGBC OTFT devices showed decent long-term stability when stored in air for up to 24 days. Finally, **PNDIOT** was used as acceptor in all-PSCs with **PTB7-Th** as donor. PCE as high as 3.25% was realized in the standard device configuration. In particular, the FF (0.61) of the **PNDIOT**-based devices is much higher than those of the NDI polymer based all-PSCs. This is due to the balanced charge transport in the polymer blend and the suppressed bimolecular recombination. Our preliminary results suggested that NDIO polymers represent a class of promising n-type semiconductors for air-stable OTFTs and high-performance organic solar cells.

The major contributions of this thesis include:

- First to report the challenging synthesis of the electron deficient building block, IBDP, and two IBDP polymers, which showed high hole mobility of 0.19 $cm^2 V^{-1} s^{-1}$ and electron mobility of 0.10 $cm^2 V^{-1} s^{-1}$ in OTFTs and demonstrated broad absorption up to 1100 nm. In the all-PSCs that use **P3HT** as donor, **P1** exhibited a decently high PCE of 3.38%. The results showed IBDP polymers are very promising materials for organic photovoltaics.
- Designed and synthesized a series of ester side chain for solution processable IBDF-polymers, which needed expensive carbon 40 side chain as solubilizing group. The resultant polymers showed excellent electron transport property with electron mobility up to 0.35 $cm^2 V^{-1} s^{-1}$.
- This new type of side chains provides a tool to solubilize other n-type semiconductors such as, PDPPT-BTz copolymers.[193,194]
- Frist to incorporate NDIO into D-A π-conjugated polymer. The resultant polymers exhibited high electron affinity, which led to enhanced electron transport property and more stable BGBC OTFT performance in the air.

- The NDIO polymer, **PNDIOT**, showed superior photovoltaic performance with PCE up to 3.25% in all-PSCs compared to its NDI analogue. In particular, the FF (0.61) is much higher than those of the NDI polymer based all-PSCs, which has been a hindrance to achieving high PCE in all-PSCs.

5.2 Recommended Future Research

As discussed in Chapter 2, the synthesis of IBDP polymers needs to be improved in terms of yield and chemical toxicity in order for further studies and optimization. The two IBDP polymers showed considerable absorption in the NIR region (800 nm to 1100 nm), which has been rarely reported for a single component organic semiconductor. Therefore, photodetection application such as phototransistor can be tried using these materials. Meanwhile, the simultaneously deep HOMO levels and excellent absorption profile of these materials make them favorable donor materials in OSCs for increasing the V_{OC} without compromising the light harvesting. With the ambipolar charge transport characteristic, the polymer can be used in ternary OSCs as the third component, which may help to improve the absorption, smoothen the exciton dissociation and tune the blend morphology.[195–197]

Although IBDF polymers have shown excellent electron transport property in OTFTs, the required bulky side chains might have greatly limited the bulk heterojunction morphology and bulk electron transport. Introducing a twisted backbone in the IBDF polymers may be a solution to both issues. For one thing, it can lower the crystallinity of the polymer to achieve better miscibility with other donors. For another, the twisted polymer may not require the bulky side chains and thus improve the bulk charge transport property.

With the introduction of alkoxy groups into NDIO, the electron affinity has been increased and the π-π interaction of the resultant polymers are much stronger. This has led to enhanced performance in OTFTs but in the same time difficulty in solubilizing the NDIO-BT copolymer, which can provide better adsorption in the visible and NIR region. Solution processable PNDIOBT can be realized by controlling the molecular weight or introducing defects into the backbone (random copolymers). On the other hand, the device performance can be substantially increased by using a donor with complementary absorption profile.

Bibliography

[1] Peaking of World Oil Production Impacts, Mitigation & Risk Management, (n.d.). https://www.netl.doe.gov/publications/others/pdf/Oil_Peaking_NETL.pdf.

[2] A. Stoppato, Life cycle assessment of photovoltaic electricity generation, Energy. 33 (2008) 224–232. doi:http://dx.doi.org/10.1016/j.energy.2007.11.012.

[3] 2015 Renewable Energy Data Book, 2015.

[4] A.M. and P.C.T. Samuel C. E. Jupe, Increasing the Energy Yield of Generation from New and Renewable Energy Resources, Renew. Energy. 14 (2009) 37–62. doi:10.5772/7379.

[5] W. a. Badawy, A review on solar cells from Si-single crystals to porous materials and quantum dots, J. Adv. Res. 6 (2015) 123–132. doi:10.1016/j.jare.2013.10.001.

[6] G.F. Brown, J. Wu, Third generation photovoltaics, Laser Photon. Rev. 3 (2009) 394–405. doi:10.1002/lpor.200810039.

[7] M. Green, Third Generation Photovoltaics: Advanced Solar Energy Conversion, 2003. doi:10.1007/b137807.

[8] Annual Energy Review, (n.d.). https://www.eia.gov/totalenergy/data/annual/.

[9] M. Green, Thin-film solar cells: review of materials, technologies and commercial status, J. Mater. Sci. Mater. Electron. 18 (2007) 15–19. doi:10.1007/s10854-007-9177-9.

[10] G. Dennler, M.C. Scharber, C.J. Brabec, Polymer-fullerene bulk-heterojunction solar cells, Adv. Mater. 21 (2009) 1323–1338. doi:10.1002/adma.200801283.

[11] Y. Liu, X. Wan, F. Wang, J. Zhou, G. Long, J. Tian, J. You, Y. Yang, Y. Chen, Spin-Coated Small Molecules for High Performance Solar Cells, Adv. Energy Mater. 1 (2011) 771–775. doi:10.1002/aenm.201100230.

[12] M. Kaltenbrunner, M.S. White, E.D. Głowacki, T. Sekitani, T. Someya, N.S. Sariciftci, S. Bauer, Ultrathin and lightweight organic solar cells with high flexibility, Nat. Commun. 3 (2012) 770. http://dx.doi.org/10.1038/ncomms1772.

[13] T. Kim, J.-H. Kim, T.E. Kang, C. Lee, H. Kang, M. Shin, C. Wang, B. Ma, U. Jeong, T.-S. Kim, B.J. Kim, Flexible, highly efficient all-polymer solar cells, Nat. Commun. 6 (2015) 8547. doi:10.1038/ncomms9547.

[14] Y. He, W. Hong, Y. Li, New building blocks for π-conjugated polymer semiconductors for organic thin film transistors and photovoltaics, J. Mater. Chem. C. 2 (2014) 8651–8661. doi:10.1039/C4TC01201A.

[15] Figure 1, (n.d.). https://www.nrel.gov/pv/advanced_concepts.html.

[16] D.L. Morel, A.K. Ghosh, T. Feng, E.L. Stogryn, P.E. Purwin, R.F. Shaw, C. Fishman, High-efficiency organic solar cells, Appl. Phys. Lett. 32 (1978) 495–497. doi:10.1063/1.90099.

[17] C.W. Tang, Two- layer organic photovoltaic cell, Appl. Phys. Lett. 48 (1986) 183–185. doi:10.1063/1.96937.

[18] N.S. Sariciftci, L. Smilowitz, A.J. Heeger, F. Wudl, Semiconducting polymers (as donors) and buckminsterfullerene (as acceptor): photoinduced electron transfer and heterojunction devices, Synth. Met. 59 (1993) 333–352. doi:http://dx.doi.org/10.1016/0379-6779(93)91166-Y.

[19] P.E. Shaw, A. Ruseckas, I.D.W. Samuel, Exciton Diffusion Measurements in Poly(3-hexylthiophene), Adv. Mater. 20 (2008) 3516–3520. doi:10.1002/adma.200800982.

[20] G. Stapper, M. Bernasconi, N. Nicoloso, M. Parrinello, Ab initio, Phys. Rev. B. 59 (1999) 797–810. https://link.aps.org/doi/10.1103/PhysRevB.59.797.

[21] G. Li, R. Zhu, Y. Yang, Polymer solar cells, Nat. Photonics. 6 (2012) 153–161. doi:10.1038/nphoton.2012.11.

[22] M. Hiramoto, H. Fujiwara, M. Yokoyama, p- i- n like behavior in three- layered organic solar cells having a co- deposited interlayer of pigments, J. Appl. Phys. 72 (1992) 3781–3787. doi:10.1063/1.352274.

[23] G. Yu, J. Gao, J.C. Hummelen, F. Wudl, A.J. Heeger, Polymer Photovoltaic Cells: Enhanced Efficiencies via a Network of Internal Donor-Acceptor Heterojunctions, Science (80-.). 270 (1995) 1789–1791. doi:10.1126/science.270.5243.1789.

[24] J. Zhao, Y. Li, G. Yang, K. Jiang, H. Lin, H. Ade, W. Ma, H. Yan, Efficient organic solar cells processed from hydrocarbon solvents, Nat. Energy. 1 (2016) 15027. doi:10.1038/nenergy.2015.27.

[25] W.L. Leong, G.C. Welch, L.G. Kaake, C.J. Takacs, Y. Sun, G.C. Bazan, A.J. Heeger, Role of trace impurities in the photovoltaic performance of solution processed small-molecule bulk heterojunction solar cells, Chem. Sci. 3 (2012) 2103–2109. doi:10.1039/C2SC20157G.

[26] M.C. Scharber, D. Mühlbacher, M. Koppe, P. Denk, C. Waldauf, A.J. Heeger, C.J. Brabec, Design Rules for Donors in Bulk-Heterojunction Solar Cells—Towards 10 % Energy-Conversion Efficiency, Adv. Mater. 18 (2006) 789–794. doi:10.1002/adma.200501717.

[27] X. Yang, J. Loos, Toward High-Performance Polymer Solar Cells: The Importance of Morphology Control, Macromolecules. 40 (2007) 1353–1362. doi:10.1021/ma0618732.

[28] H.-Y. Chen, J. Hou, S. Zhang, Y. Liang, G. Yang, Y. Yang, L. Yu, Y. Wu, G. Li, Polymer Solar Cells with Enhanced Open-Circuit Voltage and Efficiency, Nat. Photonics. 3 (2009) 649–653. doi:10.1038/nphoton.2009.192.

[29] H. Zhou, L. Yang, A.C. Stuart, S.C. Price, S. Liu, W. You, Development of Fluorinated Benzothiadiazole as a Structural Unit for a Polymer Solar Cell of 7 % Efficiency, Angew. Chemie Int. Ed. 50 (2011) 2995–2998. doi:10.1002/anie.201005451.

[30] Y. Liang, D. Feng, Y. Wu, S.-T. Tsai, G. Li, C. Ray, L. Yu, Highly Efficient Solar Cell Polymers Developed via Fine-Tuning of Structural and Electronic Properties, J. Am. Chem.

Soc. 131 (2009) 7792–7799. doi:10.1021/ja901545q.

[31] S.C. Price, A.C. Stuart, L. Yang, H. Zhou, W. You, Fluorine Substituted Conjugated Polymer of Medium Band Gap Yields 7% Efficiency in Polymer−Fullerene Solar Cells, J. Am. Chem. Soc. 133 (2011) 4625–4631. doi:10.1021/ja1112595.

[32] Y. Liang, D. Feng, Y. Wu, S.-T. Tsai, G. Li, C. Ray, L. Yu, Highly Efficient Solar Cell Polymers Developed via Fine-Tuning of Structural and Electronic Properties, J. Am. Chem. Soc. 131 (2009) 7792–7799. doi:10.1021/ja901545q.

[33] No Title, (n.d.). https://www.iasj.net/iasj?func=fulltext&aId=101545.

[34] D. Ashish, R.K. Singh, Basic Electronics Engineering & Devices, Laxmi Publications Pvt. Ltd, 2007.

[35] K. Misiakos, D. Tsamakis, Accurate measurements of the silicon intrinsic carrier density from 78 to 340 K, J. Appl. Phys. 74 (1993) 3293–3297. doi:10.1063/1.354551.

[36] Conductor, semiconductor and insulator, (n.d.). http://www.optique-ingenieur.org/en/courses/OPI_ang_M05_C02/co/Contenu_02.html.

[37] The doping of semiconductor, (n.d.). http://instrumentacion.qi.fcen.uba.ar/hbase/solids/dope.html.

[38] H. Naarmann, Polymers, Electrically Conducting, in: Ullmann's Encycl. Ind. Chem., Wiley-VCH Verlag GmbH & Co. KGaA, Weinheim, Germany, 2000. doi:10.1002/14356007.a21_429.

[39] H. Li, F.S. Kim, G. Ren, S.A. Jenekhe, High-Mobility n-Type Conjugated Polymers Based on Electron-Deficient Tetraazabenzodifluoranthene Diimide for Organic Electronics, J. Am. Chem. Soc. 135 (2013) 14920–14923. doi:10.1021/ja407471b.

[40] B.A. Jones, A. Facchetti, M.R. Wasielewski, T.J. Marks, Tuning Orbital Energetics in Arylene

Diimide Semiconductors. Materials Design for Ambient Stability of n-Type Charge Transport, J. Am. Chem. Soc. 129 (2007) 15259–15278. doi:10.1021/ja075242e.

[41] Y. Li, B. Sun, P. Sonar, S.P. Singh, Solution processable poly(2,5-dialkyl-2,5-dihydro-3,6-di-2-thienyl- pyrrolo[3,4-c]pyrrole-1,4-dione) for ambipolar organic thin film transistors, Org. Electron. 13 (2012) 1606–1613. doi:10.1016/j.orgel.2012.04.023.

[42] B. Sun, W. Hong, Z. Yan, H. Aziz, Y. Li, Record High Electron Mobility of 6.3 cm 2 V −1 s −1 Achieved for Polymer Semiconductors Using a New Building Block, Adv. Mater. 26 (2014) 2636–2642. doi:10.1002/adma.201305981.

[43] C. Guo, W. Hong, H. Aziz, Y. Li, Recent Progress in High Mobility Polymer Semiconductors for Organic Thin Film Transistors, Rev. Adv. Sci. Eng. 1 (2012) 200–224. doi:10.1166/rase.2012.1014.

[44] D. Anand, CONDUCTING FLEXIBLE PAPER BASED ON BACTERIAL CELLULOSE AND POLYANILINE COMPOSITES, University of Tokyo, 2016. doi:10.13140/RG.2.1.3321.1764.

[45] M.M. Wienk, J.M. Kroon, W.J.H. Verhees, J. Knol, J.C. Hummelen, P.A. van Hal, R.A.J. Janssen, Efficient Methano[70]fullerene/MDMO-PPV Bulk Heterojunction Photovoltaic Cells, Angew. Chemie Int. Ed. 42 (2003) 3371–3375. doi:10.1002/anie.200351647.

[46] W. Ma, C. Yang, X. Gong, K. Lee, A.J. Heeger, Thermally Stable, Efficient Polymer Solar Cells with Nanoscale Control of the Interpenetrating Network Morphology, Adv. Funct. Mater. 15 (2005) 1617–1622. doi:10.1002/adfm.200500211.

[47] C.J. Brabec, S.E. Shaheen, C. Winder, N.S. Sariciftci, P. Denk, Effect of LiF/metal electrodes on the performance of plastic solar cells, Appl. Phys. Lett. 80 (2002) 1288–1290. doi:10.1063/1.1446988.

[48] G. Li, V. Shrotriya, J. Huang, Y. Yao, T. Moriarty, K. Emery, Y. Yang, High-efficiency solution processable polymer photovoltaic cells by self-organization of polymer blends, Nat.

Mater. 4 (2005) 864–868. doi:10.1038/nmat1500.

[49] J. Peet, J.Y. Kim, N.E. Coates, W.L. Ma, D. Moses, A.J. Heeger, G.C. Bazan, Efficiency enhancement in low-bandgap polymer solar cells by processing with alkane dithiols, Nat. Mater. 6 (2007) 497–500. doi:10.1038/nmat1928.

[50] D. Mühlbacher, M. Scharber, M. Morana, Z. Zhu, D. Waller, R. Gaudiana, C. Brabec, High Photovoltaic Performance of a Low-Bandgap Polymer, Adv. Mater. 18 (2006) 2884–2889. doi:10.1002/adma.200600160.

[51] L. Lu, T. Zheng, Q. Wu, A.M. Schneider, D. Zhao, L. Yu, Recent Advances in Bulk Heterojunction Polymer Solar Cells, Chem. Rev. 115 (2015) 12666–12731. doi:10.1021/acs.chemrev.5b00098.

[52] Q. Wan, X. Guo, Z. Wang, W. Li, B. Guo, W. Ma, M. Zhang, Y. Li, 10.8% Efficiency Polymer Solar Cells Based on PTB7-Th and PC71BM via Binary Solvent Additives Treatment, Adv. Funct. Mater. 26 (2016) 6635–6640. doi:10.1002/adfm.201602181.

[53] Z. He, B. Xiao, F. Liu, H. Wu, Y. Yang, S. Xiao, C. Wang, T.P. Russell, Y. Cao, Single-junction polymer solar cells with high efficiency and photovoltage, Nat. Photonics. 9 (2015) 174–179. doi:10.1038/nphoton.2015.6.

[54] Z. Wu, C. Sun, S. Dong, X.-F. Jiang, S. Wu, H. Wu, H.-L. Yip, F. Huang, Y. Cao, n-Type Water/Alcohol-Soluble Naphthalene Diimide-Based Conjugated Polymers for High-Performance Polymer Solar Cells, J. Am. Chem. Soc. 138 (2016) 2004–2013. doi:10.1021/jacs.5b12664.

[55] I. Etxebarria, A. Guerrero, J. Albero, G. Garcia-Belmonte, E. Palomares, R. Pacios, Inverted vs standard PTB7:PC70BM organic photovoltaic devices. The benefit of highly selective and extracting contacts in device performance, Org. Electron. 15 (2014) 2756–2762. doi:10.1016/j.orgel.2014.08.008.

[56] J.-D. Chen, C. Cui, Y. Li, L. Zhou, Q.-D. Ou, C. Li, Y. Li, J.-X. Tang, Single-Junction

Polymer Solar Cells Exceeding 10% Power Conversion Efficiency, Adv. Mater. 27 (2015) 1035–1041. doi:10.1002/adma.201404535.

[57] Z. He, C. Zhong, X. Huang, W.-Y. Wong, H. Wu, L. Chen, S. Su, Y. Cao, Simultaneous Enhancement of Open-Circuit Voltage, Short-Circuit Current Density, and Fill Factor in Polymer Solar Cells, Adv. Mater. 23 (2011) 4636–4643. doi:10.1002/adma.201103006.

[58] Y. He, Y. Li, Fullerene derivative acceptors for high performance polymer solar cells, Phys. Chem. Chem. Phys. 13 (2011) 1970–1983. doi:10.1039/C0CP01178A.

[59] J.H. Youn, Y. Il Lee, H.T. Moon, M.S. Ryu, J. Kim, J. Jang, Trap energy level of P3HT: PCBM-71 bulk heterojunction solar cells with PICTS (photo-induced current transient spectroscopy), Curr. Appl. Phys. 10 (2010) S525–S527. doi:https://doi.org/10.1016/j.cap.2010.02.031.

[60] C. Groves, Suppression of geminate charge recombination in organic photovoltaic devices with a cascaded energy heterojunction, Energy Environ. Sci. 6 (2013) 1546–1551. doi:10.1039/C3EE24455E.

[61] P. Cheng, C. Yan, T.-K. Lau, J. Mai, X. Lu, X. Zhan, Molecular Lock: A Versatile Key to Enhance Efficiency and Stability of Organic Solar Cells, Adv. Mater. 28 (2016) 5822–5829. doi:10.1002/adma.201600426.

[62] P. Cheng, H. Bai, N.K. Zawacka, T.R. Andersen, W. Liu, E. Bundgaard, M. Jørgensen, H. Chen, F.C. Krebs, X. Zhan, Roll-Coated Fabrication of Fullerene-Free Organic Solar Cells with Improved Stability, Adv. Sci. 2 (2015) 1500096–n/a. doi:10.1002/advs.201500096.

[63] Y.-Y. Lai, Y.-J. Cheng, C.-S. Hsu, Applications of functional fullerene materials in polymer solar cells, Energy Environ. Sci. 7 (2014) 1866–1883. doi:10.1039/C3EE43080D.

[64] S. Falke, P. Eravuchira, A. Materny, C. Lienau, Raman spectroscopic identification of fullerene inclusions in polymer/fullerene blends, J. Raman Spectrosc. 42 (2011) 1897–1900. doi:10.1002/jrs.2966.

[65] T. Heumueller, W.R. Mateker, A. Distler, U.F. Fritze, R. Cheacharoen, W.H. Nguyen, M. Biele, M. Salvador, M. von Delius, H.-J. Egelhaaf, M.D. McGehee, C.J. Brabec, Morphological and electrical control of fullerene dimerization determines organic photovoltaic stability, Energy Environ. Sci. 9 (2016) 247–256. doi:10.1039/C5EE02912K.

[66] H. Kang, W. Lee, J. Oh, T. Kim, C. Lee, B.J. Kim, From Fullerene–Polymer to All-Polymer Solar Cells: The Importance of Molecular Packing, Orientation, and Morphology Control, Acc. Chem. Res. 49 (2016) 2424–2434. doi:10.1021/acs.accounts.6b00347.

[67] B. Fan, K. Zhang, X.-F. Jiang, L. Ying, F. Huang, Y. Cao, High-Performance Nonfullerene Polymer Solar Cells based on Imide-Functionalized Wide-Bandgap Polymers, Adv. Mater. 29 (2017) 1606396. doi:10.1002/adma.201606396.

[68] W. Zhao, D. Qian, S. Zhang, S. Li, O. Inganäs, F. Gao, J. Hou, Fullerene-Free Polymer Solar Cells with over 11% Efficiency and Excellent Thermal Stability, Adv. Mater. 28 (2016) 4734–4739. doi:10.1002/adma.201600281.

[69] J. Liu, S. Chen, D. Qian, B. Gautam, G. Yang, J. Zhao, J. Bergqvist, F. Zhang, W. Ma, H. Ade, O. Inganäs, K. Gundogdu, F. Gao, H. Yan, Fast charge separation in a non-fullerene organic solar cell with a small driving force, Nat. Energy. 1 (2016) 16089. doi:10.1038/nenergy.2016.89.

[70] Y.-J. Hwang, T. Earmme, S. Subramaniyan, S. a Jenekhe, Side chain engineering of n-type conjugated polymer enhances photocurrent and efficiency of all-polymer solar cells, Chem. Commun. 50 (2014) 10801. doi:10.1039/C4CC03722G.

[71] W. Li, W.S.C. Roelofs, M. Turbiez, M.M. Wienk, R.A.J. Janssen, Polymer solar cells with diketopyrrolopyrrole conjugated polymers as the electron donor and electron acceptor, Adv. Mater. 26 (2014) 3304–3309. doi:10.1002/adma.201305910.

[72] D. Mori, H. Benten, I. Okada, H. Ohkita, S. Ito, Highly efficient charge-carrier generation and collection in polymer/polymer blend solar cells with a power conversion efficiency of 5.7%,

Energy Environ. Sci. 7 (2014) 2939. doi:10.1039/C4EE01326C.

[73] T. Earmme, Y.-J. Hwang, N.M. Murari, S. Subramaniyan, S.A. Jenekhe, All-Polymer Solar Cells with 3.3% Efficiency Based on Naphthalene Diimide-Selenophene Copolymer Acceptor, J. Am. Chem. Soc. 135 (2013) 14960–14963. doi:10.1021/ja4085429.

[74] Y.-J. Hwang, B.A.E. Courtright, A.S. Ferreira, S.H. Tolbert, S.A. Jenekhe, 7.7% Efficient All-Polymer Solar Cells, Adv. Mater. 27 (2015) 4578–4584. doi:10.1002/adma.201501604.

[75] J.W. Jung, J.W. Jo, C.-C. Chueh, F. Liu, W.H. Jo, T.P. Russell, A.K.-Y. Jen, Fluoro-Substituted n-Type Conjugated Polymers for Additive-Free All-Polymer Bulk Heterojunction Solar Cells with High Power Conversion Efficiency of 6.71%, Adv. Mater. 27 (2015) 3310–3317. doi:10.1002/adma.201501214.

[76] C. Lee, H. Kang, W. Lee, T. Kim, K.-H. Kim, H.Y. Woo, C. Wang, B.J. Kim, High-Performance All-Polymer Solar Cells Via Side-Chain Engineering of the Polymer Acceptor: The Importance of the Polymer Packing Structure and the Nanoscale Blend Morphology, Adv. Mater. 27 (2015) 2466–2471. doi:10.1002/adma.201405226.

[77] J. Choi, K.-H. Kim, H. Yu, C. Lee, H. Kang, I. Song, Y. Kim, J.H. Oh, B.J. Kim, Importance of Electron Transport Ability in Naphthalene Diimide-Based Polymer Acceptors for High-Performance, Additive-Free, All-Polymer Solar Cells, Chem. Mater. 27 (2015) 5230–5237. doi:10.1021/acs.chemmater.5b01274.

[78] J.W. Jo, J.W. Jung, H. Ahn, M.J. Ko, A.K.-Y. Jen, H.J. Son, Effect of Molecular Orientation of Donor Polymers on Charge Generation and Photovoltaic Properties in Bulk Heterojunction All-Polymer Solar Cells, Adv. Energy Mater. 7 (2017) 1601365. doi:10.1002/aenm.201601365.

[79] X. Long, Z. Ding, C. Dou, J. Zhang, J. Liu, L. Wang, Polymer Acceptor Based on Double B←N Bridged Bipyridine (BNBP) Unit for High-Efficiency All-Polymer Solar Cells, Adv. Mater. 28 (2016) 6504–6508. doi:10.1002/adma.201601205.

[80] J. Jung, W. Lee, C. Lee, H. Ahn, B.J. Kim, Controlling Molecular Orientation of Naphthalenediimide-Based Polymer Acceptors for High Performance All-Polymer Solar Cells, Adv. Energy Mater. 6 (2016) 1600504. doi:10.1002/aenm.201600504.

[81] Z. Li, X. Xu, W. Zhang, X. Meng, W. Ma, A. Yartsev, O. Inganäs, M.R. Andersson, R.A.J. Janssen, E. Wang, High Performance All-Polymer Solar Cells by Synergistic Effects of Fine-Tuned Crystallinity and Solvent Annealing, J. Am. Chem. Soc. 138 (2016) 10935–10944. doi:10.1021/jacs.6b04822.

[82] W. Lee, C. Lee, H. Yu, D.-J. Kim, C. Wang, H.Y. Woo, J.H. Oh, B.J. Kim, Side Chain Optimization of Naphthalenediimide-Bithiophene-Based Polymers to Enhance the Electron Mobility and the Performance in All-Polymer Solar Cells, Adv. Funct. Mater. 26 (2016) 1543–1553. doi:10.1002/adfm.201504191.

[83] L. Gao, Z.-G. Zhang, L. Xue, J. Min, J. Zhang, Z. Wei, Y. Li, All-Polymer Solar Cells Based on Absorption-Complementary Polymer Donor and Acceptor with High Power Conversion Efficiency of 8.27%, Adv. Mater. 28 (2016) 1884–1890. doi:10.1002/adma.201504629.

[84] J. Yan, B.R. Saunders, Third-generation solar cells: a review and comparison of polymer:fullerene, hybrid polymer and perovskite solar cells, RSC Adv. 4 (2014) 43286–43314. doi:10.1039/C4RA07064J.

[85] B.A. Gregg, Entropy of Charge Separation in Organic Photovoltaic Cells: The Benefit of Higher Dimensionality, J. Phys. Chem. Lett. 2 (2011) 3013–3015. doi:10.1021/jz2012403.

[86] J. You, L. Dou, K. Yoshimura, T. Kato, K. Ohya, T. Moriarty, K. Emery, C.-C. Chen, J. Gao, G. Li, Y. Yang, A polymer tandem solar cell with 10.6% power conversion efficiency., Nat. Commun. 4 (2013) 1446. doi:10.1038/ncomms2411.

[87] M. Zhang, Y. Gu, X. Guo, F. Liu, S. Zhang, L. Huo, T.P. Russell, J. Hou, Efficient Polymer Solar Cells Based on Benzothiadiazole and Alkylphenyl Substituted Benzodithiophene with a Power Conversion Efficiency over 8%, Adv. Mater. 25 (2013) 4944–4949.

doi:10.1002/adma.201301494.

[88] H. Bronstein, Z. Chen, R.S. Ashraf, W. Zhang, J. Du, J.R. Durrant, P. Shakya Tuladhar, K. Song, S.E. Watkins, Y. Geerts, M.M. Wienk, R.A.J. Janssen, T. Anthopoulos, H. Sirringhaus, M. Heeney, I. McCulloch, Thieno[3,2-b]thiophene−Diketopyrrolopyrrole-Containing Polymers for High-Performance Organic Field-Effect Transistors and Organic Photovoltaic Devices, J. Am. Chem. Soc. 133 (2011) 3272–3275. doi:10.1021/ja110619k.

[89] H. Chen, Y. Guo, G. Yu, Y. Zhao, J. Zhang, D. Gao, H. Liu, Y. Liu, Highly π-Extended Copolymers with Diketopyrrolopyrrole Moieties for High-Performance Field-Effect Transistors, Adv. Mater. 24 (2012) 4618–4622. doi:10.1002/adma.201201318.

[90] J.S. Ha, K.H. Kim, D.H. Choi, 2,5-Bis(2-octyldodecyl)pyrrolo[3,4-c]pyrrole-1,4-(2H,5H)-dione-Based Donor–Acceptor Alternating Copolymer Bearing 5,5′-Di(thiophen-2-yl)-2,2′-biselenophene Exhibiting 1.5 cm2·V–1·s–1 Hole Mobility in Thin-Film Transistors, J. Am. Chem. Soc. 133 (2011) 10364–10367. doi:10.1021/ja203189h.

[91] P. Sonar, S.P. Singh, Y. Li, Z.-E. Ooi, T. Ha, I. Wong, M.S. Soh, A. Dodabalapur, High mobility organic thin film transistor and efficient photovoltaic devices using versatile donor-acceptor polymer semiconductor by molecular design, Energy Environ. Sci. 4 (2011) 2288–2296. doi:10.1039/C1EE01213D.

[92] A.J. Snell, W.E. Spear, P.G. Le Comber, K. Mackenzie, Application of amorphous silicon field effect transistors in integrated circuits, Appl. Phys. A. 26 (1981) 83–86. doi:10.1007/BF00616653.

[93] X. Guo, M. Baumgarten, K. Müllen, Designing π-conjugated polymers for organic electronics, Prog. Polym. Sci. 38 (2013) 1832–1908. doi:http://dx.doi.org/10.1016/j.progpolymsci.2013.09.005.

[94] H. Yan, Z. Chen, Y. Zheng, C. Newman, J.R. Quinn, F. Dötz, M. Kastler, A. Facchetti, A high-mobility electron-transporting polymer for printed transistors., Nature. 457 (2009) 679–

86. doi:10.1038/nature07727.

[95] R. Matsidik, H. Komber, A. Luzio, M. Caironi, M. Sommer, Defect-free naphthalene diimide bithiophene copolymers with controlled molar mass and high performance via direct arylation polycondensation, J. Am. Chem. Soc. 137 (2015) 6705. doi:10.1021/jacs.5b03355.

[96] C. Luo, A.K.K. Kyaw, L.A. Perez, S. Patel, M. Wang, B. Grimm, G.C. Bazan, E.J. Kramer, A.J. Heeger, General Strategy for Self-Assembly of Highly Oriented Nanocrystalline Semiconducting Polymers with High Mobility, Nano Lett. 14 (2014) 2764–2771. doi:10.1021/nl500758w.

[97] H. Benten, D. Mori, H. Ohkita, S. Ito, Recent research progress of polymer donor/polymer acceptor blend solar cells, J. Mater. Chem. A. 4 (2016) 5340–5365. doi:10.1039/C5TA10759H.

[98] Z. Yan, B. Sun, Y. Li, Novel stable (3E,7E)-3,7-bis(2-oxoindolin-3-ylidene)benzo[1,2-b:4,5-b[prime or minute]]difuran-2,6(3H,7H)-dione based donor-acceptor polymer semiconductors for n-type organic thin film transistors, Chem. Commun. 49 (2013) 3790–3792. doi:10.1039/C3CC40531A.

[99] T. Lei, J.-H. Dou, X.-Y. Cao, J.-Y. Wang, J. Pei, A BDOPV-Based Donor-Acceptor Polymer for High-Performance n-Type and Oxygen-Doped Ambipolar Field-Effect Transistors, Adv. Mater. 25 (2013) 6589–6593. doi:10.1002/adma.201302278.

[100] G. Zhang, P. Li, L. Tang, J. Ma, X. Wang, H. Lu, B. Kang, K. Cho, L. Qiu, A bis(2-oxoindolin-3-ylidene)-benzodifuran-dione containing copolymer for high-mobility ambipolar transistors, Chem. Commun. 50 (2014) 3180–3183. doi:10.1039/c3cc48695h.

[101] Y. Li, P. Sonar, L. Murphy, W. Hong, High mobility diketopyrrolopyrrole (DPP)-based organic semiconductor materials for organic thin film transistors and photovoltaics, Energy Environ. Sci. 6 (2013) 1684–1710. doi:10.1039/C3EE00015J.

[102] P.L.T. Boudreault, A. Najari, M. Leclerc, Processable low-bandgap polymers for photovoltaic

applications, Chem. Mater. 23 (2011) 456–469. doi:10.1021/cm1021855.

[103] K.-J. Baeg, M. Caironi, Y.-Y. Noh, Toward Printed Integrated Circuits based on Unipolar or Ambipolar Polymer Semiconductors, Adv. Mater. 25 (2013) 4210–4244. doi:10.1002/adma.201205361.

[104] J.-H. Dou, Y.-Q. Zheng, T. Lei, S.-D. Zhang, Z. Wang, W.-B. Zhang, J.-Y. Wang, J. Pei, Systematic Investigation of Side-Chain Branching Position Effect on Electron Carrier Mobility in Conjugated Polymers, Adv. Funct. Mater. 24 (2014) 6270–6278. doi:10.1002/adfm.201401822.

[105] T. Lei, J.-H. Dou, X.-Y. Cao, J.-Y. Wang, J. Pei, Electron-Deficient Poly(p-phenylene vinylene) Provides Electron Mobility over 1 cm2 V–1 s–1 under Ambient Conditions, J. Am. Chem. Soc. 135 (2013) 12168–12171. doi:10.1021/ja403624a.

[106] T. Lei, X. Xia, J.-Y. Wang, C.-J. Liu, J. Pei, "Conformation Locked" Strong Electron-Deficient Poly(p-Phenylene Vinylene) Derivatives for Ambient-Stable n-Type Field-Effect Transistors: Synthesis, Properties, and Effects of Fluorine Substitution Position, J. Am. Chem. Soc. 136 (2014) 2135–2141. doi:10.1021/ja412533d.

[107] J.W. Rumer, M. Levick, S.-Y. Dai, S. Rossbauer, Z. Huang, L. Biniek, T.D. Anthopoulos, J.R. Durrant, D.J. Procter, I. McCulloch, BPTs: thiophene-flanked benzodipyrrolidone conjugated polymers for ambipolar organic transistors, Chem. Commun. 49 (2013) 4465. doi:10.1039/c3cc40811f.

[108] Y. Cao, J.-S. Yuan, X. Zhou, X.-Y. Wang, F.-D. Zhuang, J.-Y. Wang, J. Pei, N-Fused BDOPV: a tetralactam derivative as a building block for polymer field-effect transistors, Chem. Commun. 51 (2015) 10514–10516. doi:10.1039/C5CC02026C.

[109] A.N.C. Lötter, R. Pathak, T.S. Sello, M.A. Fernandes, W.A.L. van Otterlo, C.B. de Koning, Synthesis of the dibenzopyrrocoline alkaloid skeleton: indolo[2,1-a]isoquinolines and related analogues, Tetrahedron. 63 (2007) 2263–2274. doi:https://doi.org/10.1016/j.tet.2006.12.063.

[110] O.G. Reid, R.D. Pensack, Y. Song, G.D. Scholes, G. Rumbles, Charge Photogeneration in Neat Conjugated Polymers, Chem. Mater. 26 (2014) 561–575. doi:10.1021/cm4027144.

[111] G. Zhang, J. Guo, M. Zhu, P. Li, H. Lu, K. Cho, L. Qiu, Bis(2-oxoindolin-3-ylidene)-benzodifuran-dione-based D-A polymers for high-performance n-channel transistors, Polym. Chem. 6 (2015) 2531–2540. doi:10.1039/C4PY01683A.

[112] X. Zhou, N. Ai, Z.-H. Guo, F.-D. Zhuang, Y.-S. Jiang, J.-Y. Wang, J. Pei, Balanced Ambipolar Organic Thin-Film Transistors Operated under Ambient Conditions: Role of the Donor Moiety in BDOPV-Based Conjugated Copolymers, Chem. Mater. 27 (2015) 1815–1820. doi:10.1021/acs.chemmater.5b00018.

[113] M. Zhu, S. Lv, Q. Wang, G. Zhang, H. Lu, L. Qiu, Enhanced near-infrared photoresponse of organic phototransistors based on single-component donor-acceptor conjugated polymer nanowires, Nanoscale. 8 (2016) 7738–7748. doi:10.1039/C5NR09003B.

[114] F. Li, Y. Chen, C. Ma, U. Buttner, K. Leo, T. Wu, High-Performance Near-Infrared Phototransistor Based on n-Type Small-Molecular Organic Semiconductor, Adv. Electron. Mater. (2016) 1600430. doi:10.1002/aelm.201600430.

[115] Z. Qi, J. Cao, H. Li, L. Ding, J. Wang, High-Performance Thermally Stable Organic Phototransistors Based on PSeTPTI/PC61BM for Visible and Ultraviolet Photodetection, Adv. Funct. Mater. 25 (2015) 3138–3146. doi:10.1002/adfm.201500525.

[116] K.H. Hendriks, W. Li, M.M. Wienk, R.A.J. Janssen, Small-Bandgap Semiconducting Polymers with High Near-Infrared Photoresponse, J. Am. Chem. Soc. 136 (2014) 12130–12136. doi:10.1021/ja506265h.

[117] Y. Peng, W. Lv, B. Yao, G. Fan, D. Chen, P. Gao, M. Zhou, Y. Wang, High performance near infrared photosensitive organic field-effect transistors realized by an organic hybrid planar-bulk heterojunction, Org. Electron. 14 (2013) 1045–1051. doi:https://doi.org/10.1016/j.orgel.2013.02.005.

[118] T. Lei, J.H. Dou, J. Pei, Influence of alkyl chain branching positions on the hole mobilities of polymer thin-film transistors, Adv. Mater. 24 (2012) 6457–6461. doi:10.1002/adma.201202689.

[119] S. Chen, B. Sun, W. Hong, H. Aziz, Y. Meng, Y. Li, Influence of side chain length and bifurcation point on the crystalline structure and charge transport of diketopyrrolopyrrole-quaterthiophene copolymers (PDQTs), J. Mater. Chem. C. 2 (2014) 2183–2190. doi:10.1039/c3tc32219j.

[120] E. Zhou, J. Cong, Q. Wei, K. Tajima, C. Yang, K. Hashimoto, All-Polymer Solar Cells from Perylene Diimide Based Copolymers: Material Design and Phase Separation Control, Angew. Chemie Int. Ed. 50 (2011) 2799–2803. doi:10.1002/anie.201005408.

[121] D. Mori, H. Benten, H. Ohkita, S. Ito, K. Miyake, Polymer/Polymer Blend Solar Cells Improved by Using High-Molecular-Weight Fluorene-Based Copolymer as Electron Acceptor, ACS Appl. Mater. Interfaces. 4 (2012) 3325–3329. doi:10.1021/am300623f.

[122] M. Schubert, D. Dolfen, J. Frisch, S. Roland, R. Steyrleuthner, B. Stiller, Z. Chen, U. Scherf, N. Koch, A. Facchetti, D. Neher, Influence of Aggregation on the Performance of All-Polymer Solar Cells Containing Low-Bandgap Naphthalenediimide Copolymers, Adv. Energy Mater. 2 (2012) 369–380. doi:10.1002/aenm.201100601.

[123] W. Li, Y. An, M.M. Wienk, R.A.J. Janssen, Polymer-polymer solar cells with a near-infrared spectral response, J. Mater. Chem. A. 3 (2015) 6756–6760. doi:10.1039/C5TA01042J.

[124] B.A. Jones, A. Facchetti, M.R. Wasielewski, T.J. Marks, Tuning Orbital Energetics in Arylene Diimide Semiconductors. Materials Design for Ambient Stability of n-Type Charge Transport, J. Am. Chem. Soc. 129 (2007) 15259–15278. doi:10.1021/ja075242e.

[125] D.M. de Leeuw, M.M.J. Simenon, A.R. Brown, R.E.F. Einerhand, Stability of n-type doped conducting polymers and consequences for polymeric microelectronic devices, Synth. Met. 87 (1997) 53–59. doi:10.1016/S0379-6779(97)80097-5.

[126] J. Wang, M.S. Gudiksen, X. Duan, Y. Cui, C.M. Lieber, Highly Polarized Photoluminescence and Photodetection from Single Indium Phosphide Nanowires, Science (80-.). 293 (2001) 1455 LP-1457. http://science.sciencemag.org/content/293/5534/1455.abstract.

[127] X. Gong, M. Tong, Y. Xia, W. Cai, J.S. Moon, Y. Cao, G. Yu, C.-L. Shieh, B. Nilsson, A.J. Heeger, High-Detectivity Polymer Photodetectors with Spectral Response from 300 nm to 1450 nm, Science (80-.). 325 (2009) 1665 LP-1667. http://science.sciencemag.org/content/325/5948/1665.abstract.

[128] G. Konstantatos, I. Howard, A. Fischer, S. Hoogland, J. Clifford, E. Klem, L. Levina, E.H. Sargent, Ultrasensitive solution-cast quantum dot photodetectors, Nature. 442 (2006) 180–183. http://dx.doi.org/10.1038/nature04855.

[129] R. Kim, P.S.K. Amegadze, I. Kang, H.-J. Yun, Y.-Y. Noh, S.-K. Kwon, Y.-H. Kim, High-Mobility Air-Stable Naphthalene Diimide-Based Copolymer Containing Extended π-Conjugation for n-Channel Organic Field Effect Transistors, Adv. Funct. Mater. 23 (2013) 5719–5727. doi:10.1002/adfm.201301197.

[130] B.W. D'Andrade, S. Datta, S.R. Forrest, P. Djurovich, E. Polikarpov, M.E. Thompson, Relationship between the ionization and oxidation potentials of molecular organic semiconductors, Org. Electron. 6 (2005) 11–20. doi:http://dx.doi.org/10.1016/j.orgel.2005.01.002.

[131] X. Guo, A. Facchetti, T.J. Marks, Imide- and Amide-Functionalized Polymer Semiconductors, Chem. Rev. 114 (2014) 8943–9021. doi:10.1021/cr500225d.

[132] J.D. Yuen, F. Wudl, Strong acceptors in donor-acceptor polymers for high performance thin film transistors, Energy Environ. Sci. 6 (2013) 392–406. doi:10.1039/C2EE23505F.

[133] J. Mei, D.H. Kim, A.L. Ayzner, M.F. Toney, Z. Bao, Siloxane-Terminated Solubilizing Side Chains: Bringing Conjugated Polymer Backbones Closer and Boosting Hole Mobilities in Thin-Film Transistors, J. Am. Chem. Soc. 133 (2011) 20130–20133. doi:10.1021/ja209328m.

[134] W. Hong, C. Guo, Y. Li, Y. Zheng, C. Huang, S. Lu, A. Facchetti, Synthesis and thin-film transistor performance of benzodipyrrolinone and bithiophene donor-acceptor copolymers, J. Mater. Chem. 22 (2012) 22282–22289. doi:10.1039/C2JM34867E.

[135] W. Hong, B. Sun, C. Guo, J. Yuen, Y. Li, S. Lu, C. Huang, A. Facchetti, Dipyrrolo[2,3-b:2′,3′-e]pyrazine-2,6(1H,5H)-dione based conjugated polymers for ambipolar organic thin-film transistors, Chem. Commun. 49 (2013) 484–486. doi:10.1039/C2CC37266E.

[136] J.Y. Back, H. Yu, I. Song, I. Kang, H. Ahn, T.J. Shin, S.-K. Kwon, J.H. Oh, Y.-H. Kim, Investigation of Structure–Property Relationships in Diketopyrrolopyrrole-Based Polymer Semiconductors via Side-Chain Engineering, Chem. Mater. 27 (2015) 1732–1739. doi:10.1021/cm504545e.

[137] Lyn (Beijing) Science & Technology Co., Ltd, (n.d.).

[138] J.D. Jian Pei, Ting Lei, Compound with branching alkyl chains, method for preparing the same, and use thereof in photoelectric device, US 2014011973 A1, 2014.

[139] W. Hong, C. Guo, B. Sun, Y. Li, (3Z,3'Z)-3,3'-(Hydrazine-1,2-diylidene)bis(indolin-2-one) as a new electron-acceptor building block for donor-acceptor [small pi]-conjugated polymers for organic thin film transistors, J. Mater. Chem. C. 3 (2015) 4464–4470. doi:10.1039/C5TC00447K.

[140] F.C. Spano, The Spectral Signatures of Frenkel Polarons in H- and J-Aggregates, Acc. Chem. Res. 43 (2010) 429–439. doi:10.1021/ar900233v.

[141] J. Zaumseil, H. Sirringhaus, Electron and Ambipolar Transport in Organic Field-Effect Transistors, Chem. Rev. 107 (2007) 1296–1323. doi:10.1021/cr0501543.

[142] Y. Zhao, Y. Guo, Y. Liu, 25th Anniversary Article: Recent Advances in n-Type and Ambipolar Organic Field-Effect Transistors, Adv. Mater. 25 (2013) 5372–5391. doi:10.1002/adma.201302315.

[143] G. Zhang, G. Yang, H. Yan, J.H. Kim, H. Ade, W. Wu, X. Xu, Y. Duan, Q. Peng, Efficient Nonfullerene Polymer Solar Cells Enabled by a Novel Wide Bandgap Small Molecular Acceptor, Adv. Mater. (2017). doi:10.1002/adma.201606054.

[144] Y. He, C. Guo, B. Sun, J. Quinn, Y. Li, (3E,7E)-3,7-Bis(2-oxoindolin-3-ylidene)-5,7-dihydropyrrolo[2,3-f]indole-2,6(1H,3H)-dione based polymers for ambipolar organic thin film transistors, Chem. Commun. 51 (2015) 8093–8096. doi:10.1039/C5CC01021G.

[145] M.J. Winokur, D. Spiegel, Y. Kim, S. Hotta, A.J. Heeger, Structural and absorption studies of the thermochromic transition in poly(3-hexylthiophene), Synth. Met. 28 (1989) 419–426. doi:10.1016/0379-6779(89)90554-7.

[146] H. Sirringhaus, P.J. Brown, R.H. Friend, M.M. Nielsen, K. Bechgaard, B.M.W. Langeveld-Voss, A.J.H. Spiering, R.A.J. Janssen, E.W. Meijer, P. Herwig, D.M. de Leeuw, Two-dimensional charge transport in self-organized, high-mobility conjugated polymers, Nature. 401 (1999) 685–688.

[147] Y. Wang, H. Benten, S. Ohara, D. Kawamura, H. Ohkita, S. Ito, Measurement of Exciton Diffusion in a Well-Defined Donor/Acceptor Heterojunction based on a Conjugated Polymer and Cross-Linked Fullerene Derivative, ACS Appl. Mater. Interfaces. 6 (2014) 14108–14115. doi:10.1021/am503434p.

[148] S. Fabiano, Z. Chen, S. Vahedi, A. Facchetti, B. Pignataro, M.A. Loi, Role of photoactive layer morphology in high fill factor all-polymer bulk heterojunction solar cells, J. Mater. Chem. 21 (2011) 5891–5896. doi:10.1039/C0JM03405C.

[149] U. W?rfel, D. Neher, A. Spies, S. Albrecht, Impact of charge transport on current?voltage characteristics and power-conversion efficiency of organic solar cells, Nat. Commun. 6 (2015) 6951. doi:10.1038/ncomms7951.

[150] J.D. Kotlarski, D.J.D. Moet, P.W.M. Blom, Role of balanced charge carrier transport in low band gap polymer:Fullerene bulk heterojunction solar cells, J. Polym. Sci. Part B Polym. Phys.

49 (2011) 708–711. doi:10.1002/polb.22243.

[151] Q. Fan, W. Su, X. Guo, Y. Wang, J. Chen, C. Ye, M. Zhang, Y. Li, Side-chain engineering for efficient non-fullerene polymer solar cells based on a wide-bandgap polymer donor, J. Mater. Chem. A. 5 (2017) 9204–9209. doi:10.1039/C7TA02075A.

[152] Q. Tu, D. Cai, L. Wang, J. Wei, Q. Shang, S.-C. Chen, Y. Ma, Z. Yin, C. Tang, Q. Zheng, Side-chain engineering of diindenocarbazole-based large bandgap copolymers toward high performance polymer solar cells, J. Mater. Chem. C. 4 (2016) 6160–6168. doi:10.1039/C6TC01778A.

[153] E. Wang, L. Hou, Z. Wang, Z. Ma, S. Hellström, W. Zhuang, F. Zhang, O. Inganäs, M.R. Andersson, Side-Chain Architectures of 2,7-Carbazole and Quinoxaline-Based Polymers for Efficient Polymer Solar Cells, Macromolecules. 44 (2011) 2067–2073. doi:10.1021/ma102783d.

[154] C. Cabanetos, A. El Labban, J.A. Bartelt, J.D. Douglas, W.R. Mateker, J.M.J. Fréchet, M.D. McGehee, P.M. Beaujuge, Linear Side Chains in Benzo[1,2-b:4,5-b′]dithiophene–Thieno[3,4-c]pyrrole-4,6-dione Polymers Direct Self-Assembly and Solar Cell Performance, J. Am. Chem. Soc. 135 (2013) 4656–4659. doi:10.1021/ja400365b.

[155] J. Lee, J.W. Chung, J. Jang, D.H. Kim, J.-I. Park, E. Lee, B.-L. Lee, J.-Y. Kim, J.Y. Jung, J.S. Park, B. Koo, Y.W. Jin, D.H. Kim, Influence of Alkyl Side Chain on the Crystallinity and Trap Density of States in Thiophene and Thiazole Semiconducting Copolymer Based Inkjet-Printed Field-Effect Transistors, Chem. Mater. 25 (2013) 1927–1934. doi:10.1021/cm400592b.

[156] T. Wang, M.K. Ravva, J.-L. Brédas, Impact of the Nature of the Side-Chains on the Polymer-Fullerene Packing in the Mixed Regions of Bulk Heterojunction Solar Cells, Adv. Funct. Mater. 26 (2016) 5913–5921. doi:10.1002/adfm.201601134.

[157] M. Le Borgne, J. Quinn, J. Martín, N. Stingelin, G. Wantz, Y. Li, Synthesis and properties of a

novel narrow band gap oligomeric diketopyrrolopyrrole-based organic semiconductor, Dye. Pigment. 131 (2016) 160–167. doi:10.1016/j.dyepig.2016.04.002.

[158] M. Le Borgne, J. Quinn, J. Martin, N. Stingelin, Y. Li, G. Wantz, New 3,3′-(ethane-1,2-diylidene)bis(indolin-2-one) (EBI)-based small molecule semiconductors for organic solar cells, J. Mater. Chem. C. 5 (2017) 5143–5153. doi:10.1039/C7TC00711F.

[159] S. Shi, J. Yuan, G. Ding, M. Ford, K. Lu, G. Shi, J. Sun, X. Ling, Y. Li, W. Ma, Improved All-Polymer Solar Cell Performance by Using Matched Polymer Acceptor, Adv. Funct. Mater. 26 (2016) 5669–5678. doi:10.1002/adfm.201601037.

[160] A. Roosjen, J. Šmisterová, C. Driessen, J.T. Anders, A. Wagenaar, D. Hoekstra, R. Hulst, J.B.F.N. Engberts, Synthesis and Characteristics of Biodegradable Pyridinium Amphiphiles Used for in vitro DNA Delivery, European J. Org. Chem. 2002 (2002) 1271–1277. doi:10.1002/1099-0690(200204)2002:7<1271::AID-EJOC1271>3.0.CO;2-G.

[161] Y. Li, Monomeric, oligomeric and polymeric semiconductors containing fused rings and their devices, WO 2014071524 A1, 2014.

[162] J. Pommerehne, H. Vestweber, W. Guss, R.F. Mahrt, H. Bassler, M. Porsch, J. Daub, Efficient two layer leds on a polymer blend basis, Adv. Mater. 7 (1995) 551–554. doi:10.1002/adma.19950070608.

[163] X. Guo, F.S. Kim, M.J. Seger, S.A. Jenekhe, M.D. Watson, Naphthalene Diimide-Based Polymer Semiconductors: Synthesis, Structure–Property Correlations, and n-Channel and Ambipolar Field-Effect Transistors, Chem. Mater. 24 (2012) 1434–1442. doi:10.1021/cm2034273.

[164] H. Kang, M.A. Uddin, C. Lee, K.H. Kim, T.L. Nguyen, W. Lee, Y. Li, C. Wang, H.Y. Woo, B.J. Kim, Determining the role of polymer molecular weight for high-performance all-polymer solar cells: Its effect on polymer aggregation and phase separation, J. Am. Chem. Soc. 137 (2015) 2359–2365. doi:10.1021/ja5123182.

[165] K.D. Deshmukh, T. Qin, J.K. Gallaher, A.C.Y. Liu, E. Gann, K. O'Donnell, L. Thomsen, J.M. Hodgkiss, S.E. Watkins, C.R. McNeill, Performance, morphology and photophysics of high open-circuit voltage, low band gap all-polymer solar cells, Energy Environ. Sci. 8 (2015) 332–342. doi:10.1039/C4EE03059A.

[166] C. Mu, P. Liu, W. Ma, K. Jiang, J. Zhao, K. Zhang, Z. Chen, Z. Wei, Y. Yi, J. Wang, S. Yang, F. Huang, A. Facchetti, H. Ade, H. Yan, High-Efficiency All-Polymer Solar Cells Based on a Pair of Crystalline Low-Bandgap Polymers, Adv. Mater. 26 (2014) 7224–7230. doi:10.1002/adma.201402473.

[167] M. Sommer, Conjugated polymers based on naphthalene diimide for organic electronics, J. Mater. Chem. C. 2 (2014) 3088–3098. doi:10.1039/C3TC31755B.

[168] X. Zhan, A. Facchetti, S. Barlow, T.J. Marks, M.A. Ratner, M.R. Wasielewski, S.R. Marder, Rylene and related diimides for organic electronics, Adv. Mater. 23 (2011) 268–284. doi:10.1002/adma.201001402.

[169] S. Hüttner, M. Sommer, M. Thelakkat, n-type organic field effect transistors from perylene bisimide block copolymers and homopolymers, Appl. Phys. Lett. 92 (2008) 93302. doi:10.1063/1.2885712.

[170] J.A. Letizia, M.R. Salata, C.M. Tribout, A. Facchetti, M.A. Ratner, T.J. Marks, n-Channel Polymers by Design: Optimizing the Interplay of Solubilizing Substituents, Crystal Packing, and Field-Effect Transistor Characteristics in Polymeric Bithiophene-Imide Semiconductors, J. Am. Chem. Soc. 130 (2008) 9679–9694. doi:10.1021/ja710815a.

[171] X. Zhan, Z. Tan, B. Domercq, Z. An, X. Zhang, S. Barlow, Y. Li, D. Zhu, B. Kippelen, S.R. Marder, A High-Mobility Electron-Transport Polymer with Broad Absorption and Its Use in Field-Effect Transistors and All-Polymer Solar Cells, J. Am. Chem. Soc. 129 (2007) 7246–7247. doi:10.1021/ja071760d.

[172] J.R. Moore, S. Albert-Seifried, A. Rao, S. Massip, B. Watts, D.J. Morgan, R.H. Friend, C.R.

McNeill, H. Sirringhaus, Polymer Blend Solar Cells Based on a High-Mobility Naphthalenediimide-Based Polymer Acceptor: Device Physics, Photophysics and Morphology, Adv. Energy Mater. 1 (2011) 230–240. doi:10.1002/aenm.201000035.

[173] Z. Li, W. Zhang, X. Xu, Z. Genene, D. Di Carlo Rasi, W. Mammo, A. Yartsev, M.R. Andersson, R.A.J. Janssen, E. Wang, High-Performance and Stable All-Polymer Solar Cells Using Donor and Acceptor Polymers with Complementary Absorption, Adv. Energy Mater. 201602722 (2017) 1602722. doi:10.1002/aenm.201602722.

[174] B. Fan, L. Ying, Z. Wang, B. He, X.-F. Jiang, F. Huang, Y. Cao, Optimisation of processing solvent and molecular weight for the production of green-solvent-processed all-polymer solar cells with a power conversion efficiency over 9%, Energy Environ. Sci. 10 (2017) 1243–1251. doi:10.1039/C7EE00619E.

[175] S. Dai, S. Huang, H. Yu, Q. Ling, X. Zhan, Perylene and naphthalene diimide copolymers for all-polymer solar cells: Effect of perylene/naphthalene ratio, J. Polym. Sci. Part A Polym. Chem. 55 (2017) 682–689. doi:10.1002/pola.28392.

[176] S.-H. Liao, H.-J. Jhuo, Y.-S. Cheng, S.-A. Chen, Fullerene Derivative-Doped Zinc Oxide Nanofilm as the Cathode of Inverted Polymer Solar Cells with Low-Bandgap Polymer (PTB7-Th) for High Performance, Adv. Mater. 25 (2013) 4766–4771. doi:10.1002/adma.201301476.

[177] Q.-Y. Li, J. Xiao, L.-M. Tang, H.-C. Wang, Z. Chen, Z. Yang, H.-L. Yip, Y.-X. Xu, Thermally stable high performance non-fullerene polymer solar cells with low energy loss by using ladder-type small molecule acceptors, Org. Electron. 44 (2017) 217–224. doi:https://doi.org/10.1016/j.orgel.2017.02.008.

[178] C. Weng, L. Gao, Z. Zhang, Z. Liu, S. Tan, Y. Li, A new polymer acceptor containing naphthalene diimide and 1,3,4-thiadiazole for all-polymer solar cells, J. Polym. Sci. Part B Polym. Phys. 55 (2017) 990–996. doi:10.1002/polb.24347.

[179] E.A.B. Kantchev, H.S. Tan, T.B. Norsten, M.B. Sullivan, O,O′ -Disubstituted N,N′ -

Dihydroxynaphthalenediimides (DHNDI): First Principles Designed Organic Building Blocks for Materials Science, Org. Lett. 13 (2011) 5432–5435. doi:10.1021/ol201906z.

[180] N. Cho, C.W. Schlenker, K.M. Knesting, P. Koelsch, H.-L. Yip, D.S. Ginger, A.K.-Y. Jen, High-Dielectric Constant Side-Chain Polymers Show Reduced Non-Geminate Recombination in Heterojunction Solar Cells, Adv. Energy Mater. 4 (2014) 1301857. doi:10.1002/aenm.201301857.

[181] Y.-Q. Zheng, T. Lei, J.-H. Dou, X. Xia, J.-Y. Wang, C.-J. Liu, J. Pei, Strong Electron-Deficient Polymers Lead to High Electron Mobility in Air and Their Morphology-Dependent Transport Behaviors, Adv. Mater. 28 (2016) 7213–7219. doi:10.1002/adma.201600541.

[182] G. Wei, S. Wang, K. Sun, M.E. Thompson, S.R. Forrest, Solvent-Annealed Crystalline Squaraine: PC70BM (1:6) Solar Cells, Adv. Energy Mater. 1 (2011) 184–187. doi:10.1002/aenm.201100045.

[183] Y. Zheng, S. Li, D. Zheng, J. Yu, Effects of different polar solvents for solvent vapor annealing treatment on the performance of polymer solar cells, Org. Electron. 15 (2014) 2647–2653. doi:https://doi.org/10.1016/j.orgel.2014.07.026.

[184] C.V. Kumar, L. Cabau, A. Viterisi, S. Biswas, G.D. Sharma, E. Palomares, Solvent Annealing Control of Bulk Heterojunction Organic Solar Cells with 6.6% Efficiency Based on a Benzodithiophene Donor Core and Dicyano Acceptor Units, J. Phys. Chem. C. 119 (2015) 20871–20879. doi:10.1021/acs.jpcc.5b07130.

[185] A. Zhang, Q. Wang, R.A.A. Bovee, C. Li, J. Zhang, Y. Zhou, Z. Wei, Y. Li, R.A.J. Janssen, Z. Wang, W. Li, Perfluoroalkyl-substituted conjugated polymers as electron acceptors for all-polymer solar cells: the effect of diiodoperfluoroalkane additives, J. Mater. Chem. A. 4 (2016) 7736–7745. doi:10.1039/C6TA00962J.

[186] P. Deng, C.H.Y. Ho, Y. Lu, H.-W. Li, S.-W. Tsang, S.K. So, B.S. Ong, Naphthalene diimide-difluorobenzene-based polymer acceptors for all-polymer solar cells, Chem. Commun. 53

(2017) 3249–3252. doi:10.1039/C6CC09724C.

[187] K. Zhou, R. Zhang, J. Liu, M. Li, X. Yu, R. Xing, Y. Han, Donor/Acceptor Molecular Orientation-Dependent Photovoltaic Performance in All-Polymer Solar Cells, ACS Appl. Mater. Interfaces. 7 (2015) 25352–25361. doi:10.1021/acsami.5b07605.

[188] B. Mukherjee, Flexible organic N-channel phototransistor and integrated logic devices, Opt. - Int. J. Light Electron Opt. 139 (2017) 48–55. doi:10.1016/j.ijleo.2017.03.119.

[189] T. Lee, D. Bang, Y. Park, S.H. Kim, J. Choi, J. Park, D. Kim, E. Kim, J.-S. Suh, Y.-M. Huh, S. Haam, Gadolinium-Enriched Polyaniline Particles (GPAPs) for Simultaneous Diagnostic Imaging and Localized Photothermal Therapy of Epithelial Cancer, Adv. Healthc. Mater. 3 (2014) 1408–1414. doi:10.1002/adhm.201300636.

[190] J. Zhou, Z. Lu, X. Zhu, X. Wang, Y. Liao, Z. Ma, F. Li, NIR photothermal therapy using polyaniline nanoparticles, Biomaterials. 34 (2013) 9584–9592. doi:https://doi.org/10.1016/j.biomaterials.2013.08.075.

[191] H. Gong, L. Cheng, J. Xiang, H. Xu, L. Feng, X. Shi, Z. Liu, Near-Infrared Absorbing Polymeric Nanoparticles as a Versatile Drug Carrier for Cancer Combination Therapy, Adv. Funct. Mater. 23 (2013) 6059–6067. doi:10.1002/adfm.201301555.

[192] D.H. Sliney, R.T. Wangemann, J.K. Franks, M.L. Wolbarsht, Visual sensitivity of the eye to infrared laser radiation, J. Opt. Soc. Am. 66 (1976) 339–341. doi:10.1364/JOSA.66.000339.

[193] J. Quinn, H. Patel, F. Haider, D.A. Khan, Y. Li, Converting a Semiconducting Polymer from Ambipolar into n-Type Dominant by Amine End-Capping, ChemElectroChem. 4 (2017) 256–260. doi:10.1002/celc.201600628.

[194] C. Guo, J. Quinn, B. Sun, Y. Li, Dramatically different charge transport properties of bisthienyl diketopyrrolopyrrole-bithiazole copolymers synthesized via two direct (hetero)arylation polymerization routes, Polym. Chem. 7 (2016) 4515–4524. doi:10.1039/C6PY00762G.

[195] H. Huang, L. Yang, B. Sharma, Recent advances in organic ternary solar cells, J. Mater. Chem. A. 0 (2017) 1–17. doi:10.1039/C7TA00887B.

[196] D. Angmo, M. Bjerring, N.C. Nielsen, B.C. Thompson, F.C. Krebs, Fullerene alloy formation and the benefits for efficient printing of ternary blend organic solar cells, J. Mater. Chem. C. 3 (2015) 5541–5548. doi:10.1039/C5TC00781J.

[197] H. Xu, H. Ohkita, Y. Tamai, H. Benten, S. Ito, Interface Engineering for Ternary Blend Polymer Solar Cells with a Heterostructured Near-IR Dye, Adv. Mater. 27 (2015) 5868–5874. doi:10.1002/adma.201502773.

Appendix

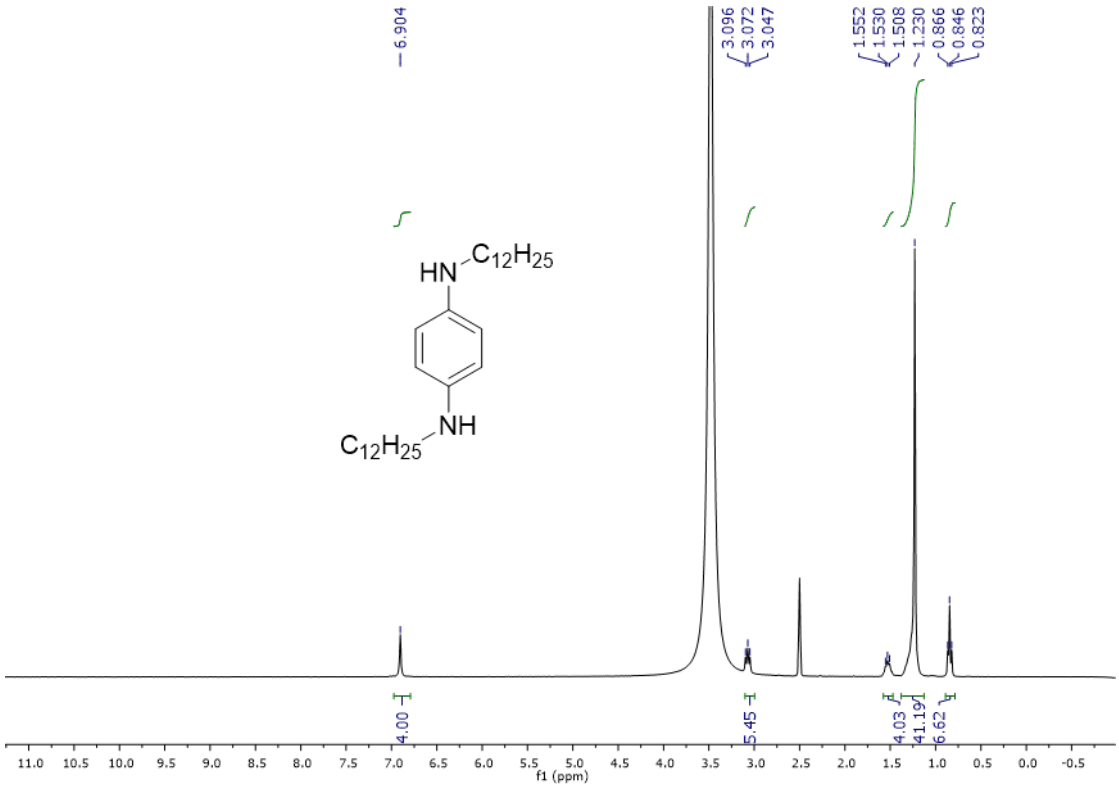

Figure A-1 300 MHz ^{1}H NMR spectrum for *N*,*N'*-didodecylbenzene-1,4-diamine (**1**) in DMSO-d6.

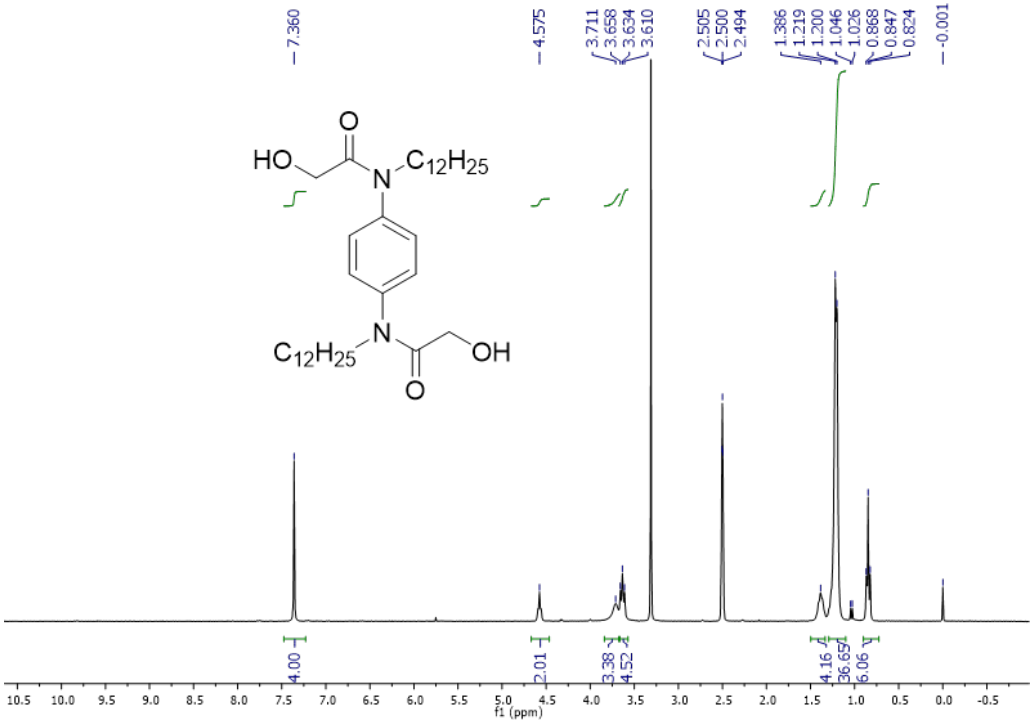

Figure A-2 300 MHz ^{1}H NMR spectrum for *N*,*N*'-(1,4-phenylene)bis(N-dodecyl-2-hydroxyacetamide) (**2)** in DMSO-d_6.

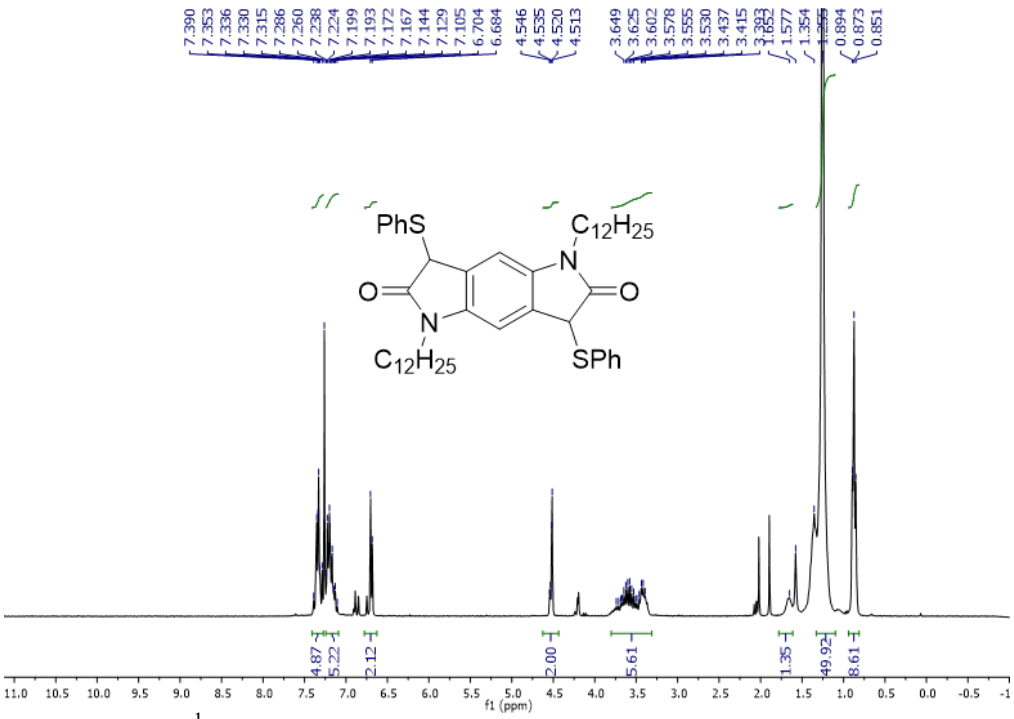

Figure A-3 300 MHz ^{1}H NMR spectrum for 1,5-didodecyl-3,7-bis(phenylthio)-5,7-dihydropyrrolo[2,3-*f*]indole-2,6(1*H*,3*H*)-dione (**3**) in chloroform-d.

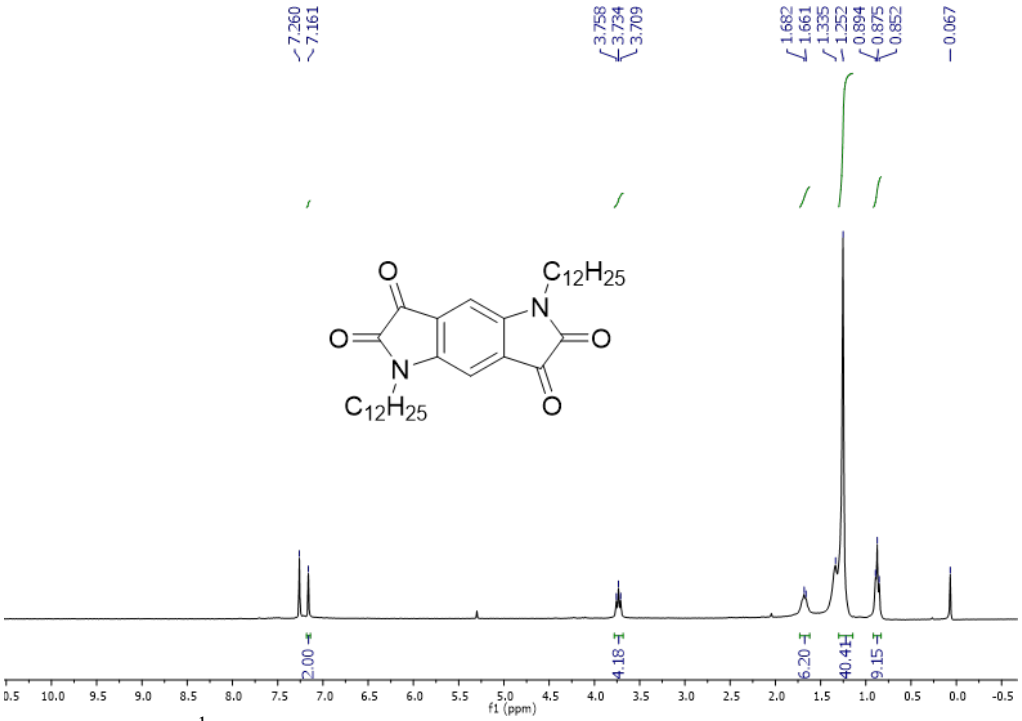

Figure A-4 300 MHz ^{1}H NMR spectrum for 1,5-didodecylpyrrolo[2,3-*f*]indole-2,3,6,7(1*H*,5*H*)-tetraone (**4**) in chloroform-d.

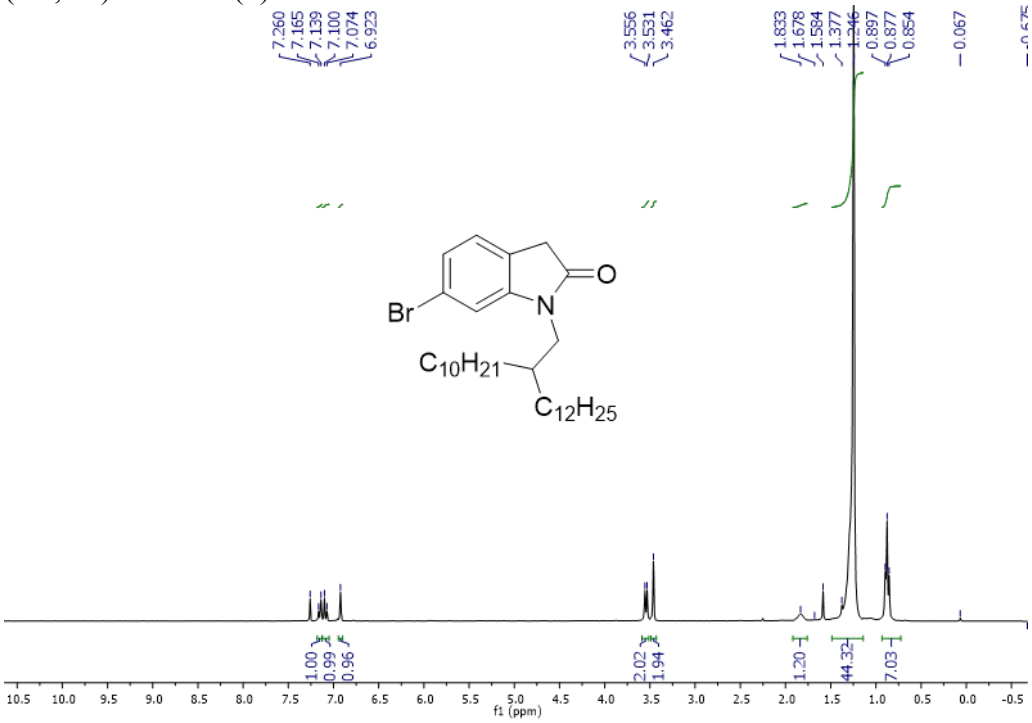

Figure A-5 300 MHz ^{1}H NMR spectrum for 6-bromo-1-(2-decyltetradecyl)indolin-2-one (**6**) in chloroform-d.

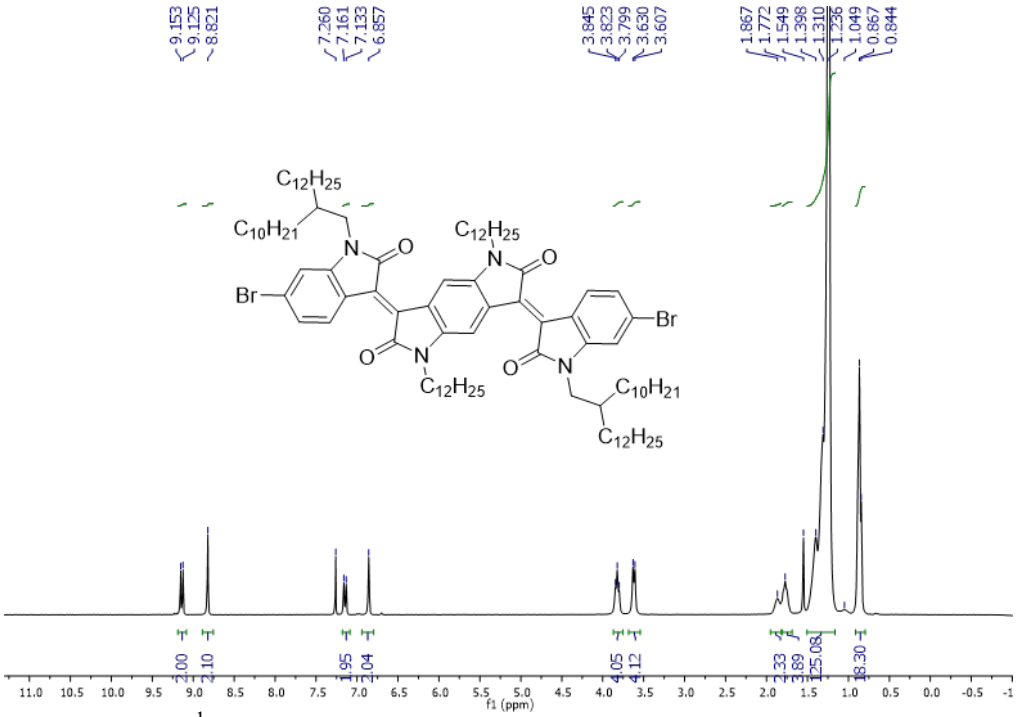

Figure A-6 300 MHz ^{1}H NMR spectrum for (3*E*,7*E*)-3,7-bis(6-bromo-1-(2-decyltetradecyl)-2-oxoindolin-3-ylidene)-1,5-didodecyl-5,7-dihydropyrrolo[2,3-*f*]indole-2,6(1*H*,3*H*)-dione (**7**) in chloroform-d.

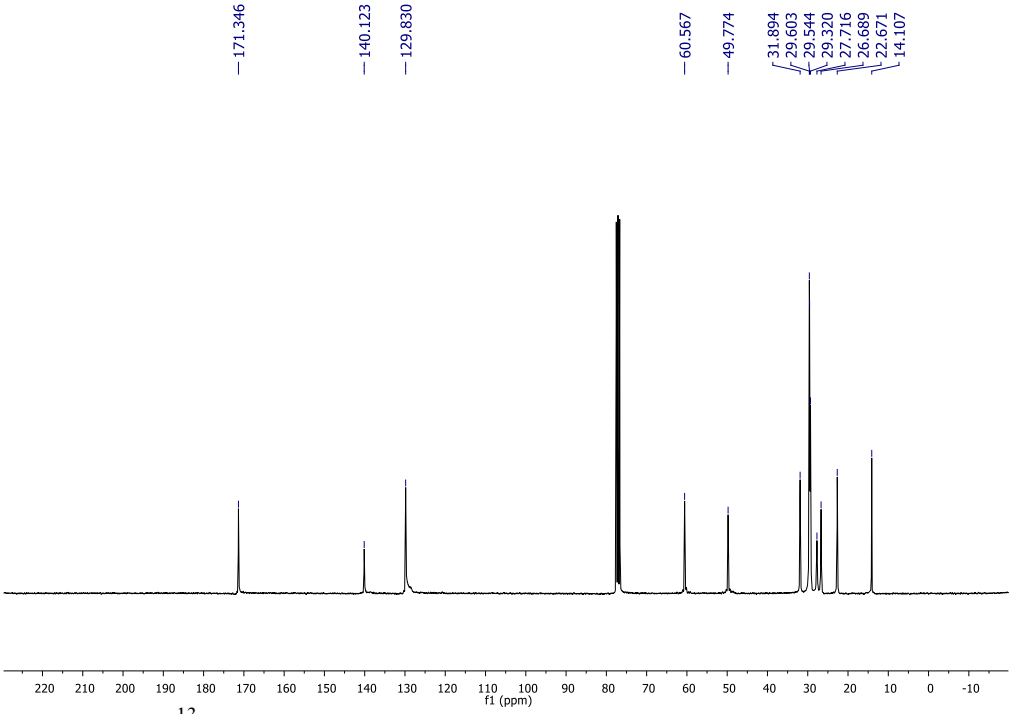

Figure A-7 75 MHz ^{13}C NMR spectrum for *N*,*N*'-(1,4-phenylene)bis(N-dodecyl-2-hydroxyacetamide) (**2)** in chloroform-d.

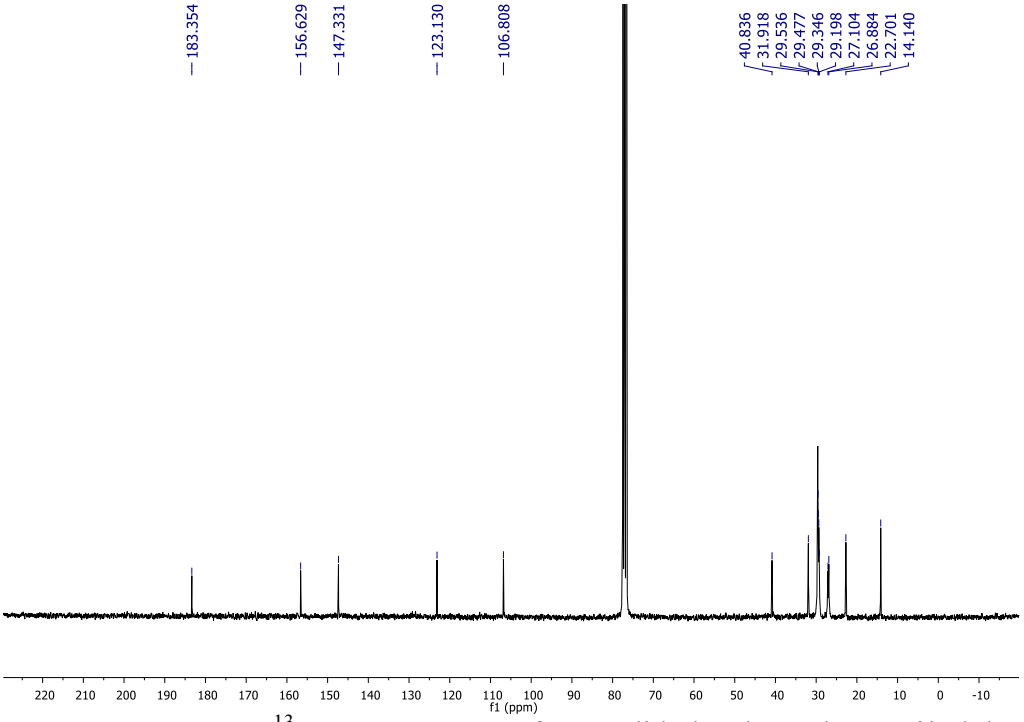

Figure A-8 75 MHz ^{13}C NMR spectrum for 1,5-didodecylpyrrolo[2,3-*f*]indole-2,3,6,7(1*H*,5*H*)-tetraone (**4**) in chloroform-d.

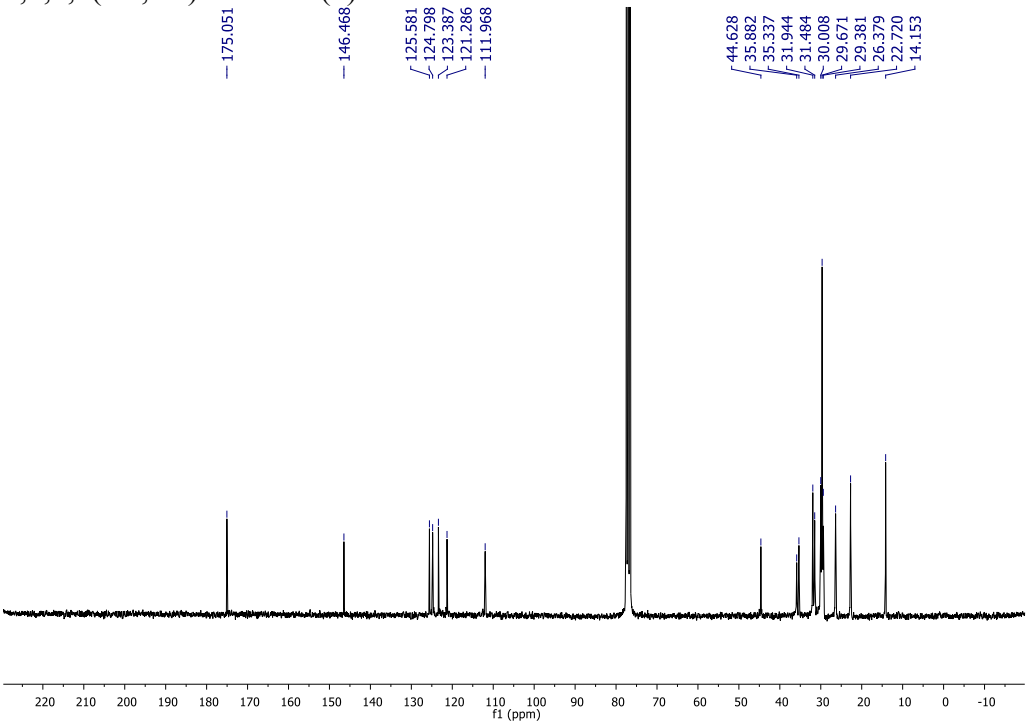

Figure A-9 75 MHz ^{13}C NMR spectrum for 6-bromo-1-(2-decyltetradecyl)indolin-2-one (**6**) in chloroform-d.

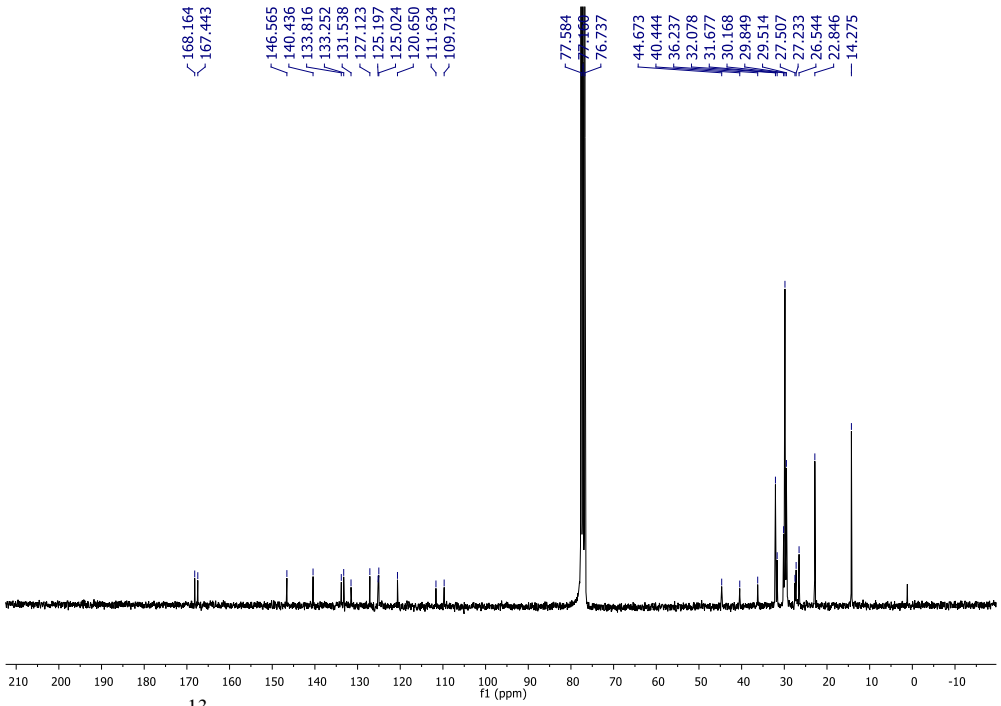

Figure A-10 75 MHz ^{13}C NMR spectrum for (3*E*,7*E*)-3,7-bis(6-bromo-1-(2-decyltetradecyl)-2-oxoindolin-3-ylidene)-1,5-didodecyl-5,7-dihydropyrrolo[2,3-*f*]indole-2,6(1*H*,3*H*)-dione (**7**) in chloroform-d.

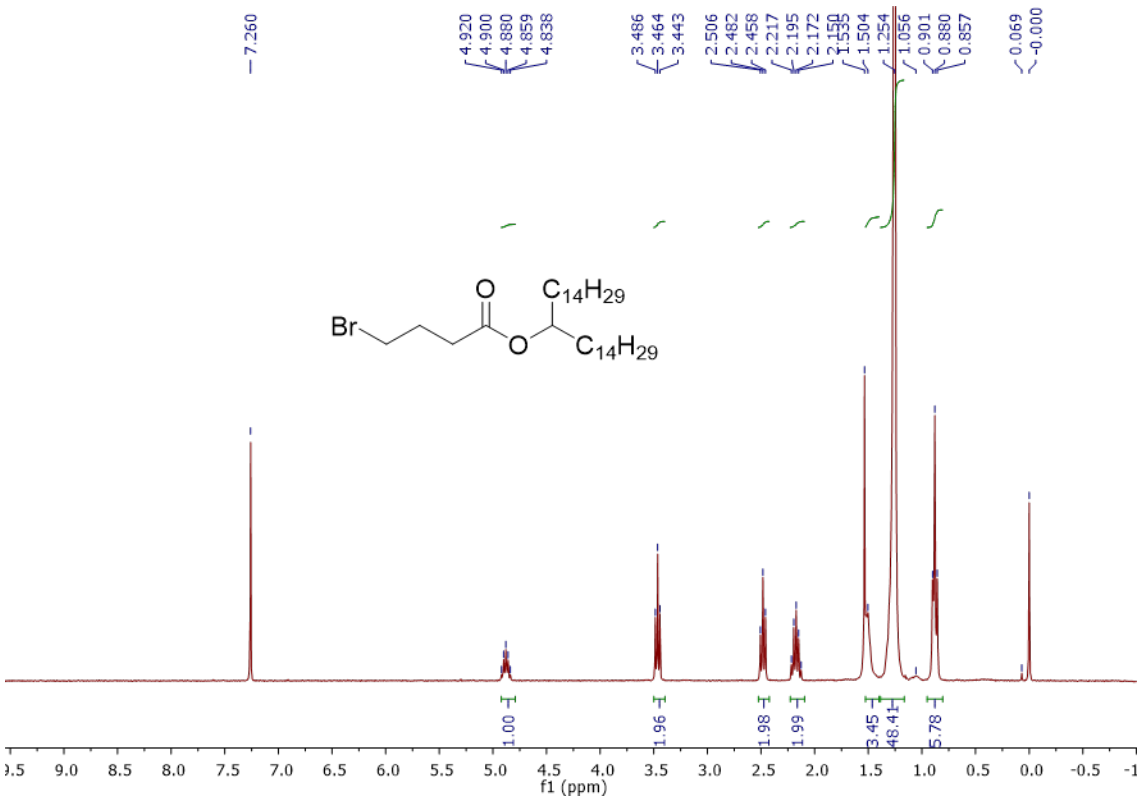

Figure A-11 300 MHz ^{1}H NMR spectrum for nonacosan-15-yl 4-bromobutanoate (**1a**) in $CDCl_3$.

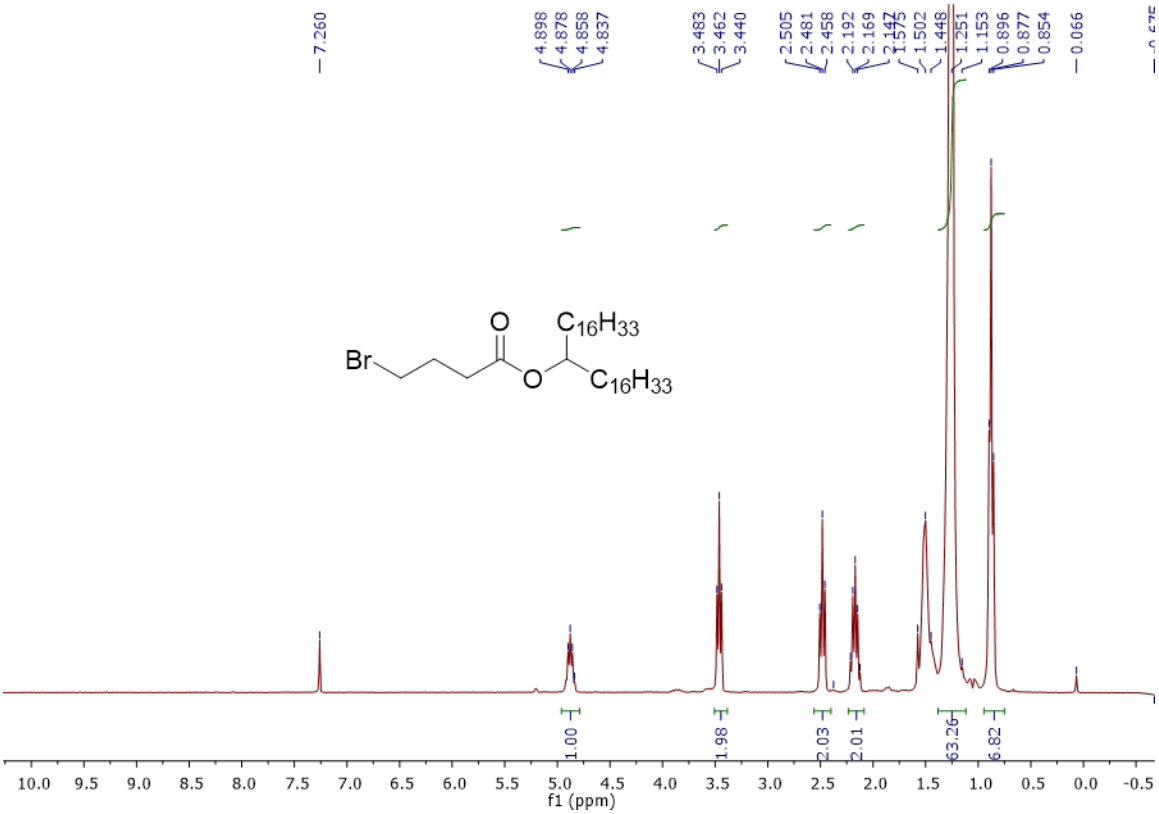

Figure A-12 300 MHz ^{1}H NMR spectrum for tritriacontan-17-yl 4-bromobutanoate (**1b**) in $CDCl_3$.

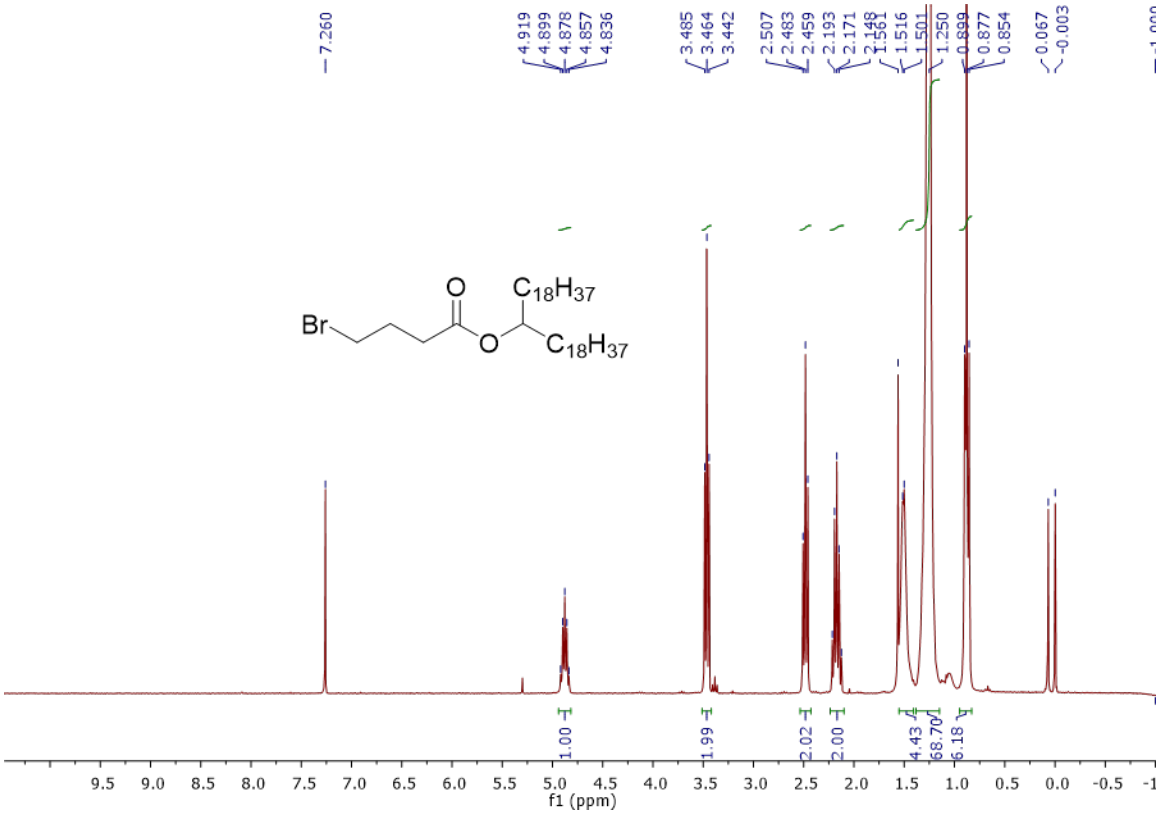

Figure A-13 300 MHz ^{1}H NMR spectrum for heptatriacontan-19-yl 4-bromobutanoate (**1c**) in $CDCl_3$.

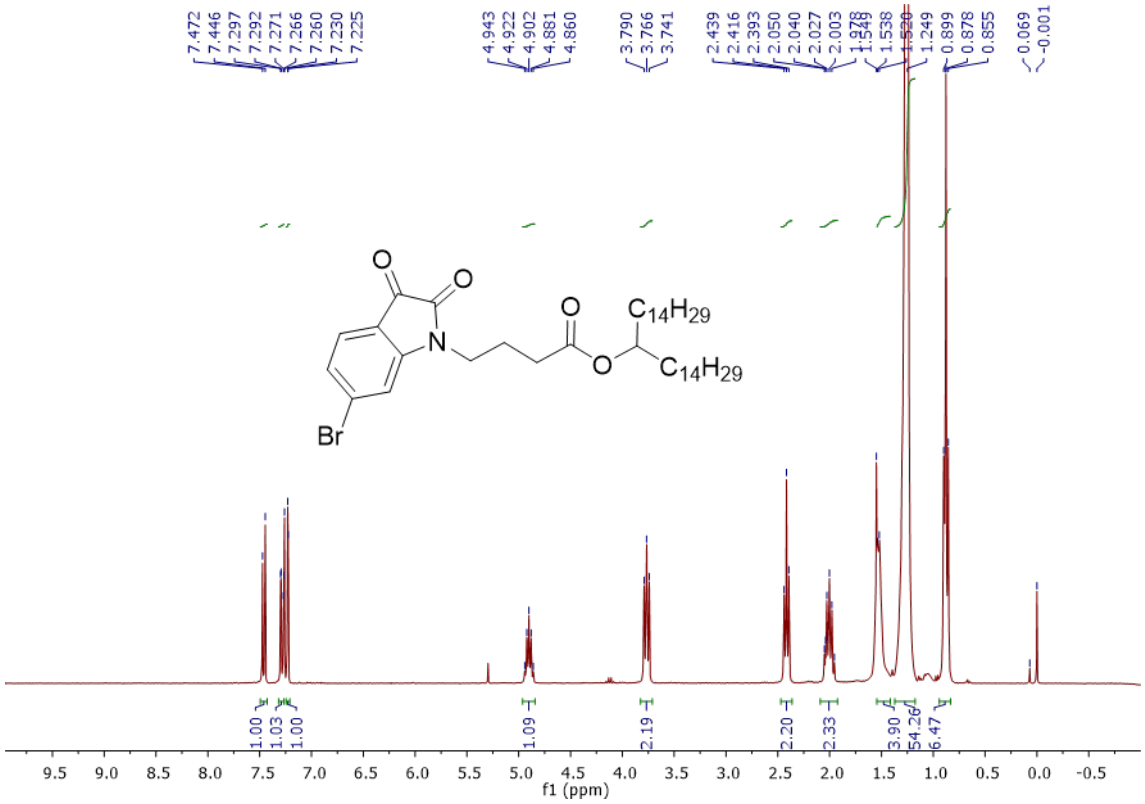

Figure A-14 300 MHz ^{1}H NMR spectrum for nonacosan-15-yl 4-(6-bromo-2,3-dioxoindolin-1-yl)butanoate **(2a)** in $CDCl_3$.

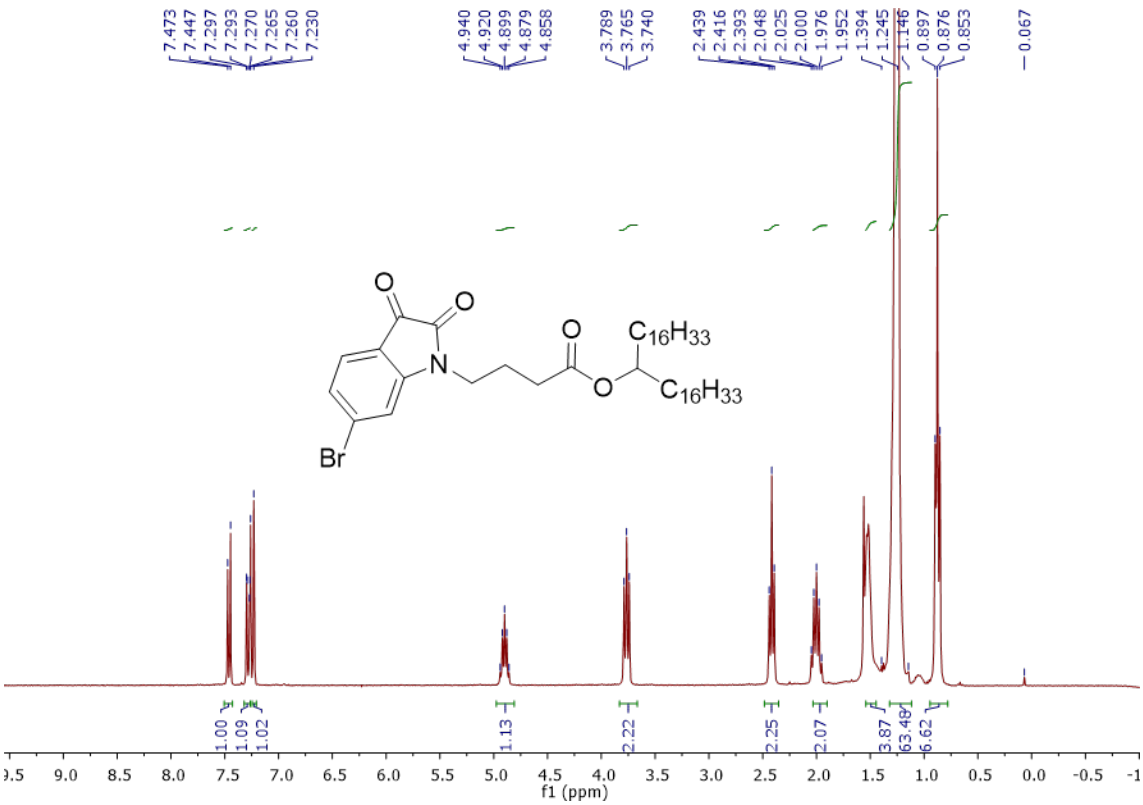

Figure A-15 300 MHz ^{1}H NMR spectrum for tritriacontan-17-yl 4-(6-bromo-2,3-dioxoindolin-1-yl)butanoate **(2b)** in $CDCl_3$.

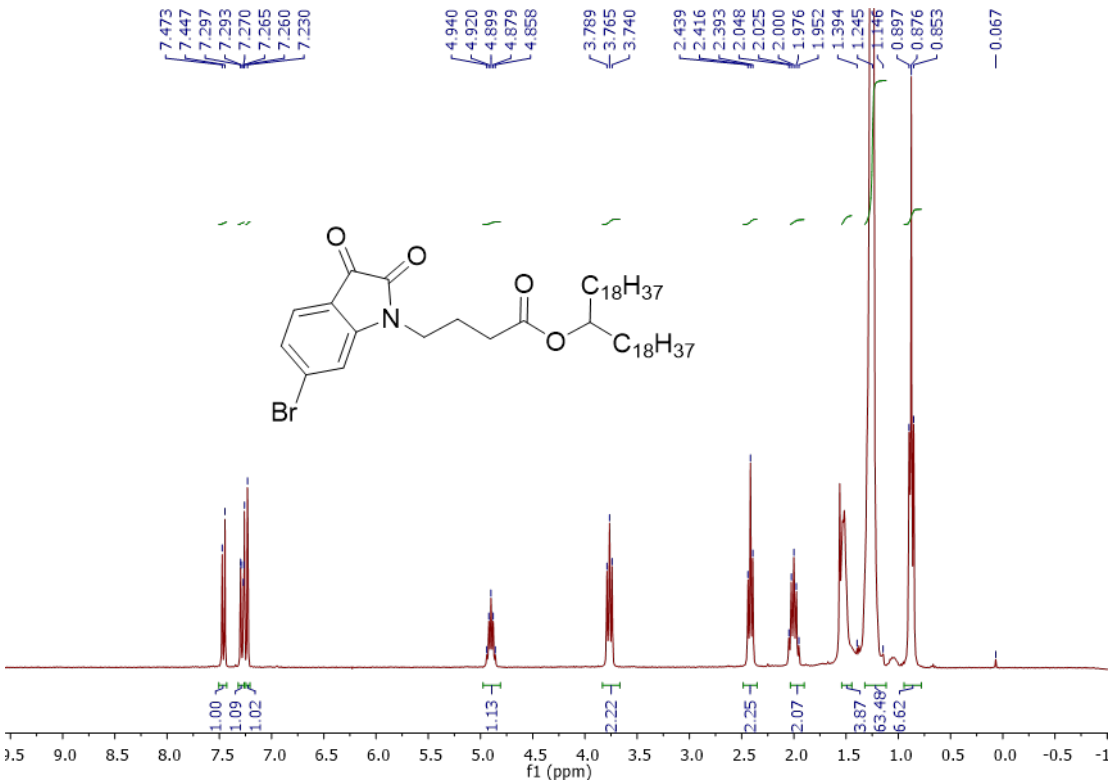

Figure A-16 300 MHz ^{1}H NMR spectrum for heptatriacontan-19-yl 4-(6-bromo-2,3-dioxoindolin-1-yl)butanoate **(2b)** in $CDCl_3$.

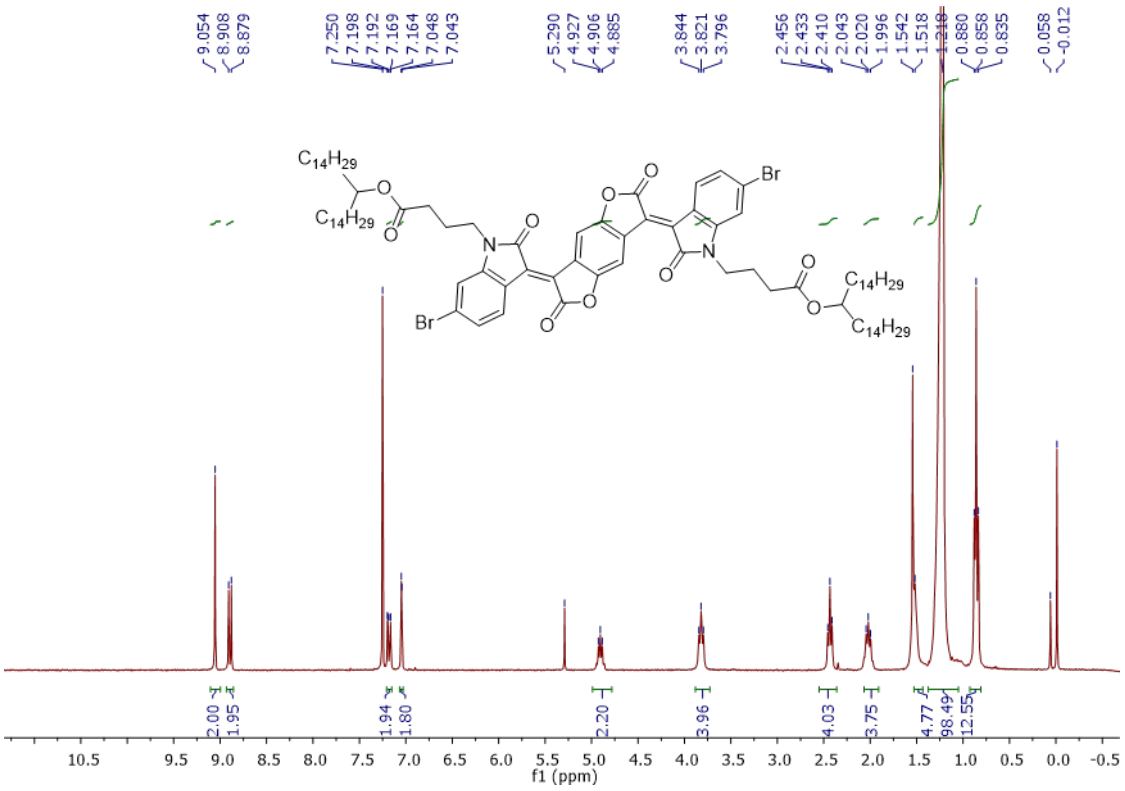

Figure A-17 300 MHz ^{1}H NMR spectrum for di(nonacosan-15-yl) 4,4'-((3*E*,3'*E*)-(2,6-dioxobenzo[1,2-*b*:4,5-*b*']difuran-3,7(2*H*,6*H*)-diylidene)bis(6-bromo-2-oxoindoline-1-yl-3-ylidene))dibutyrate **(3a)** in $CDCl_3$.

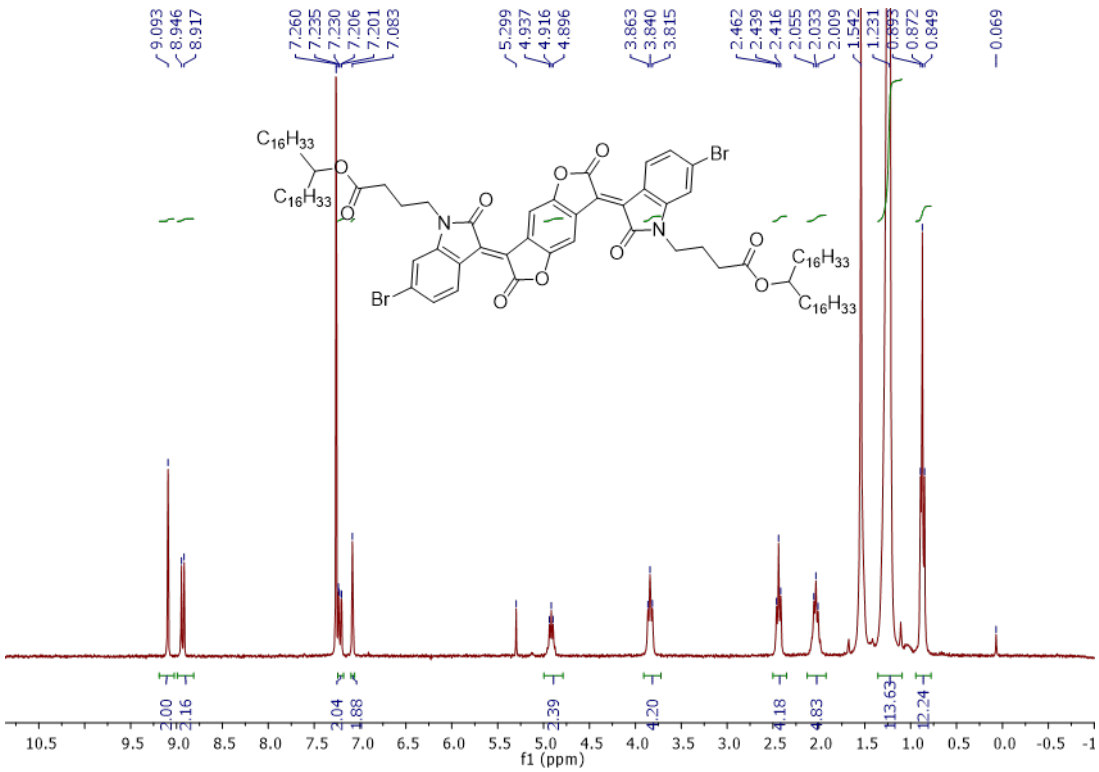

Figure A-18 300 MHz ^{1}H NMR spectrum for di(tritriacontan-17-yl) 4,4'-((3*E*,3'*E*)-(2,6-dioxobenzo[1,2-*b*:4,5-*b*']difuran-3,7(2*H*,6*H*)-diylidene)bis(6-bromo-2-oxoindoline-1-yl-3-ylidene))dibutyrate **(3b)** in $CDCl_3$.

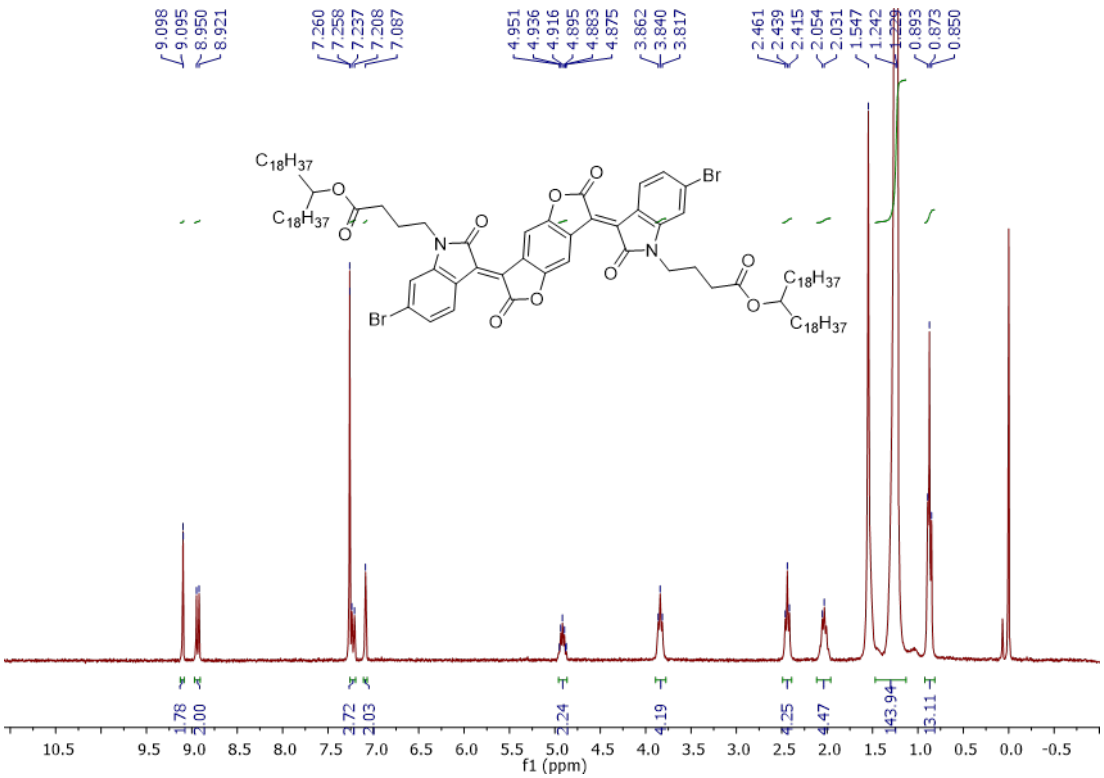

Figure A-19 300 MHz ^{1}H NMR spectrum for di(heptatriacontan-19-yl) 4,4'-((3*E*,3'*E*)-(2,6-dioxobenzo[1,2-*b*:4,5-*b*']difuran-3,7(2*H*,6*H*)-diylidene)bis(6-bromo-2-oxoindoline-1-yl-3-ylidene))dibutyrate **(3c)** in $CDCl_3$.

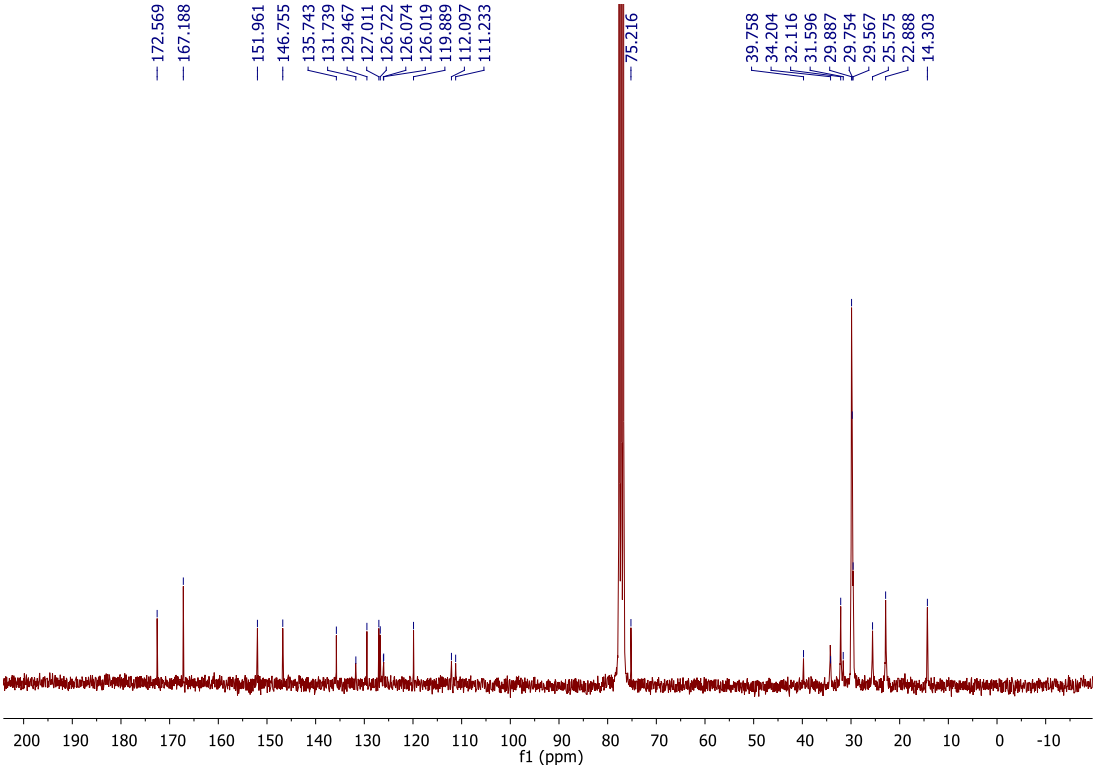

Figure A-20 75 MHz ^{13}C NMR spectrum for di(nonacosan-15-yl) 4,4'-((3*E*,3'*E*)-(2,6-dioxobenzo[1,2-*b*:4,5-*b*']difuran-3,7(2*H*,6*H*)-diylidene)bis(6-bromo-2-oxoindoline-1-yl-3-ylidene))dibutyrate **(3a)** in $CDCl_3$.

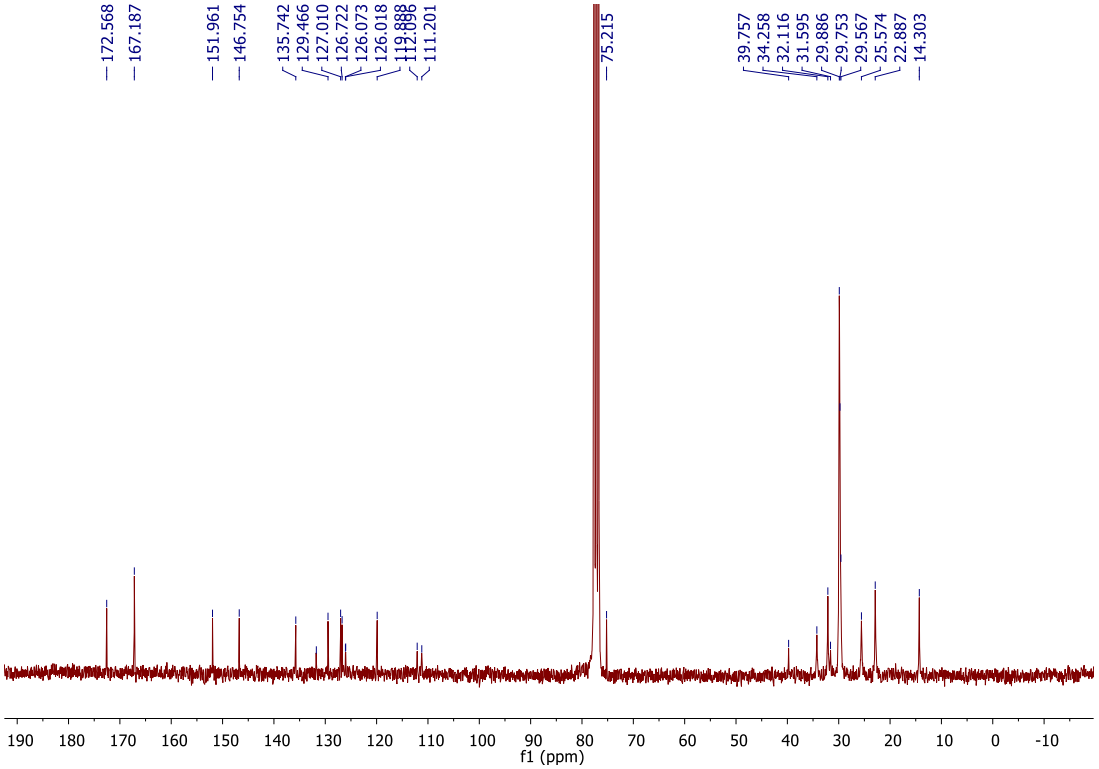

Figure A-21 75 MHz ^{13}C NMR spectrum for di(tritriacontan-17-yl) 4,4'-((3*E*,3'*E*)-(2,6-dioxobenzo[1,2-*b*:4,5-*b*']difuran-3,7(2*H*,6*H*)-diylidene)bis(6-bromo-2-oxoindoline-1-yl-3-ylidene))dibutyrate **(3b)** in $CDCl_3$.

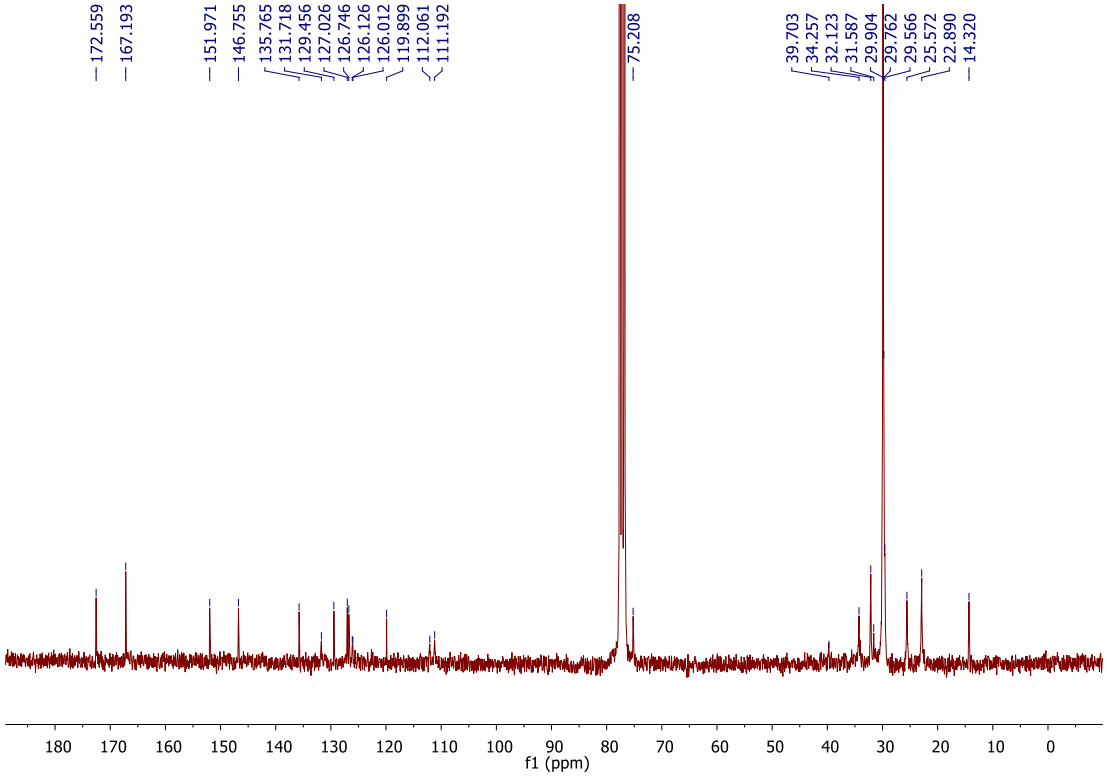

Figure A-22 75 MHz ^{13}C NMR spectrum for di(heptatriacontan-19-yl) 4,4'-((3*E*,3'*E*)-(2,6-dioxobenzo[1,2-*b*:4,5-*b*']difuran-3,7(2*H*,6*H*)-diylidene)bis(6-bromo-2-oxoindoline-1-yl-3-ylidene))dibutyrate **(3c)** in $CDCl_3$.

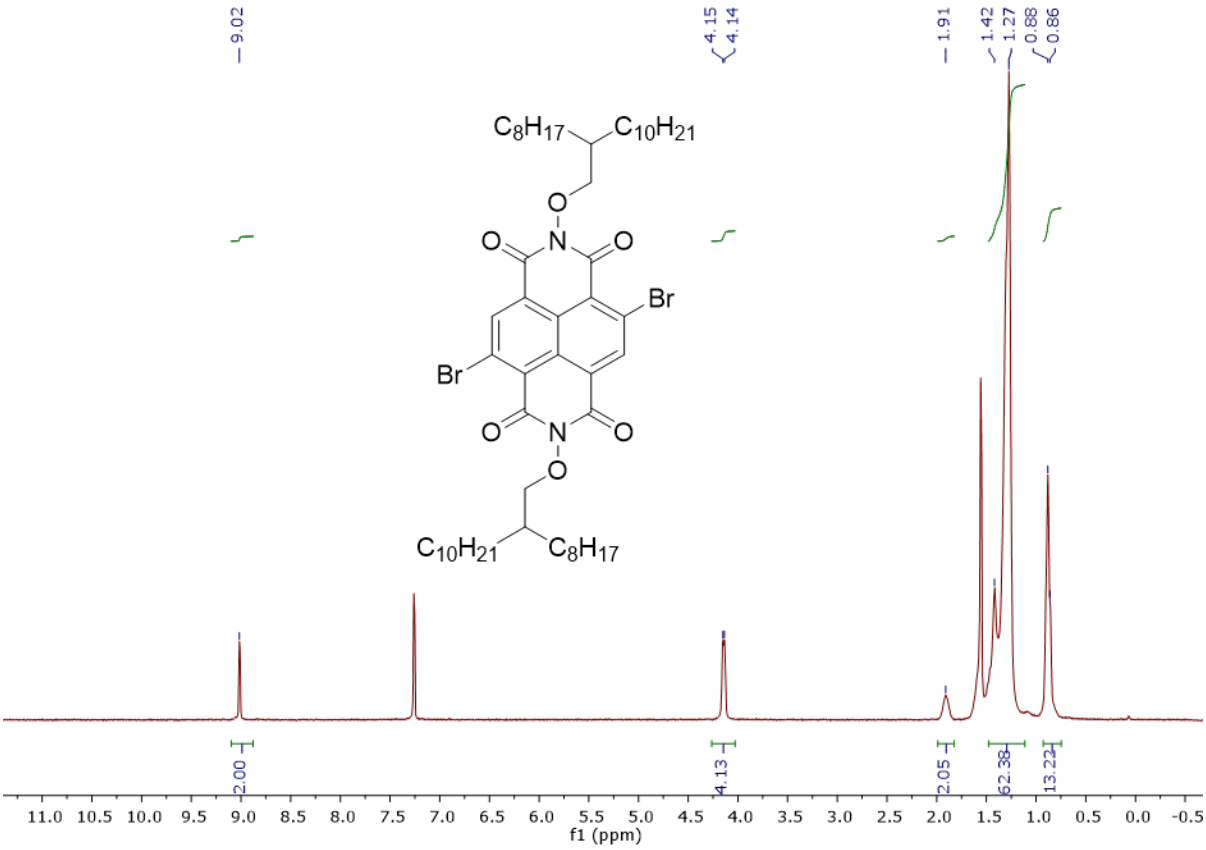

Figure A-23 300 MHz ^{1}H-NMR spectrum for 4,9-dibromo-2,7-bis((2-octyldodecyl)oxy)benzo[lmn][3,8]phenanthroline-1,3,6,8(2*H*,7*H*)-tetraone (**NDIO20-Br**) in $CDCl_3$.